ESA CONTRACT REPORT

European Space Agency Contract Report

The ECMWF Contribution to the Characterisation, Interpretation, Calibration and Validation of ERS-1 Scatterometer Backscatter Measurements and Winds, and their use in Numerical Weather Prediction Models

Authors: Ad Stoffelen and David Anderson

European Centre for Medium-Range Weather Forecasts
Europäisches Zentrum für mittelfristige Wettervorhersage
Centre européen pour les prévisions météorologiques à moyen terme

European Centre for Medium-Range Weather Forecasts
Shinfield Park, Reading, Berkshire, UK

European Space Agency Contract Report

The ECMWF contribution to the characterisation, interpretation, calibration and validation of ERS-1 scatterometer backscatter measurements and winds, and their use in numerical weather prediction models

by

Ad Stoffelen
David Anderson

originally formulated as:

"ECMWF technical support for global validation of ERS-1 AMI wind data"
under ESA contract number: 9097/90/NL/BI

February 1995

CONTENTS Page No.

1. INTRODUCTION

The ERS-1 satellite was launched on 17 July 1991, carrying a C-band scatterometer. This project is concerned with various steps in the conversion of normalised radar backscatter measurements, frequently called sigma-naughts (σ^0), into geophysically useful information, viz wind speed, V, and direction, φ, at 10 m above the ocean surface. Many of the steps necessary to make that conversion had been tested prior to launch, but not with real satellite data. As a result many changes or modifications were necessary.

The ERS-1 scatterometer has three independent antennae pointing in a horizontal plane towards a direction of 45°, 90°, and 135° with respect to satellite propagation. Therefore, a site in the scatterometer swath is illuminated three times, respectively by the fore, mid and aft beam. The incidence angle of the radar beam varies from 18° to 47° for the mid beam, and from 24° to 57° for the fore and aft beams. The swath, approximately 500 km wide, is sampled every 25 km resulting in 19 measurement nodes across the swath; along the swath the sampling distance is also equal to 25 km. The nodes are not independent, however, and the effective spatial resolution of the instrument on the Earth's surface (footprint) is approximately 50 km. The C-band radar frequency used is 5.3 GHz and its polarisation is vertical.

Two major steps are involved in deriving winds from sigma naughts. First, a relationship between the radar backscatter and wind speed and direction is needed, called the model function or transfer function. This is derived in the form $\sigma^0 = f(V,\phi)$ where ϕ is the wind direction relative to the antenna, but is then used in an inverse way to derive wind speeds and directions from σ^0 measurements. It has frequently been suggested that σ^0 is a function of more geophysical parameters than neutral 10 m wind speed and direction (eg *Donelan and Pierson*, 1987), but it will be shown that these effects, if present, are secondary and that an accurate wind inversion procedure is, in general, possible based on a σ^0-to-wind relationship only. We made no correction for stability in the lowest 10 m of the atmosphere, since stability will in general be close to neutral over the oceans, and a stability correction can not be computed with great accuracy. Therefore, our results are valid for average stability conditions (at each wind speed).

At each node, multiple solutions for (V,φ) exist so a step is necessary to select the most plausible solution from those possible. Finding the possible solutions is called inversion, while making a selection from those possible is called ambiguity removal. Before presenting our contribution, we describe the pre-launch transfer function CMOD2 and the inversion and ambiguity removal scheme used by ESA, called CREO.

1.1 The pre-launch transfer function

From pre-launch field campaigns an empirical relationship between σ^0, and wind speed V_N and direction ϕ_N for neutral stratification at 10 m height was found by *Long* (1985), called CMOD2. It has the form

$$\sigma^0=10^{\alpha}.V_N^{\gamma}.[1+B_1\cos(\phi_N)+B_2\cos(2\phi_N)] \quad (1.1)$$

where: $$B_1=b_1^1+b_1^2.V_N \quad (1.2)$$

and: $$B_2=b_2^1+b_2^2.V_N \quad (1.3)$$

The coefficients α, γ, b_1^1, b_1^2, b_2^1 and b_2^2 are specified by a sum of a tuning coefficient times a Legendre polynomial of order 0, 1, and 2 in $x=(\theta - 25°)/40°$, with θ the radar beam incidence angle, e.g. $\alpha = \alpha_1 + \alpha_2.x + \alpha_3.(3x^2-1)/2$. The resulting 18 tuning coefficients were determined from pre-launch field campaigns. In this report, the first and largest term in Eqn (1.1), i.e. $10^{\alpha}V_N^{\gamma}$ will be referred to as the "bias" term, the smaller harmonic coefficient B_1 as the "upwind/downwind amplitude", and B_2 as the "upwind/crosswind amplitude", (although the latter is strictly 50% of the average of the differences between upwind and crosswind, and between downwind and crosswind, divided by the bias term). We will further ignore the stability correction in these equations and replace (V_N,ϕ_N) by (V,ϕ).

1.2 The operational wind retrieval and ambiguity removal suite: CREO

ESA's operational scheme called CREO performs several steps in order to retrieve a wind field:

- Firstly, the transfer function is used inversely in the wind inversion algorithm. It is based on minimisation of the following maximum likelihood estimator (MLE) for varying wind speed and direction:

$$\text{MLE} = \sum_{i=1}^{3} \left[\frac{\sigma^0_{Oi} - \sigma^0_{Si}}{SD(\sigma^0_{Si})} \right]^2 \quad (1.4)$$

where σ^0_{Oi} is the measured (observed) value, and σ^0_{Si} is the simulated value obtained from the σ^0-to-wind transfer function for a trial value of the wind vector. The index i indicates beam: 1 = fore, 2 = mid, 3 = aft. $SD(\sigma^0_{Si})$ is a measure of the noise in σ^0 and has the form $Kp_i.\sigma^0_{Si}$, where Kp_i is a constant in the search for a minimum, with a value determined by instrument noise which is typically 0.05. The minimisation is done for each node, i.e. triplet of measured σ^0 values (σ^0 pairs corresponding to two-beam operation can also be processed by CREO but we do not consider such

nodes in this report). Over the full wind domain this objective function will have several local minima, with the two most probable solutions in general approximately 180° degrees apart, due to the small upwind/downwind amplitude in the transfer function. These local minima are ranked in order of decreasing probability and stored as the possible solutions for wind speed and direction.

- In the second step of CREO, two fields are compiled across the full swath and a maximum distance of 3000 km along the swath. The two fields are supposedly blowing in opposite directions. Directional consistency between neighbouring points is the main constraint in the compilation. Information on potential skill in discrimination between upwind and downwind is used in this step.
- The third step is called "autonomous ambiguity removal", in which one of the two fields is selected when it has a sufficiently low MLE averaged over all nodes. (Actually, the selection is made based on the number of rank 1 solutions in the fields). Optionally this third step can be dispensed with.
- If step 3 is unsuccessful, step four is to check which wind vector field is best correlated with a background wind field over an area typically 500 km X 3000 km. The background field used operationally by ESA is a 24-48 hour forecast from ECMWF. If the large scale fit of the closest field is not acceptable, no solution is given. This occurs in ~ 30% of cases. The processed areas overlap by one-third in order to be able to check for consistency.

1.3 **Overview of the report**

The objectives of the initial contract were to provide quality assurance on the scatterometer data and to check for technical problems with the data. In our early comparisons of the ERS-1 scatterometer data with the ECMWF forecast and analysis winds, an interbeam σ^0 bias was revealed, together with other technical problems, as will be discussed in section 2. We also found large average σ^0 departures. By intrinsic quality control of the σ^0 triplets we were able to prove that the pre-launch transfer function CMOD2 needed modification. The characterisation of the quality of σ^0 measurements and the formulation and tuning of new transfer functions (CMOD3 and CMOD4) will be discussed in section 3. Further it proved necessary to optimise the inversion procedure as discussed in section 4. In section 5, the ambiguity removal procedure is discussed and a new procedure is proposed in the light of a lower than expected upwind/downwind sensitivity and problems with the directional-consistency filter in CREO. The new ECMWF processing procedure is called PRESCAT. The impact of the improved scatterometer winds on the ECMWF forecasting system is considered in section 6. The report concludes with a summary (section 7), and recommendations (section 8).

2. DATA HANDLING AND QUALITY ASSURANCE

At an operational weather centre, such as ECMWF, large amounts of data from a variety of measurement systems are processed daily in a routine manner. This resource makes such a location ideal for quality

controlling and calibrating any new instrument, such as the scatterometer on ERS-1. The scatterometer data (labelled UWI by ESA) may be compared directly with other instruments, such as ships, buoys or island stations. However, it takes time for a reliable data set to be assembled, as the number of collocations per day is not very high. So, comparison between the UWI and other in-situ data such as ships was not carried out extensively because instrument calibrations by ESA were expected (and occurred) rather frequently during the early stages, preventing the acquisition of a comprehensive data set of consistent collocations. An alternative, and in this respect more profitable, comparison is between the UWI and either the ECMWF analysis or short range forecast, called "guess field" and denoted FG or FGAT[1].

All the above surface data (excluding the scatterometer), together with upper air and other satellite observations and information from earlier times, are synthesised into a dynamically consistent analysis (*Lönnberg and Shaw*, 1987). Subsequently, the ECMWF forecast model is used to carry information extracted from the observations from one analysis time to the next (6 hours later). The operational forecast model had a resolution of 125 km at the start of the project although this was soon improved to 60 km (in October '91). Every UWI measurement has an analysis and forecast equivalent, so collocation statistics can be built up quickly and the UWI instrument validated in near real time. For this reason most of our validation work has used the ECMWF wind fields. Both global and regional comparisons can be made with the UWI. A drawback in using ECMWF wind fields may be that any systematic error present in the ECMWF forecast model or introduced by the assimilation procedure may be passed through to the analysis, possibly affecting collocation statistics. However, the continuous monitoring and improvement of ECMWF meteorological fields, using observational data, is a safeguard against the occurrence of large errors.

2.1 Collocation files

Software to collocate UWI data with conventional data and the ECMWF model analysis and guess field has been run routinely. The files containing collocations with the ECMWF meteorological model include measured σ^0s, estimates of the model 10 m winds and simulated σ^0s from both the analysis and FGAT. Such collocation files for the period 1 March 1992 to 28 February 1993 have been prepared and delivered to ESA.

UWI data are also collocated with conventional observations including SHIP, BUOY and SYNOP[2] from islands (which are less than 100 km^2, low-lying, and away from any continent). The conventional

---

[1] FGAT = (First Guess at Appropriate Time). A forward integration is stored after 3 hrs, 6 hrs and 9 hrs and a cubic interpolation made in order to obtain the model first guess at the appropriate measurement time. Alternatively, only 6 hr forecasts are saved (FG) and all measurements in the 3 to 9 hr window are assigned to 6 hrs, giving time differences between the measurements and the FG of up to 3 hrs.

[2] Surface observations of several meteorological quantities including 10 m winds.

observations are flagged against the ECMWF operational guess field, and observations from high quality stations are indicated. These collocation files also contain interpolated pressure, height, temperature and humidity at all model levels below 850 mb, both at the sites of the conventional observation and of the scatterometer measurement nodes. A detailed description of the collocation files is given in appendix A. They are available from ESA to those wishing to make comparisons between UWI and other conventional measurements.

2.2 UWI product validation

Our initial comparisons included σ^0 departure statistics of measured minus simulated values, obtained using the ECMWF analysed wind and the CMOD2 transfer function. Although we are interested in a wind-velocity comparison, there are advantages in comparing in measurement (σ^0) space, as this avoids the inversion and ambiguity removal processes, to which we shall return later. In a σ^0 comparison, several sources of error can contribute to the differences between observed and measured values of σ^0. These are errors in the observed σ^0, errors in the specification of the transfer function, errors in the ECMWF winds, and the representativeness 'error' (i.e. the 'error' which occurs when two measurements are representative of different space and time scales). Fig 2.1a shows the differences between the observed values of σ^0 and those simulated using CMOD2. Not only are these differences substantial but they are also horizontally correlated. Although wind errors in the ECMWF model will contribute to these departures and are known to be horizontally correlated, it is not clear that this is the explanation of the differences seen in Fig 2.1a. Because of the strongly non-linear relationship of wind speed and direction with σ^0, especially at low wind speeds, it is not straightforward to interpret σ^0 departure statistics in terms of wind errors (see also section 3.3.4c). Therefore we used other methods of validation to try to identify the cause of the errors. These are discussed below in section 3.

Some points in Fig 2.1a were identified as ice, and a filter based on analysis Sea Surface Temperature was then devised to exclude ice points. From the start we also made speed comparisons between UWI and ECMWF fields. These comparisons showed a bias, with UWI speeds much higher than the ECMWF analysed speed, especially for higher speeds. Further, application of our ambiguity removal software, closely based on CREO, showed a preponderance of winds blowing up or down the mid beam at low incidence angles.

A particularly useful way of showing the σ^0 bias was to plot the mean ratio of the observed value of σ^0 to that derived from the ECMWF analysis as a function of incidence angle (Fig 2.2). Care has to be taken to avoid inhomogeneous wind direction sampling, so a filter was applied to obtain a uniform ECMWF wind

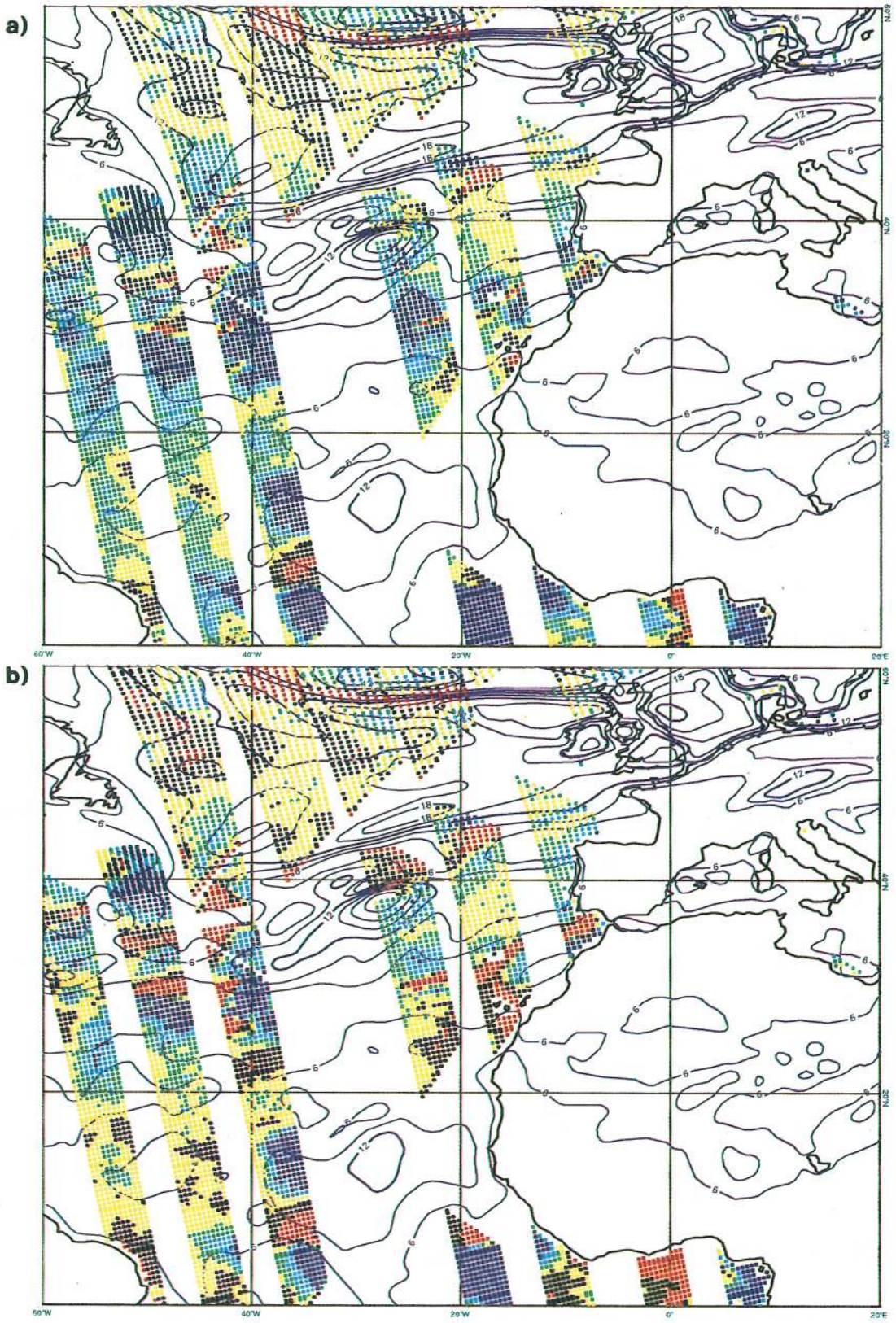

Fig 2.1 a) Map of σ^0 differences between the observed value (σ^0_O) and that simulated using CMOD2 and ECMWF analysis winds (σ^0_M). UWI data are for the period 2100 **UTC** on 26 September 1992 to 2100 **UTC** on 29 September 1992. Contours of speed are for 1200 **UTC** on 28 September. Colour coding of $\Delta\sigma = \sigma^0_O - \sigma^0_M$ in dB is

Brown $\Delta\sigma > 20$ Black $10 > \Delta\sigma > 3$ Green $-3 > \Delta\sigma < -10$ Dark blue $-20 > \Delta\sigma$

Red $20 > \Delta\sigma > 10$ Yellow $3 > \Delta\sigma > -3$ Light blue $-10 > \Delta\sigma < -20$

b) As for a) but for CMOD4.

direction distribution over the full range of wind speeds. Plots such as Fig 2.2 can be produced from just 6 hours worth of data (as in Fig 2.2), so monitoring of bias can be usefully carried out in near real time. In fact, ECMWF detected that the new calibration tables were applied incorrectly at the first engineering calibration being carried out by ESA, and ECMWF notified ESA of this within one day.

Fig 2.2 shows that there are further biases between the measured and simulated data. These could arise from instrumental bias, from a speed bias in the ECMWF model, or from an incorrect transfer function. The trend of the bias we compute with θ is mainly caused by an erroneous transfer function, and in Fig 2.3 this trend has been removed by using the transfer function CMOD4 (see section 3). Furthermore, the three beams do not overlap over the range of common incidence angle, indicative of an interbeam bias still present after the engineering calibrations on 14 and 18 September 1991. ESA validated the σ^0 bias over the rain forest. Their calibration results are also shown in Fig 2.2, verifying our relative interbeam biases. The last engineering calibration was carried out on 24 February 1992 in order to reduce the interbeam biases and remove the linear trend.

Fig 2.3 shows that the engineering calibrations between 14 September 1991 and 24 February 1992 resulted in an improvement in mutual fit of the three beams, but with small inconsistencies still existing. Figures such as 2.2 were used frequently during the instrument calibrations to monitor the changes and to check if there were differences in ascending/descending passes. No significant differences (< 0.2 dB) were found, implying that day-night temperature variations across the antennae were not leading to any significant biases. Geographical variations in the biases were also considered but no significant effects were found. From diagnostics with both analysis and forecast winds for different seasons corresponding to different geographical wind distributions, we believe the method has a relative accuracy of approximately 0.2 dB. The method does not provide an absolute calibration capability, but may be used to monitor instrument changes in time.

During the early phase, data coverage was monitored regularly and reported to ESA. A number of technical issues were also uncovered and reported, such as problems with flags (e.g. where flags indicate a good σ^0, but in fact σ^0 had a missing value), problems with σ^0 values in orbits south of Australia, and the fact that increased instrumental noise is present when switching on/off a beam (e.g. going from two to three beam operation).

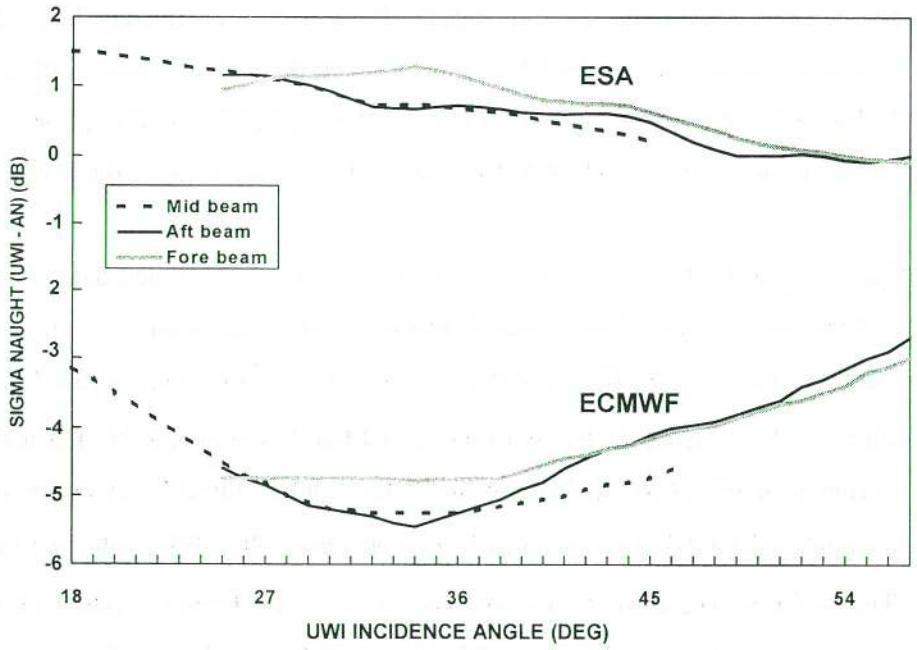

Fig 2.2 Plot of the bias between mean σ^0_O, and σ^0_M, as a function of incidence angle, θ, for the 3 beams for the 6 hour time interval 0900 to 1500 on 16 September 1991. Ideally, the fore and aft beams should lie on top of each other, but do not, indicating an interbeam bias. Likewise, over the common range of incidence angle, the mid beam should lie on top of the other two. This figure shows, however, that the mid beam appears to be biased high at low incidence angle. For comparison the ESA rainforest calibration is shown for 18 September 1991 14:29 UTC. (Based on Guignard 1991. A $\cos\theta$ factor has been removed to make the results directly comparable with the ECMWF calibration.) The ECMWF calibration is offset by -3 dB.

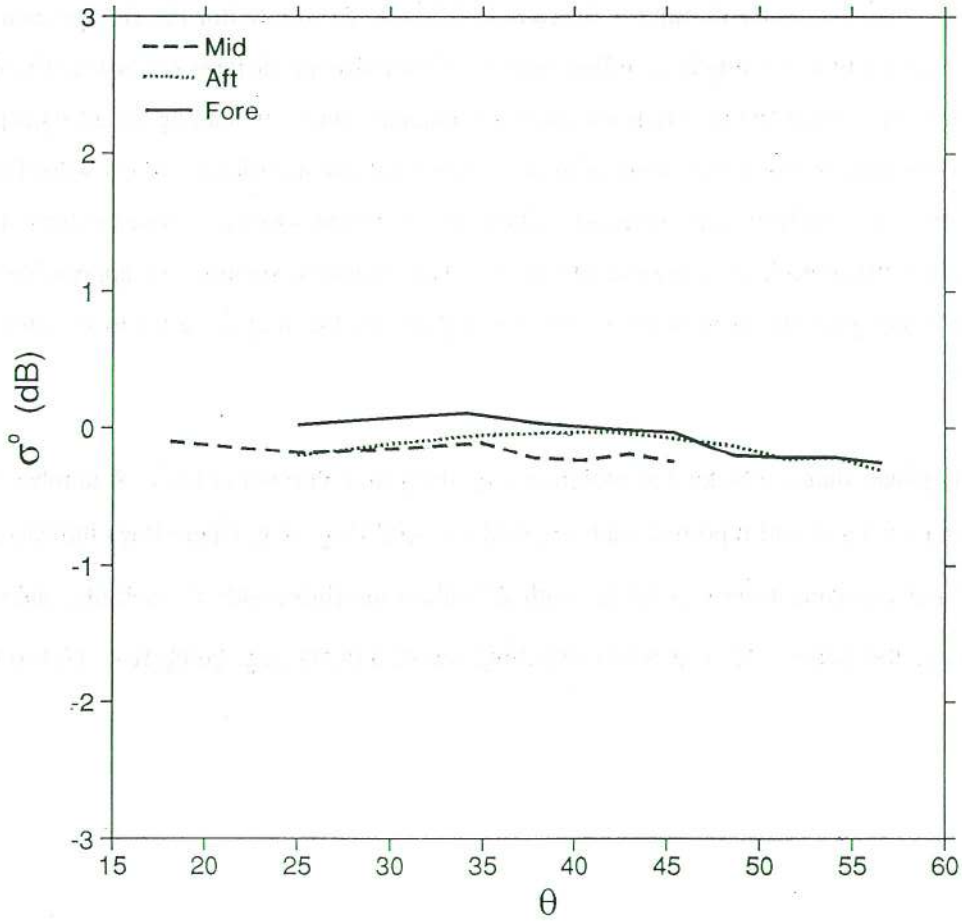

Fig 2.3 As for Fig 2.2 but an average for the period 1/12/93 to 11/12/93, using CMOD4.

2.3 Summary

In this section we have shown that the wealth of data available at an operational NWP centre provides an excellent basis for a rapid calibration and validation of satellite products. The real-time availability of ERS-1 data to ECMWF and other users also helped to reveal and then remedy technical problems at an early stage. The next sections will show that the scientific interpretation of the data has been further developed. Real-time access to the data and the existence of an analysis team, as organised by ESA, have contributed to the rapid and successful validation of the ERS-1 scatterometer.

3. CHARACTERIZATION OF THE MEASUREMENT SPACE AND DERIVATION OF THE TRANSFER FUNCTION

The observed trend in the ocean σ^0 calibrations as a function of θ shown in Fig 2.2 indicated that there was a problem with the transfer function CMOD2. Our confidence in the ocean calibration was increased when we showed that removal of the computed biases on the measured σ^0s improved the wind retrieval and ambiguity removal (with CREO). However, using this method did not remove all problems with the retrieved winds, such as unrealistic wind speed and direction distributions, and the dependency of these distributions on incidence angle (i.e. across swath node number).

By plotting each measured σ^0 triplet in a 3D space, where the three axes represent the fore, mid and aft beam measurements respectively, the full characteristics of the measurements can be obtained. Visualisation of the 3D σ^0 measurement space allowed us to obtain the noise characteristics of the measurements, and gave further evidence of problems with the transfer function (section 3.1). We therefore started to reformulate and recompute the coefficients of the transfer function.

The procedure used for the transfer function tuning was based on software provided by A Long (ESA, ESTEC) using the algorithm of *Britt and Luecke* (1973). This procedure allowed for errors in both the UWI and in the ground calibration 'instrument', in this case the ECMWF analysis wind fields. Results were sensitive to the estimated error. So, in order to carry out tuning, it was necessary to have estimates of the error in the ECMWF winds as well as in σ^0s. Error estimates for σ^0s are given in section 3.1, and for ECMWF winds in section 3.2. In section 3.3 we consider tuning. Here, a number of problems were identified which are illustrated in section 3.3.1. The way data were filtered for tuning is described in section 3.3.2, and the tuning of the transfer functions CMOD3 and CMOD4 discussed in section 3.3.3. Finally in section 3.3.4 we consider a postiori verification where again 3D σ^0 space plays an important role.

3.1 Visualisation in measurement space

The transfer function CMOD2 relates σ^0 to the two geophysical parameters V_N and ϕ_N. There is a third parameter, incidence angle, θ, but we interpret that as a known parameter, determined from the geometry of the instrument and orbit. Small errors in θ could give rise to substantial errors in σ^0 as the θ dependence is very strong, especially for low θ values. For example, the 0.1 degree θ sampling in the UWI product is found to give approximately a 6% variation in σ^0 values at θ=18°. (Because the θ dependence of σ^0 is strongest at low θ, it would be more convenient for data characterization to have yaw steering result in a constant θ for the mid beam at node 1 (θ=18°) rather than at θ=40°.)

Strictly, σ^0 could be a function of parameters other than the local wind velocity, such as wave age, temperature, surfactants etc. Before trying to derive a new transfer function based on two parameters, it is important to know if there is substantial evidence for a departure from a two-parameter function. One way to do this which does not depend on external measurement is to plot the data in measurement space. If the transfer function depends on only two parameters, then the data should lie on a surface in 3D σ^0 space.

Following *Cavanié and Lecomte* (1987) we plot σ^0 triplets in the 3D-space (measurement space) spanned by the σ^0s of the fore mid and aft beams (respectively called 1, 2 and 3) (see Fig 3.1). Quantitative use and visualisation of such a cone in three dimensions is rather difficult, so we took sections through the cone. Initially, three sections were used (i) a vertical cross-section with $\sigma_1^0 + \sigma_3^0$ = constant, (ii) a vertical cross-section along the plane with $\sigma_1^0 = \sigma_3^0$, (iii) a horizontal section with σ_2^0 = constant and the data projected onto that plane. The thickness of the cross-sections (i) and (ii) is made equal to the expected noise contribution from fore, mid and aft beams in the direction normal to the plane of the section. An example of the data in section (i) is shown in Fig 3.2 for node 11 at speeds of approximately (a) 4 ms^{-1}, (b) 8 ms^{-1} and (c) 15 ms^{-1}. Clearly the data do not lie exactly on a surface (a Lissajous-type figure in this section), nor should they because of instrumental noise. An estimate of instrumental noise is given by K_p. The width of 2 K_p is plotted on Fig 3.2, to show the extent to which data do in fact lie within this distance of the surface. The appropriate curves for CMOD2 and CMOD4 are also shown.

3.1.1 *Validation of the existence of a solution surface*

Subjectively we estimated the scatter around a hypothetical surface from type (i) cross-sections for different values of $\sigma_1^0 + \sigma_3^0$ and for nodes 1, 3, .. 19. The distribution of measurement points near the bottom of the curve was used to obtain a scatter estimate for the mid beam and the distributions at the sides to give

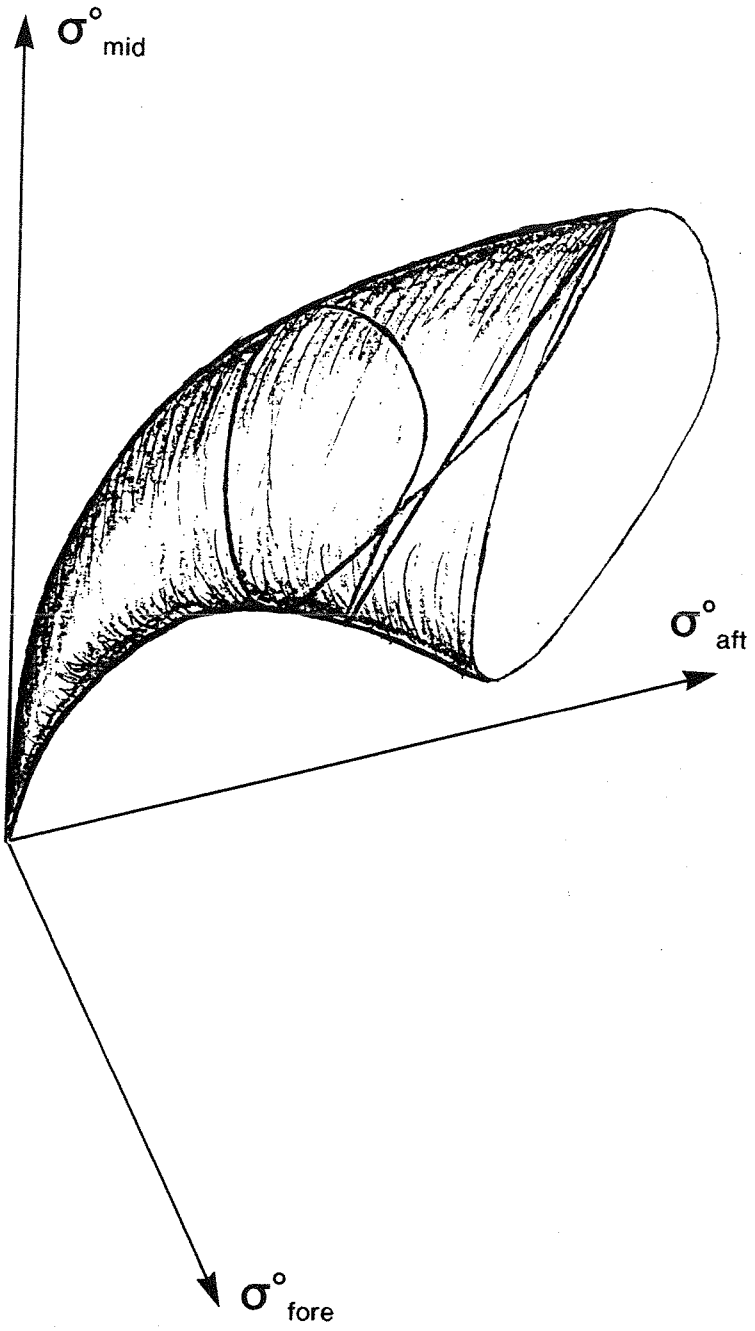

Fig 3.1 Schematic representation of the surface on which σ^0 triplets should lie for a given node. The surface actually consists of two skins which can intersect, but this is not shown in the schematic. The shape and proximity to each other of the two skins is a function of node number across the swath. A schematic curve of constant speed is drawn on the surface of the cone. Based on *Cavanie and Lecomte* (1987).

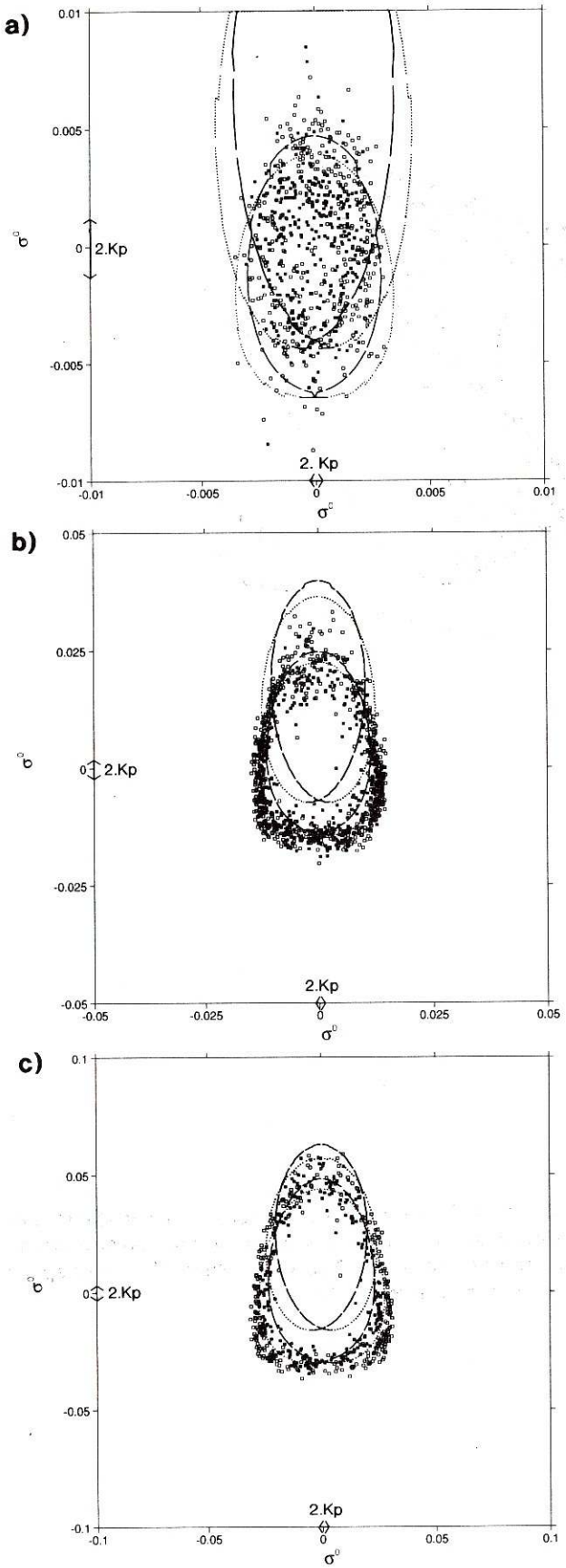

Fig 3.2 (a) Vertical slice through the cone for node 11 along the line $\sigma_1^0 + \sigma_3^0 = const$, corresponding approximately to a speed of 4 ms^{-1}. The thickness of the slice is 5% of $\sigma_1^0 + \sigma_3^0$. A measure of instrumental noise 2 Kp is shown. The curves for CMOD2 (upper pair) and for CMOD4 (lower pair) are plotted on top of the measured σ^0 triplets. Triplets associated with a wind component upwind to the midbeam are represented by an open square and downwind by a solid square. The solid curve marks upwind and the dotted curve downwind flow. The top of the curve corresponds to winds exactly along the mid beam, whereas at the lowest points the wind blows roughly across the mid beam. The curves are broken at every 10 degrees in wind direction to show the wind direction dependency.
(b) As a), but for an approximate speed of 8 ms^{-1}.
(c) As a), but for an approximate speed of 12 ms^{-1}.

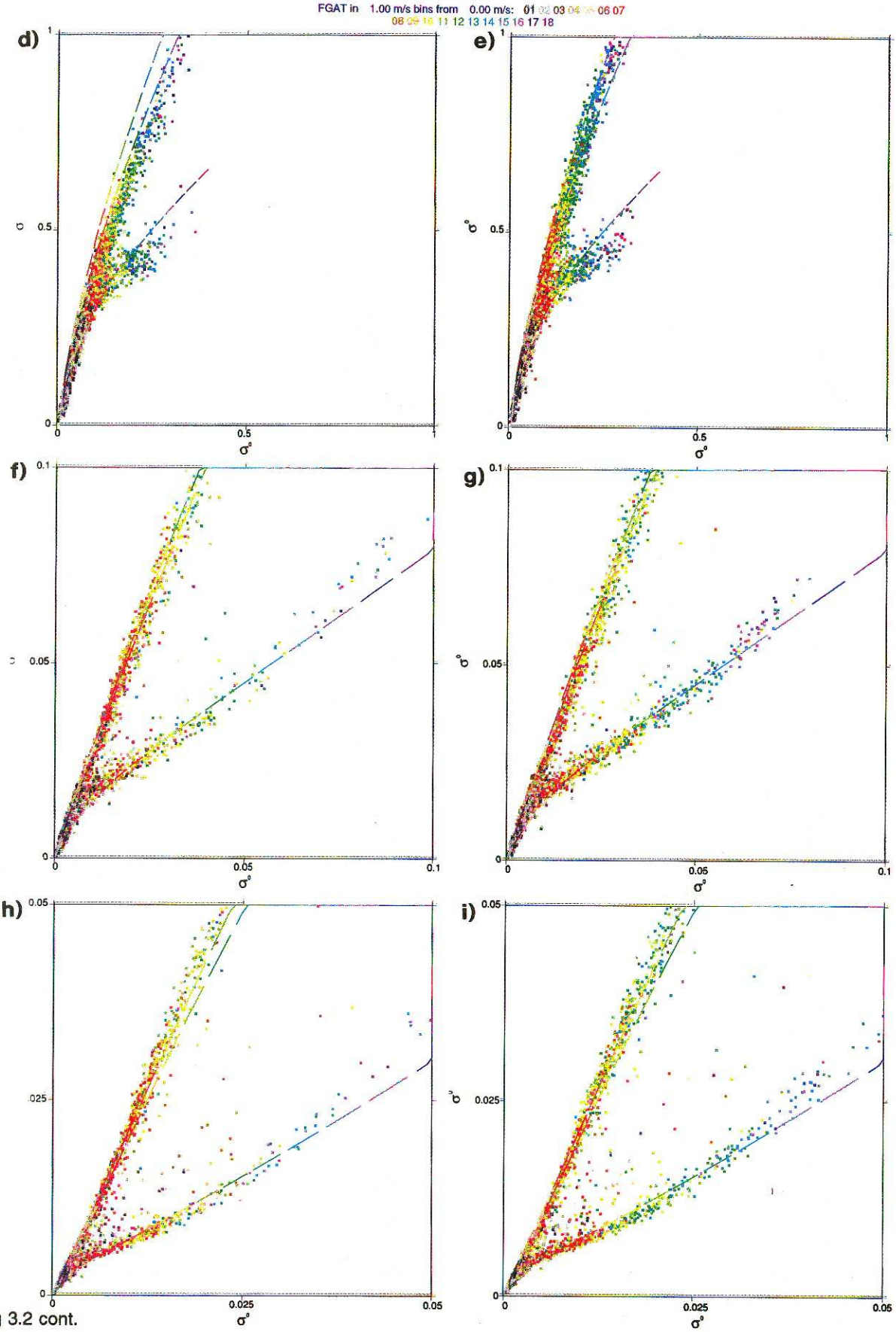

Fig 3.2 cont.

(d) A vertical slice through the cone for node 3 along the line σ_1^0 - σ_3^0, with a thickness 5% of σ^0. The σ^0 triplets are classified as upwind. Colour coding shows ECMWF wind speed in 1 ms^{-1} intervals as indicated at the top. The curves show CMOD4 at upwind, downwind and approximately crosswind to the mid beam.
(e) As d), but for downwind, (f) As d), but for node 11, (g) As f), but for downwind, (h) As d), but for node 19, (i) As h), but for downwind.

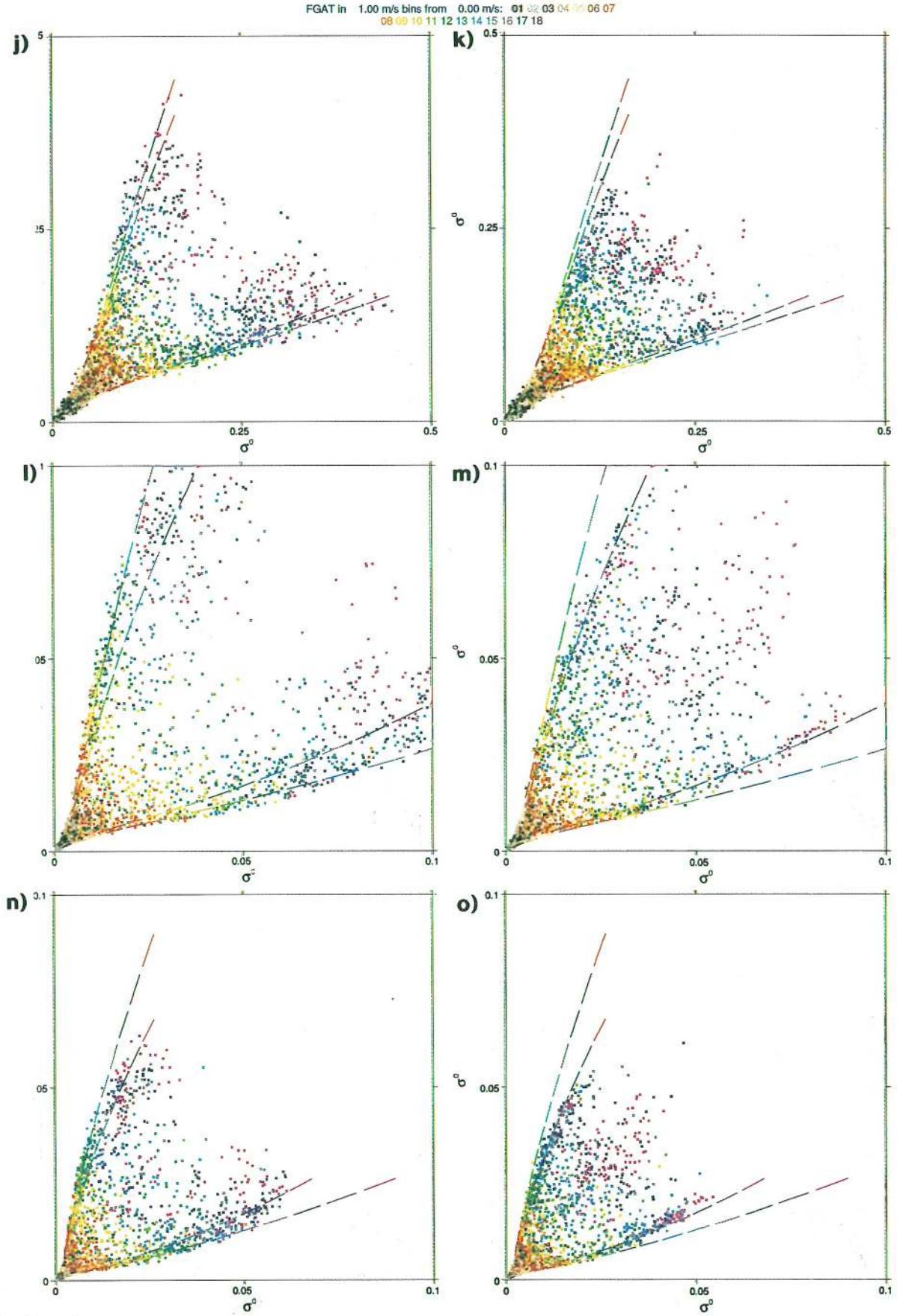

Fig 3.2 cont

(j) The projection of σ^0 data onto a plane σ_2^0 = constant for node 3 and upwind. Colour coding as in d). The curves show the extreme values of CMOD4 for approximately upwind and downwind wind directions with respect to the fore and aft beams. (k) As j), but for downwind, (l) As j), but for node 11, (m) As l), but for downwind,(n) As j), but for node 19, (o) As n), but for downwind.

estimates of scatter for the fore and aft beams. A normalised measure of the scatter, similar to K_p, was calculated. For the mid beam, the normalisation was the local value of σ_2^0, and for the fore and aft beams, the average of σ_1^0 and σ_3^0. We collocated the points in cross-section (i) with ECMWF wind speed, to refer the value of $\sigma_1^0 + \sigma_3^0$ to a specific wind speed obtained from the collocated wind speed Probability Density Function (PDF). As shown in Fig 3.3, the variance of the scatter present in σ^0 is generally of the order of instrumental noise (~ 5 %) which implies that instrumental noise is the main contribution to the scatter of Fig 3.2. However, for low wind speeds, a wind speed dependency is evident. We have assumed that the total error in Fig 3.3 can be separated into an instrumental error of approximately 5% which varies per beam, and a geophysical relative error $\frac{\Delta\sigma_g^0}{\sigma^0}$ which is the same for the three beams and the root-mean-square of which can be expressed as:

$$rms\left(\frac{\Delta\sigma_g^0}{\sigma^0}\right) = 6.44\ 10^{-4}(V-16)^2 \qquad (3.1)$$

where wind speed V is in m/s. Further, for small incidence angles (high σ^0) the variance of the scatter is larger than for large incidence angles (low σ^0) implying processes other than implied by Eqn (3.1) are causing scatter. A possible explanation may be in the strong non-linear θ dependence of σ^0 at these angles, combined with the variability of wind and waves on scales smaller than the scatterometer footprint size (50 km x 50 km). Because of the non-linearity, the scatterometer will be most sensitive to the ocean conditions at the inner part (lowest θ) of the footprint and therefore have an effective footprint size which is smaller than 50 km x 50 km. So, for inner nodes (low θ), the effective sampling area is not the same for the mid, and fore and aft beams. Geophysical variability on scales not effectively sampled by the mid beam will decrease the coherence within a triplet, and therefore increase the scatter. Avoiding measurements at low θ, or correcting measurements made at a higher resolution may relieve this problem. In the spatial filtering of σ^0s the non-linearity should be accounted for.

For low wind speeds of order 2 m/s the scatter increases to approximately 15%. It is likely that this is a result of geophysical effects, but this has not been further investigated since 15% at 2 m/s results in only a small wind speed variance. Using the relationship between σ^0 and wind velocity from CMOD2, the σ^0 scatter was estimated to correspond to a wind vector RMS error of only 0.3 m/s on average (see also table 3.1). Therefore we conclude that the ERS-1 scatterometer is performing very well, and that we may in general regard the triplets as being scattered around a surface.

Cross-sections of type (i) are very useful for considering the directional response of the transfer function at a particular speed. A cross-section of type (ii), shown in Figs 3.2 d-i, is useful to define wind speed dependence. For illustration, the nodes 3, 11 and 19 are shown. The diameter of the cone relative to the scatter normal to its surface can be seen to be much smaller for low speeds and low node number. Figs 3.2 d, f, and h show "upwind" triplets, and Figs 3.2 e, g, and i "downwind" triplets. We note that the location of "upwind" and "downwind" triplets is similar in the direction perpendicular to the cone. The distribution of triplets along the cone is however different for "upwind" and "downwind". At low node numbers, the downwind distribution extends further along the cone than the upwind distribution, but for high node numbers the opposite is true. The projection of type (iii) is shown in figure 3.2 j-o for "upwind" and "downwind" nodes 3, 11, and 19. In this type of projection the upwind/downwind effect can be verified, as well as the upwind/crosswind effect. Figs 3.2 d-i show the directional effects on the mid beam, whereas Figs 3.2 j-o provide information on the fore and aft beam directional sensitivity. The wind speed dependence can be verified as well to some extent in Figs 3.2 d-o. Other sections were also made, but they did not yield any new information.

In principle, one could attempt to find a mathematical description of this surface for each node and then relate the two mathematical parameters describing the surface to useful geophysical parameters. Upwind/downwind aliasing could be avoided by finding a mathematical description of the surface separately for upwind and downwind, relying on external wind direction data. Care would have to be taken to allow for a continuous functionality on the directional parameter when going from upwind to downwind. We did not try to solve this problem, but instead a posteriori verified the fit of our tuned transfer functions with the measured σ^0 triplets in the 3D σ^0 space. As a consequence, in our case the two parameters used to describe the surface can be interpreted directly as the wind vector.

The wind vector interpretation, although the most practical, is not without difficulty. The ERS-1 scatterometer has a footprint size of 50 km diameter. The radar return therefore is probably best related to the mean wind speed over the footprint area, and not to the amplitude of the mean vector wind. Especially for low wind speeds this difference is significant; for example for a zero mean vector wind, the average wind speed is approximately equal to 1.5 times the wind vector variability (resulting in roughly 1.5 X 1.2 = 1.8 m/s). Similarly, other non-linear aspects of the σ^0-to-wind vector relationship, i.e. in σ^0-to-ϕ or σ^0-to-θ, will make the wind vector interpretation physically more complicated. These effects are especially relevant when comparing scatterometer measurements with small footprint instruments such as SAR. Also, CMOD2 was derived from aircraft campaigns and, given the small footprint size in this case, CMOD2 would not have been generally valid for the σ^0-to-wind relationship applicable for the ERS-1 scatterometer footprint size.

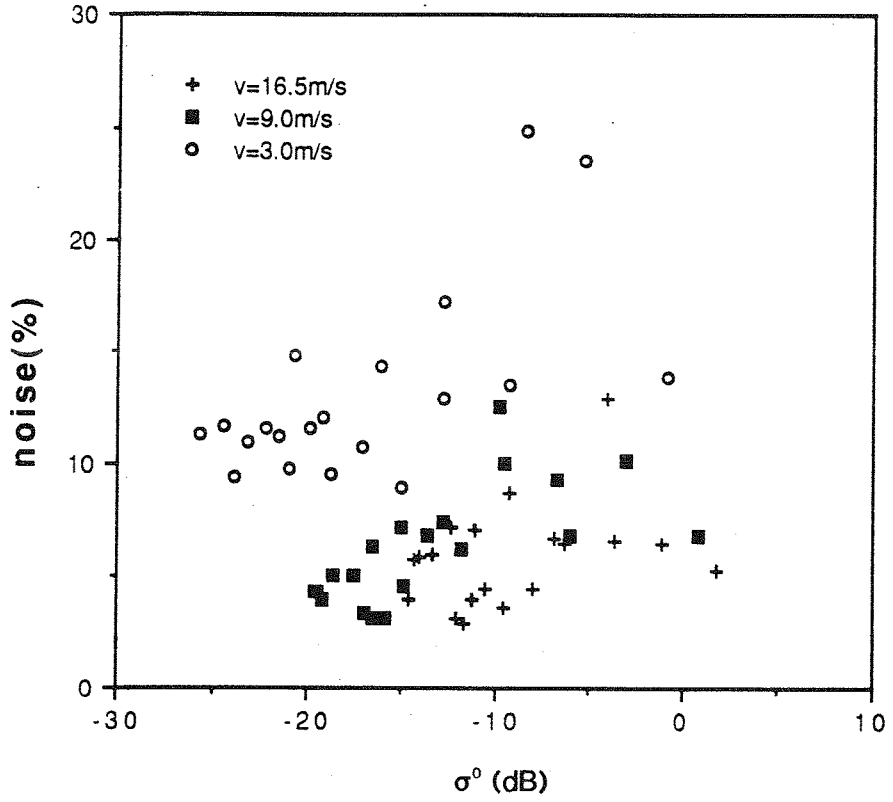

Fig 3.3 Estimated scatter against incidence angle for speeds of 3, 9 and 16.5 m/s.

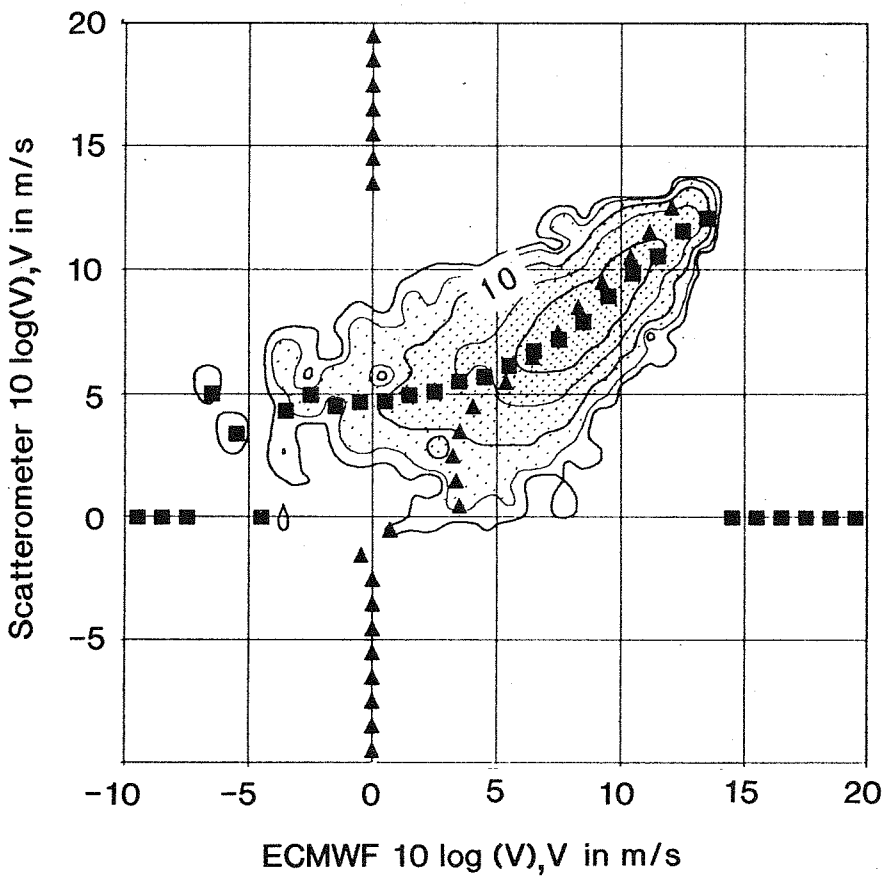

Fig 3.4 Two-dimensional distribution in 10 log V, with V in m/s. The vertical axis is V estimated from the fore and aft beam measurements, while the horizontal axis is the collocated ECMWF speed. Solid squares represent vertical averages over the distribution and solid triangles, horizontal averages. Node 17 data from 30/9/'91 and 1/10/'91.

3.1.2 *Wind speed dependence of* σ^0

Cross-section (i) is approximately a cross-section at constant wind speed, as can be verified by collocation with ECMWF analysis wind speeds. Knowing the 3D σ^0 offset vector for the centre of gravity of the data distribution in cross-sections at different wind speeds, one can plot an estimate of the bias term ($10^{\alpha}V^{\gamma}$ in Eqn 1.1) as a function of wind speed V for each incidence angle (θ). Eqn (1.1) suggests that σ^0 (in dB) should have a $\log(V)$ dependence viz $10(\alpha+\gamma\log V)$, but we found a non-logarithmic relationship particularly at low wind speeds. However, given the uncertainty in ECMWF model wind speed and the non-symmetric error distribution for low wind speeds (see section 3.3) it is very difficult to draw any firm conclusion from this method.

So, in order to study the wind speed dependence of σ^0, we averaged σ_1^0 and σ_3^0 and compared the average to ECMWF wind speed. As implied by Eqn (1.1), this average is independent of the upwind/crosswind amplitude, and is only slightly dependent on the upwind/downwind amplitude. Fig 3.4 shows a 2D histogram of wind speeds estimated from the average of σ_1^0 and σ_3^0 collocated with ECMWF analysed wind speeds. From such plots it was found that the distributions calculated with a $\log(V)$ dependence were not realistic for any value of α and γ, particularly for the lower wind speeds. For example, the number of points above a line at 45° is much greater than the number below; an asymmetry is especially noticeable for low values of $\log V$. (The values of α and γ used in Fig 3.4 were optimised to give the optimal fit of x and y.) Moreover, the resulting distributions were dependent on incidence angle. When the $\log(V)$ dependence was modified to a $\log(V+\beta(\theta))$ dependence, the distributions became more realistic. A stronger modification, like a $\sqrt{V}$ dependence gave unrealistic distributions for the lower wind speeds, but a more realistic distribution for high wind speeds. We modified the transfer function CMOD2 to include the parameter β, the log-dependency for low wind speeds and the $\sqrt{V}$ dependency for average and high speeds.

3.1.3 *Upwind/crosswind amplitude*

By subjectively estimating the diameter of the cone in the horizontal and vertical directions, see Fig 3.2a-c, the upwind/crosswind amplitude for the fore/aft and mid beam (i.e. B_2 as defined in Eqn 1.1) was calculated. Using simple vector algebra and ignoring the upwind/downwind amplitude for the moment, the resulting dependence of B_2 on θ could be calculated as shown in Fig 3.5. For low incidence angles, the scatter in σ^0 is comparable to the upwind/crosswind amplitude, leading to low skill in wind direction retrieval. For higher wind speeds and higher incidence angles, the upwind/crosswind amplitude saturates at a value of 0.6, peaking at around 12 m/s and dropping a little for the highest wind speeds and incidence

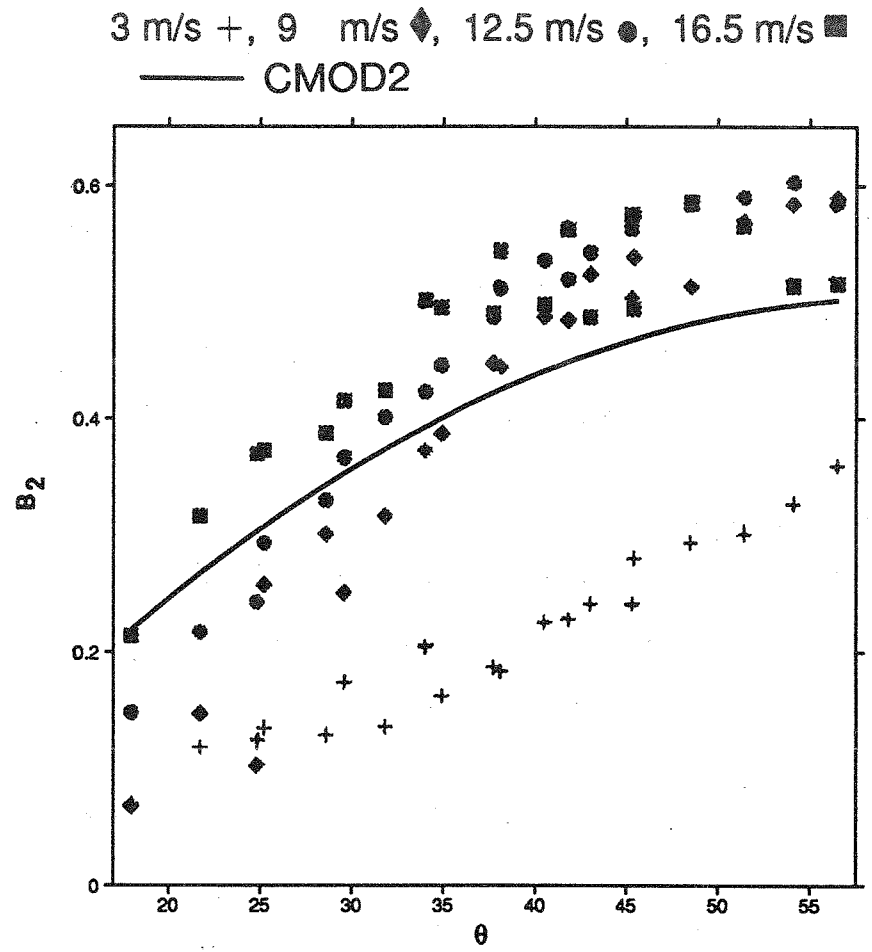

Fig 3.5 Estimated value of B2 against incidence angle, θ, for speeds of 3, 9, 12.5 and 16.5 m/s. The curve shows the CMOD2 relationship.

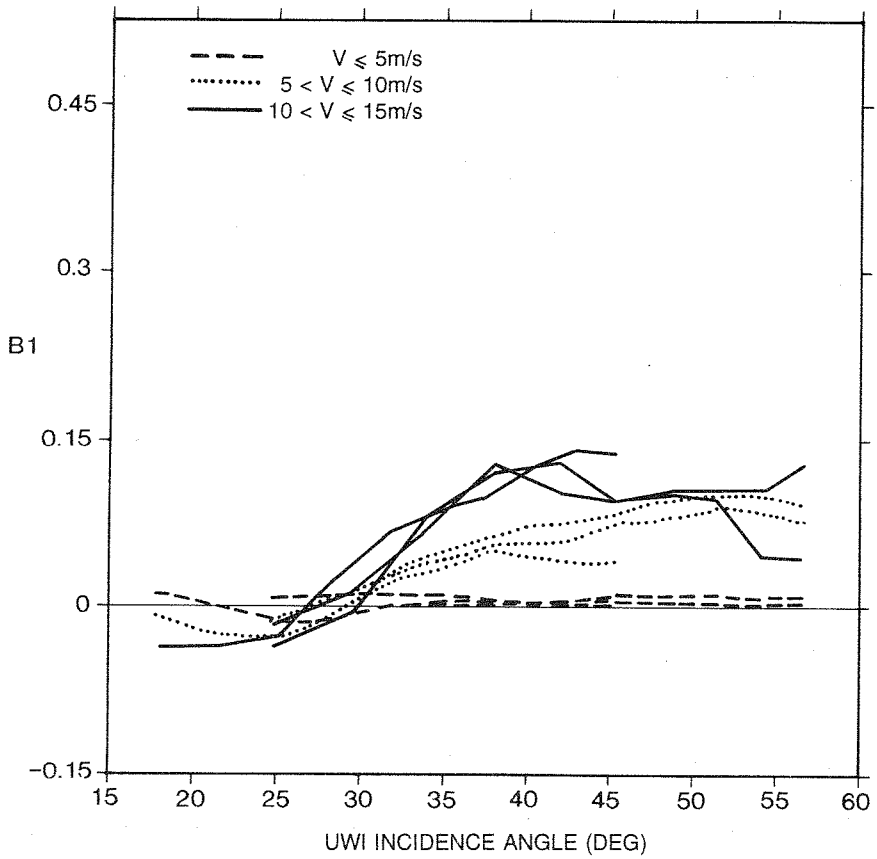

Fig 3.6 Upwind/downwind amplitude versus incidence angle for different wind speed intervals, based on the average of the scatterometer and ECMWF wind speed. The 3 beams are shown separately for each speed.

angles. Since this behaviour cannot be described with a parabolic θ dependence and a linear wind speed dependence as assumed in Eqn (1.3) for B_2, it follows that CMOD2 has to be revised in this respect.

An important point evident from Fig 3.2 b and c is the almost triangular shape of the solution surface. This means that higher harmonics besides $\cos(\phi)$ and $\cos(2\phi)$ are involved in Eqn (1.1). We found that replacing $[1+B_1\cos(\phi)+B_2\cos(2\phi)]$ by $[1+B_1\cos(\phi)+B_2\cos(2\phi)]^{1.6}$ allows an accurate fit to the triangular shape, and so this is the form used subsequently.

3.1.4 *Upwind/downwind amplitude*

Although the cross-sections in σ^0 space can provide considerable information about the geophysical processes affecting C-band radar backscatter and about σ^0 measurement characteristics, they do not provide a quantitative measure of the upwind/downwind amplitude. Therefore we tried to estimate this amplitude by another method. First, we filtered a σ^0 and ECMWF analysis wind collocation data set to a flat wind direction distribution over a large range of wind speeds. Then we defined an upwind bin for $|\phi| < 90°$, and a downwind bin for $|\phi - 180°| < 90°$. The average upwind value minus the average downwind value divided by the sum of upwind and downwind values is proportional to the upwind/downwind amplitude (B_1 in Eqn 1.1). On the assumption of a $\cos(\phi)$ relationship and symmetry around $\phi = 90°$ for the remaining harmonic terms, the proportionality constant can be shown to be $\pi/2$. The standard deviation of error in the ECMWF analysis wind direction as a function of wind speed was estimated, and a correction made for the effect of this wind direction error on the calculated amplitudes. This correction was not very significant because the upwind/downwind amplitude is small for low wind speeds, and it is only for low wind speeds that the standard deviation of wind direction error is large (i.e. a substantial fraction of 90°). Fig 3.6 shows our estimated upwind/downwind amplitude. It is in general small and negative for low incidence angle, but shows large wind speed dependence for mid range incidence angles. Again saturation can be observed for high wind speeds and incidence angles. This behaviour cannot be described by the CMOD2 formulation of Eqn (1.1-1.3).

3.1.5 *Ice and SST effects*

We also used cross-section (ii) to investigate the sensitivity of the distribution of σ^0 triplets to SST (from 0° C to 30° C) for low wind speeds (< 2 m/s) and found no sensitivity. At mid swath, cross-section (ii) reveals a considerable overlap in the distribution of σ^0 triplets from ice with the distribution from wind. Time or space continuity could be used to distinguish open sea from ice (eg *Lecomte*, 1993). At inner and outer swath, the distributions are largely distinct and so ice and wind effects can be separated.

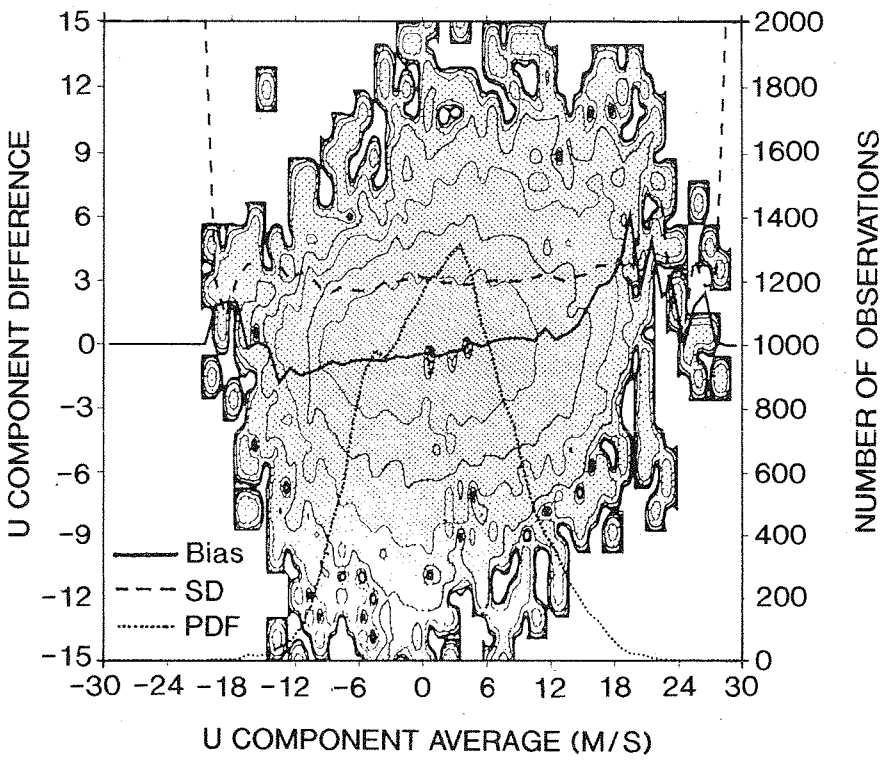

Fig 3.7 2D distribution of departures in the East-West component of the wind of "automatic" SHIP from the ECMWF guess field, plotted versus the average of SHIP and guess field East-West component. The solid line shows the bias and the dashed line the standard deviation of the departures. The dotted line is the distribution of average East-West components and is quantified on the right vertical axis. Contour levels are logarithmic and 21270 entries are used.

3.2 Error level of the ECMWF winds

Fig 3.7 shows an example of a distribution of departures in the east-west component of the wind, of "automatic" SHIP observations from the ECMWF guess field plotted against the average of SHIP and guess field. In general the bias (solid curve) between conventional observations and guess field is below 10% and positive, i.e. the conventional observations are higher than the guess field. However, the space and time representativeness of observed and model data are not the same, leading to different statistical characteristics for the two systems. The standard deviation is rather constant over the components of the wind. In speed scatter plots we verified that the departure error depends only weakly on wind speed. Similar scatter plots for wind direction, however, show a strong variation of wind direction error with wind speed indicating that error estimates are more easily quoted in terms of wind components than in terms of speed and direction. Assuming equal portions of the standard deviation derived from Fig 3.7 to be in SHIP observation and guess field, the guess field error is approximately 2.25 ms^{-1} in the components irrespective of wind component amplitude. We found no evidence of marked regional variations. In retrospect, the error estimate of 2.25 ms^{-1} is pessimistic (see table 3.2).

3.3 Estimation of the σ^0-to-wind relationship

The MLE procedure of Britt and Luecke can be used to estimate the most probable σ^0, wind speed and direction, and coefficients of an implicitly defined σ^0-to-wind transfer function as given for example in Eqns (1.1-1.3). Using this MLE procedure and assuming Gaussian statistics for error in σ^0, V and ϕ, we found that the resulting transfer functions were not significantly better than CMOD2. This unsatisfactory result prompted us to review the nature of the estimation problem. The assumption of Gaussian distributions of error in wind speed and direction is not supported by the results from section 3.2, where it was shown that the standard deviation of error in the components of the wind is approximately 2.25 m/s and constant over all wind speeds. Therefore, we assumed an isotropic error distribution in the components of the wind. Then the standard deviation of wind speed error is approximately 2.6 m/s which implies that the correlation between "true" wind speed and ECMWF analysis wind speed should start to drop below 8 m/s and approach zero around 2 m/s. For speeds below 2 m/s, the speed error distributions are very asymmetric. Furthermore, for low speeds the direction error distribution is strongly dependent on wind speed. Since the statistical properties of errors in the components of the wind are much closer to the requirements of the MLE procedure than the statistical properties of errors in wind speed and direction, it is more constructive to derive a transfer function using wind components rather than speed and direction. A second consideration is the consequence of proportional errors for MLE. The expected value of the standard deviation of error in σ^0 is proportional to the "true" value of σ^0. In Appendix B.1 we show that this type of variation in standard deviation causes the MLE procedure to be inexact.

It is shown in Appendix B.1 that one way to accommodate proportional error is to perform the estimation using σ^0 measured in dBs, rather than as a physical quantity. The advantage is that the error (K_p) is approximately constant at 5%, or 0.2 dB. A possible disadvantage is that the error distribution, which is probably Gaussian in physical space, will not be strictly so in logarithmic space. We will consider the relative advantages/disadvantages of estimation in logarithmic space further in section 3.3.1.

The transfer function is a strongly nonlinear function of wind speed and direction, and this nonlinearity can give rise to difficulties in estimating the transfer function parameters, as illustrated in Appendix B.2. In the problem of estimating the scatterometer transfer function, we have highly non-linear relationships between σ^0 and wind speed and direction, invalidating the use of a linear MLE method. Some non-linear aspects of the problem are reduced by posing it in $\ln\sigma^0$ rather than σ^0. If we are unable to estimate the bias term in the transfer function correctly, we will have problems with the upwind/crosswind and upwind/downwind term similar to those introduced by the β term in Appendix B2. The "aliasing" problem will occur for low wind speeds, where the wind direction standard error is close to 90° and therefore comparable to the upwind/crosswind angle difference. Finally we note that if the data selected for the estimation procedure represents an inhomogeneous distribution of the parameters involved in the estimation, then further errors in the MLE procedure may result.

3.3.1 *Tuning simulations using wind components and logarithmic space*

Given the considerations above, we re-examined the estimation procedure to see whether the problem was properly posed. To this end we studied the behaviour of the MLE procedure using simulated data for which the true solution was known. Analysis winds were chosen to be "true" winds, and "true" σ^0s were simulated from them using CMOD2. In sections 3.1.1 and 3.2 we estimated the noise characteristics of both the σ^0s and the winds to be used in the estimation of the transfer function coefficients. In our simulations noise was added to the "true" winds with a Gaussian standard deviation of 2.25 m/s in the wind components. At the time we did the simulations we were not yet able to accurately estimate the noise level in σ^0. The noise estimates used in the simulations vary slightly, but in retrospect were a little too high (we used 10% rather than 5%-8% as seen in Fig 3.3).

The simulation will be most meaningful when the noise specification resembles the noise that will be experienced in the real problem. For example, specification of the noise in the wind as 20% in wind speed and 20° in direction for all wind velocities (as was used in deriving the CMOD2 model function for example) will give misleading simulations, since in reality such a noise specification is not tenable (see section 3.2). We also found that the selection of data used in the estimation plays an important rôle, and in the next examples we use the same wind distributions that were used for tuning with real data (see 3.3.2).

In Fig 3.8 we compare the upwind/crosswind amplitude for two simulations, different only in the sense that we used wind speed and direction in one case, and wind components in the other case as input to the MLE procedure. The 'true' solution is also plotted. It is evident that estimation using wind components gives a much closer fit to the 'true' solution than using speed and direction.

Fig 3.9 shows the upwind/crosswind amplitude for two simulation cases differing only in that the upper curve is obtained by MLE in physical space, whereas the lower curve is obtained by MLE in logarithmic space for σ^0. Not only is the upwind/crosswind amplitude in error, but the bias term and upwind/downwind amplitude are also significantly worse when estimation is made in physical space. Experiments where we varied the σ^0 error standard deviation to be Gaussian in either physical or logarithmic space did not show any significant difference in results (not shown).

In most experiments the upwind/crosswind amplitude was found to be very sensitive to slight changes in the bias term, indicating that we need a formulation for the bias term which fits the data accurately.

Different, but reasonably uniform wind distributions containing up to 20,000 points, gave slightly different answers after convergence of the MLE procedure, but in general there was no dependence of the result on initial conditions, and in most cases 25 iterations were sufficient to converge to the solution.

3.3.2 *Data Selection*

Since we found that the MLE procedure is not particularly stable, it appears to be important to select a high quality and statistically well-conditioned input data set. In deriving our data sets a number of aspects were considered. These are listed as follows:

- Spatial correlation in the data introduces local minima in solution space. Therefore input winds and σ^0s should be spatially decorrelated. We created data sets where the spatial separation was at least 300 km between one selected data point and the next.
- Ice and fractional ice were filtered by an SST filter; if the SST was below 6°C no data were extracted.
- The distribution of incidence angles covered is irregular because the fore and aft beams have a range of incidence angles only partly overlapping the mid beam incidence angle range. We used a filter to achieve a smooth distribution of incidence angles over all three beams.
- We also made a filter selecting beams in such a way as to achieve equal coverage for all three beams. If there were no relative biases between the three antennae this filter would be redundant.
- Steadiness: We used a filter selecting only those winds which were sufficiently steady over a certain time period. For each selected ERS-1 scatterometer node we compared the ECMWF guess field wind vector difference between the 3 and 6, and the 6 and 9 hour forecasts. The average of both vector

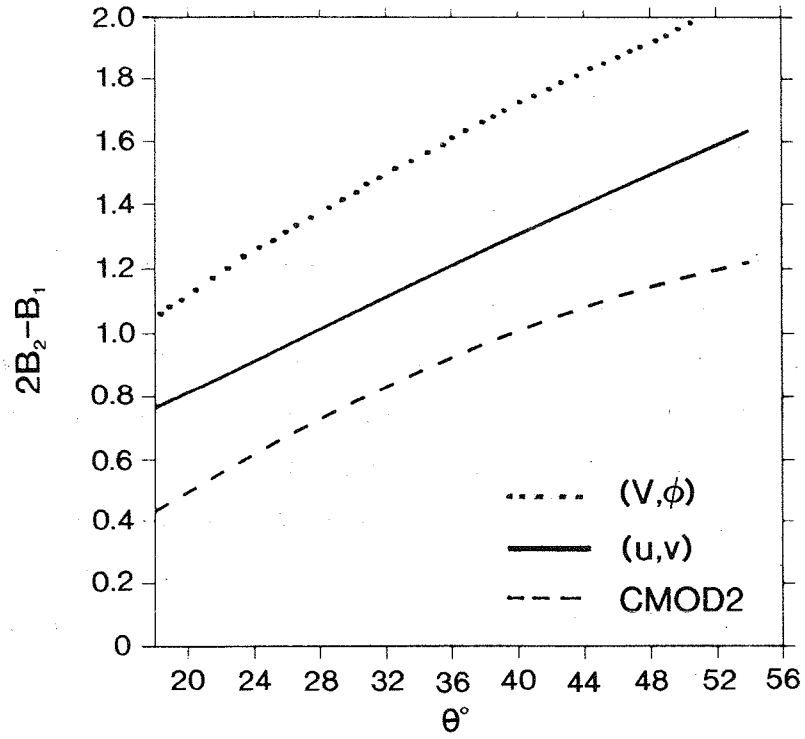

Fig 3.8 Upwind/crosswind amplitude as a function of incidence angle derived using speed and direction as input to the Britt-Luecke tuning algorithm (dotted) and wind components (solid) as input. The 'correct' solution is shown by the dashed curve. The wind speed is 10 m/s.

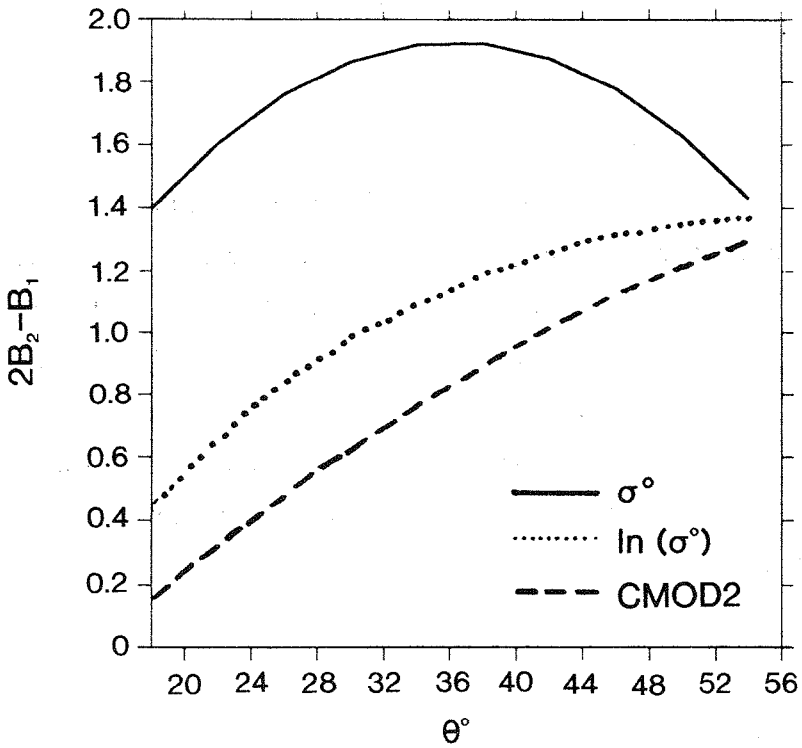

Fig 3.9 Upwind/crosswind amplitude as a function of incidence angle derived using σ^0 (solid) and $\ln\sigma^0$ (dotted). The wind speed is 5 m/s. Wind input to the tuning algorith is supplied in component form, not in terms of speed and direction. The correct solution is shown by the dashed curve.

differences was normalised by 5 m/s plus the average of wind speed over the three times considered. The normalisation is such that this steadiness filter excludes both high and low winds, if unsteady. The selection threshold was set to 0.2.

- The data were filtered to achieve a more uniform wind speed distribution than the usual Weibull distribution seen in nature. Although the wind direction PDF over the globe and several days varies by a factor of two with wind direction with respect to one particular beam, for all three beams together the variation is less than 10 %. Therefore after performing a limited number of tests, wind direction filtering was eventually not used.
- We also performed experiments with time filters. Normally ERS-1 observations differing up to three hours with the analysis time were selected. Bringing the time window down to two hours did not show any impact in our initial experiments using CMOD2. With hindsight we would recommend using FGAT rather than the analysis winds, in which case time filtering becomes redundant.
- The ECMWF analyses are believed to be more accurate in the Atlantic than for instance in the southern hemisphere. However, we did not see any statistical difference for surface wind speed verifications between those areas so we have not experimented with filtering different regions of the globe.
- If a reasonable transfer model already existed, then one could reject σ^0 data if the triplet of measurements had too large a distance to the transfer function solution surface in measurement space. This filter has to be used carefully since it could bias the MLE result towards the transfer function used for selection. The filter was not used in the results presented in this section, but a similar filter is used in the retrieval stage (see section 4).

3.3.3 *Estimation with real data*

In section 3.1, it was shown that all major terms of the transfer function CMOD2 needed revision. The formulation of CMOD2 contains 18 coefficients. The new formulation also contains 18 coefficients. Our experience with MLE for this problem is that more degrees of freedom lead to instability, although this depends on how well the transfer function formulation can potentially fit the data. Because of the non-linearities in the transfer function relationship, our feeling is that even a perfectly formulated function with too many degrees of freedom would show aberrations after estimation. Therefore the philosophy we adopted to develop a formulation, was to constrain the solution as much as possible using the diagnostics described in sections 3.1 and 3.2.

As discussed in section 3.3.2, the MLE software was adapted to work in logarithmic space for σ^0, and in the components of the wind. It is defined as

$$\mathrm{MLE_T} = \sum_{i=1}^{N} \left(\frac{10\log[\sigma_i^0/\sigma_{si}^0]}{0.2} \right)^2 + \frac{(u_i-u_{si})^2+(v_i-v_{si})^2}{(2.25)^2} \qquad (3.2)$$

where σ_i^0 is the measured value, σ_{si}^0 is $f(u_{si},v_{si})$, (u_i,v_i) are the wind components of the ECMWF model, (u_{si},v_{si}) are the estimated true wind components and f is the transfer function with 18 coefficients. The perceived noise in σ^0 is 0.2 dB, and the perceived noise in the wind components is 2.25 ms^{-1} (see section 3.2). N is the number of measurements σ_i^0 collocated with (u_i,v_i). Typically we used N ~ 20,000.

Several tests with slightly different transfer function formulations were carried out, resulting in different values for $\mathrm{MLE_T}/N$. The lowest value found was 1.4 corresponding to CMOD4. A noise formulation taking into account increased σ^0 noise for low wind speeds failed to give better results, probably as a result of the strong non-linearity in the transfer function for low wind speed.

The transfer function CMOD3 was tuned to ECMWF analyses, using data for the period November 1991. Subsequently, there was a further engineering correction to the beams carried out by ESA. The transfer function was therefore adjusted for that, using the bias calculation method as described in section 2, and CMOD4 produced. The B2 coefficient as found in section 3.1.1 is used in CMOD4 and replaces the tuned B2 coefficient. The revision does not result in a different performance of CMOD4. A revision of the B1 coefficient has not been tested, although the tuned and statistically retrieved values are close. A specification of CMOD4 is given in Appendix C.

3.3.4 *A postiori verification*

a) Validation in σ^0 space

A fundamental test of a newly derived transfer function is its ability to describe the cone's surface to within the measurement scatter. We therefore made several cross-sections of type (i), (ii) and (iii) for the transfer functions we computed. Measured σ^0 triplets and the transfer function CMOD4 are plotted together in Fig 3.2 for various cross-sections. It can be seen that, in general, CMOD4 fits the distribution of σ^0 triplets very well. Without exception we found a positive correlation between the fits in σ^0 space and $\mathrm{MLE_T}/N$ (as defined in Eqn 3.2) found as a result of the tuning. To have an objective score for the fit in σ^0 space, we compute for each measured triplet the distance to the cone's surface. This distance is normalised by the

scatter we estimate for this triplet (as derived in section 3.1.1). For CMOD4 the average of the squared normalised distance (defined as MLE in Eqn 4.1) versus node number, wind speed and wind direction is fairly constant. The squared normalised distance to the cone is on average 1.7. This verifies the good fit of CMOD4 to the cone's surface and the validity of our σ^0 noise estimates. For comparison the corresponding value for CMOD2 is 4.7. A perfect transfer function would ideally score 1.0.

The normalised distances can also be plotted on a geographical map, as shown in Fig 3.10a for CMOD4. Again, we can verify that most values are smaller than 2. Larger values occur within 100 to 150 km of intense fronts and low pressure centres, which could result from the sea state not being in equilibrium with the local wind, from rain effects or from variability in the wind on a scale smaller than the footprint. Spatial correlation of the normalised distances is evident which will translate into horizontally correlated errors in the retrieved winds. However, we expect the measurement noise to result in a wind error of only ~ 0.3 m/s, which is small compared to errors in the ECMWF model or other observational systems (typically 2 m/s). Therefore, we do not expect the correlation in normalised distances evident in Fig 3.10a to lead to a substantial correlation of wind errors. In Fig 3.10b the same plot is shown for CMOD2. In this case the picture is dominated by problems in the fit of CMOD2 to the cone's surface, since the distances are correlated with wind speed, wind direction and node number.

Having a function (CMOD4) that fits the general solution surface well, more detailed studies could be made to investigate geophysical parameters that may cause deviations from the two parameter model (e.g. wave parameters or rain). These parameters should then be correlated with the normalised distances, which could be investigated both qualitatively with figures like Fig 3.10, or quantitatively. We have shown above that effects from other geophysical parameters may be relevant for low wind speeds and incidence angles and in situations connected with high temporal wind variability.

In table 3.1 we compute departure statistics between winds retrieved from simulated values of σ^0 and "true" analysis winds. The simulation is done by computing values of σ^0 from the ECMWF analysis winds using CMOD4, perturbing them by the σ^0 scatter quantified in section 3.1.1 and then retrieving winds from the perturbed σ^0s using the retrieval scheme described later in section 4.1. From table 3.1, we observe that the scatter in σ^0 leads to small errors in the winds and accounts for only a small part of the total scatterometer wind error. (Comparisons between retrieved winds and analysis winds are shown later in table 3.3, where the vector RMS error is typically 6 times larger than that estimated to arise from scatter in σ^0 suggesting that the errors resulting from scatter in σ^0 contribute only ~ 3% of the wind vector variance.) Deviations from a two parameter transfer function will therefore generally not have a significant impact on the global quality of the scatterometer wind product, but may reveal local information on other geophysical processes.

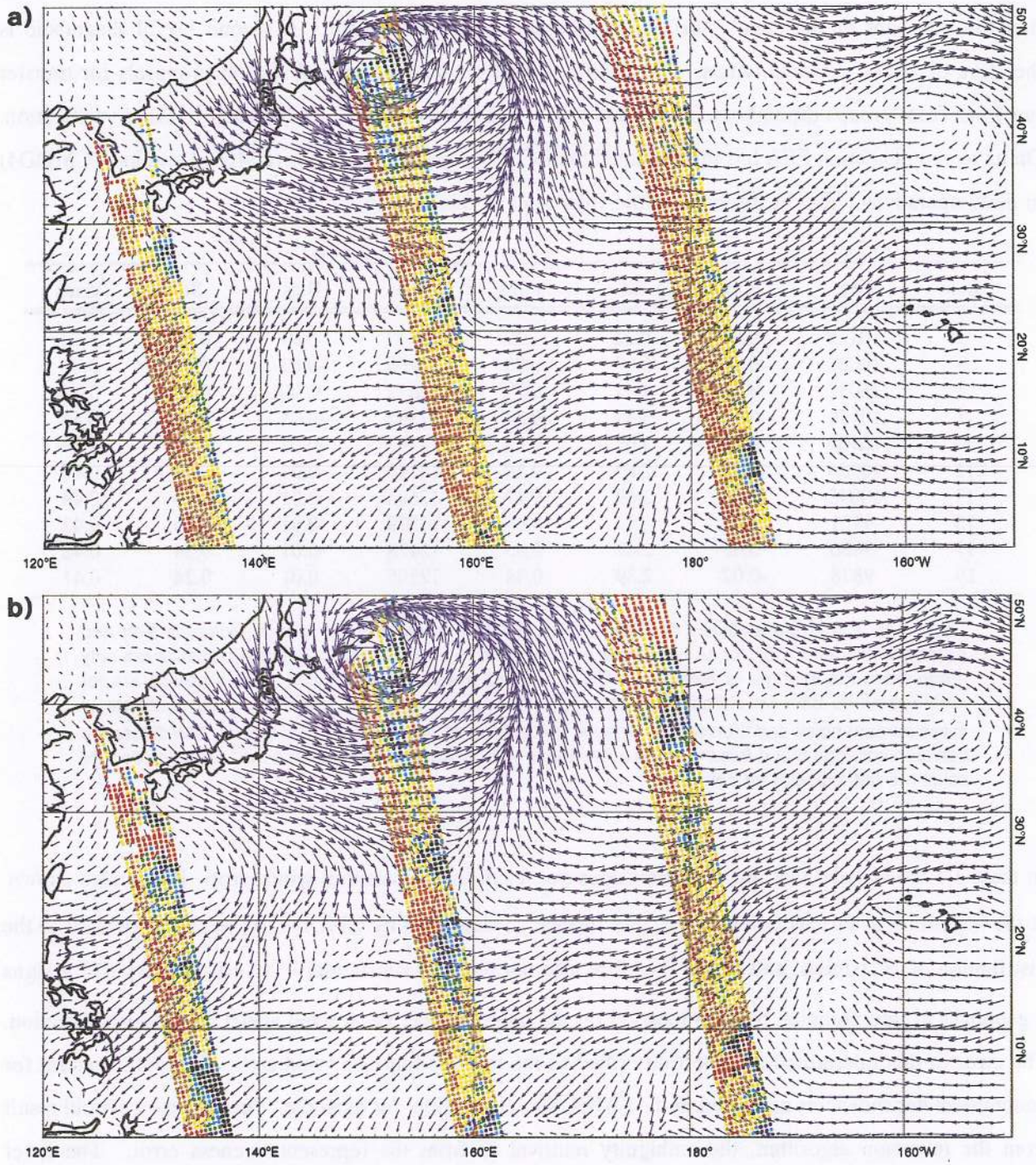

Fig 3.10 Spatial plot of the normalised distance to the cone surface defined in Eqn (4.1) for a) CMOD4 and b) CMOD2. Data are for 12UTC∓ 2 on 13 February 1994 and the ECMWF model first guess and wind vectors for 13 February 1994 12UTC. The colour coding is:

< 0.5 = red	1-1.5 = yellow	2-2.5 = light blue	> 3 = black
0.5-1 = brown	1.5-2 = green	2.5-3 = dark blue	

b) Validation against winds

In the above section we characterised the fit of CMOD4 to the distribution of σ^0 triplets in σ^0 space and showed that the associated error on retrieved winds was small. However, we will show that if the transfer function does not fit the cone's surface, **systematic** wind errors result. A second useful diagnostic is therefore to verify retrieved winds. ESA's ERS-1 analysis team compared several proposals for transfer functions from groups throughout Europe and a proposal from the USA, on the basis of wind verification. On its recommendation ESA has implemented the ECMWF transfer functions (CMOD3 and later CMOD4) in daily operations. This is discussed more fully later in this section.

Node	Nbr.	Bias	Sd	Vrms	Nbr.	Bias	Sd	Vrms
1	10128	-0.06	8.22	1.29	12317	-0.01	0.60	1.12
3	10032	0.10	5.89	0.95	12205	-0.01	0.47	0.89
5	10082	-0.01	4.92	0.79	12372	0.00	0.40	0.74
7	10139	0.10	3.37	0.57	12585	-0.01	0.30	0.54
9	10101	0.00	3.09	0.53	12597	-0.01	0.28	0.49
11	10085	-0.03	2.83	0.50	12590	-0.01	0.27	0.46
13	10045	0.00	2.69	0.47	12604	-0.01	0.26	0.44
15	9921	-0.01	2.54	0.45	12579	-0.01	0.24	0.42
17	9830	0.03	2.47	0.45	12478	-0.01	0.24	0.42
19	9878	-0.02	2.39	0.44	12505	0.01	0.24	0.41

Table 3.1: Departure statistics of ERS-1 minus ECMWF analysis wind speeds (columns 6-9) and directions (columns 2-5), for all odd nodes (numbered from inside swath). Direction statistics are only made when the average of ERS-1 and ECMWF wind speed exceeds 4 m/s. The statistics are for retrieved winds from simulated σ^0s. The ECMWF analysis σ^0s were distorted by our estimate of measurement noise and then winds retrieved and compared with the analysed winds. The difference between columns 5 and 9 is that wind collocations with average speed below 4 ms^{-1} are excluded for column 5 but included for column 9.

In table 3.1 we showed that the σ^0 scatter does not result in a substantial wind error. It was also shown, at the beginning of this section that the cone surface, as described by CMOD4, represents a good fit to the distribution of σ^0 triplets, and would therefore also not result in substantial wind errors. CMOD4 assigns a geophysical interpretation to each location on the cone surface, i.e. a wind speed and a wind direction. The error in this interpretation is best described as the transfer function wind error. It would account for geophysical dependencies neglected in the CMOD4 interpretation, for example. Further errors would result from the inversion algorithm, the ambiguity removal or from the representativeness error. The latter accounts for the mismatch in spatial and temporal scales between the observations and the Numerical Weather Prediction (NWP) model.

A statistical comparison between the ERS-1 wind speed retrieved using CMOD4 and FGAT is shown in Fig 3.11a for node 11 for a 3 day period. A similar comparison for the wind component along the mid beam and wind direction are given in 3.11b and c respectively. These figures illustrate the good fit between

ECMWF model and scatterometer retrieved winds. For comparison, the corresponding plots for CMOD2 are shown in Fig 3.12. An erroneous transfer function not only distorts the speed distribution (panels a), but also the angular distribution (panels c) giving rise to the S-shaped distribution for the wind component along the mid beam seen in panel (b) of Fig 3.12. (The same retrieval procedure, discussed in section 4.1, was used to derive the winds in both Figs 3.11 and 3.12.) We further note that the ECMWF and CMOD4 direction distributions are not uniform due to the sampling of the trades and the westerlies in the extratropics. Differences between the two PDFs arise because of errors in both ECMWF and CMOD4 inverted wind directions. The statistical problems, evident for CMOD2, can be easily verified by inspection of the fit of CMOD2 to σ^0 triplets in σ^0 space, again illustrating the importance of the transfer function visualisation discussed in section 3.3.4a (see e.g. Figs 3.2a, b, and c).

For comparison with Figs 3.11 and 3.12, histograms of collocations of automatic and non-automatic SHIP winds (i.e. reports from buoys and platforms which are described as (non-)automatic SHIP in the WMO coding conventions) and FGAT winds for the East-West component of the wind were made. These results are summarised in table 3.2. These departure statistics incorporate not only instrument and representativeness error, but also the ECMWF model error, including an error due to the extrapolation from the lowest model level (~ 30 m) to 10 m height - the nominal height of ship winds. Table 3.2 shows that there is a difference in quality of non-automatic and automatic SHIP measurements. We made similar statistics for other data sets operationally available on the Global Telecommunication System (GTS), i.e. moored and drifting buoys and automatic and non-automatic island stations, which again show differences. There may be several reasons for these, such as different distributions of the observational data across the globe, a difference of quality in the observational systems and no, or insufficient, height correction (WMO requires a measurement to be reported at 10 m height).

	Std dev	Correlation	Bias
(a)	3.5	0.93	1.41
(b)	2.8	0.95	0.73
(c)	2.2	0.97	-0.2

Table 3.2 The standard deviation and correlation of the wind component departures, and the mean wind speed departure for (a) non automatic ship, (b) automatic ship and (c) scatterometer data compared to FGAT. SHIP data are for March 1993, mainly in the northern hemisphere, and scatterometer data are global for the period 18 March 1993 to 28 March 1993. The scatterometer statistics are for node 11, for the wind component along the mid beam.

In table 3.2, we also give statistics for retrieved scatterometer winds compared to FGAT for node 11 for the wind component along the mid beam. Table 3.2 shows that the highest correlations with the NWP model are for the scatterometer (97%). This indicates that the scatterometer winds are more accurate than any other operationally available surface wind data set.

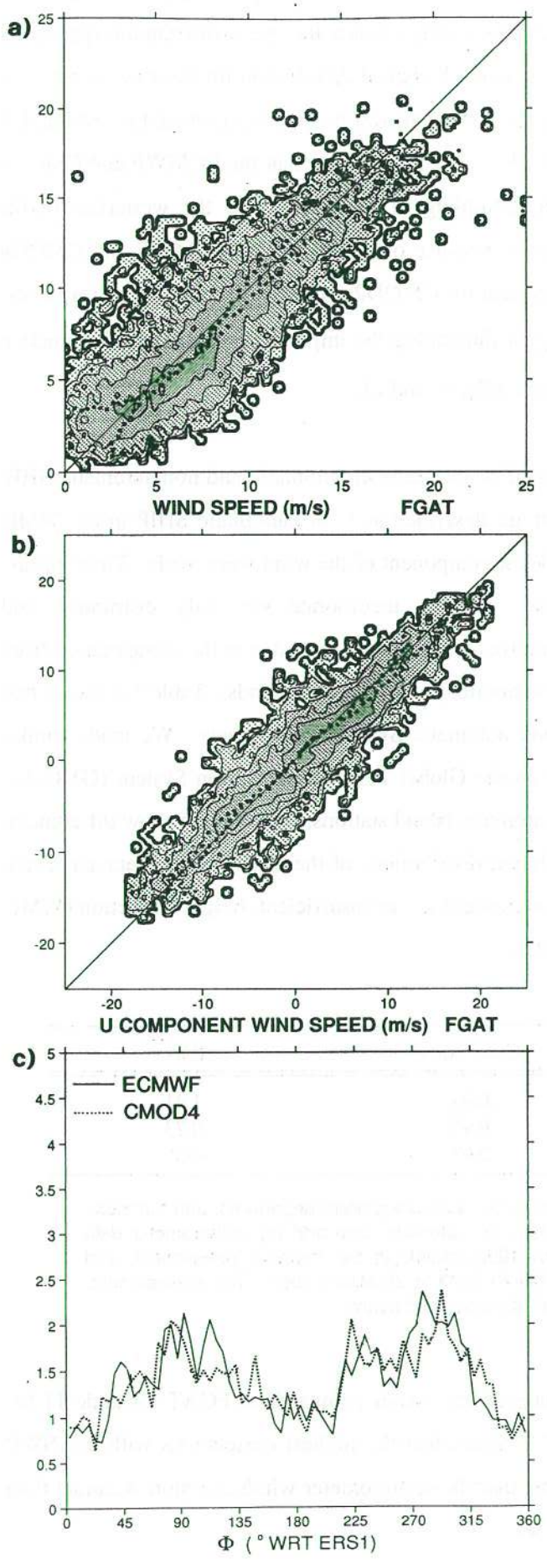

Fig 3.11 a) Retrieved speed versus FGAT speed
b) Component of retrieved speed along the mid beam versus the corresponding FGAT component
c) Distribution of wind direction measured relative to the satellite direction for ECMWF (solid) and retrieved directions (dotted).
The transfer function CMOD4 was used, together with the inversion scheme described in section 4.1. Data are over the 3 day period 13 February to 15 February 1994 for node 11. Panels a and b show a good speed agreement between CMOD4 and ECMWF from 5 to 15 m/s. Above 15 m/s, it is difficult to reach a conclusion. Panel c shows that the angular distributions are also similar.

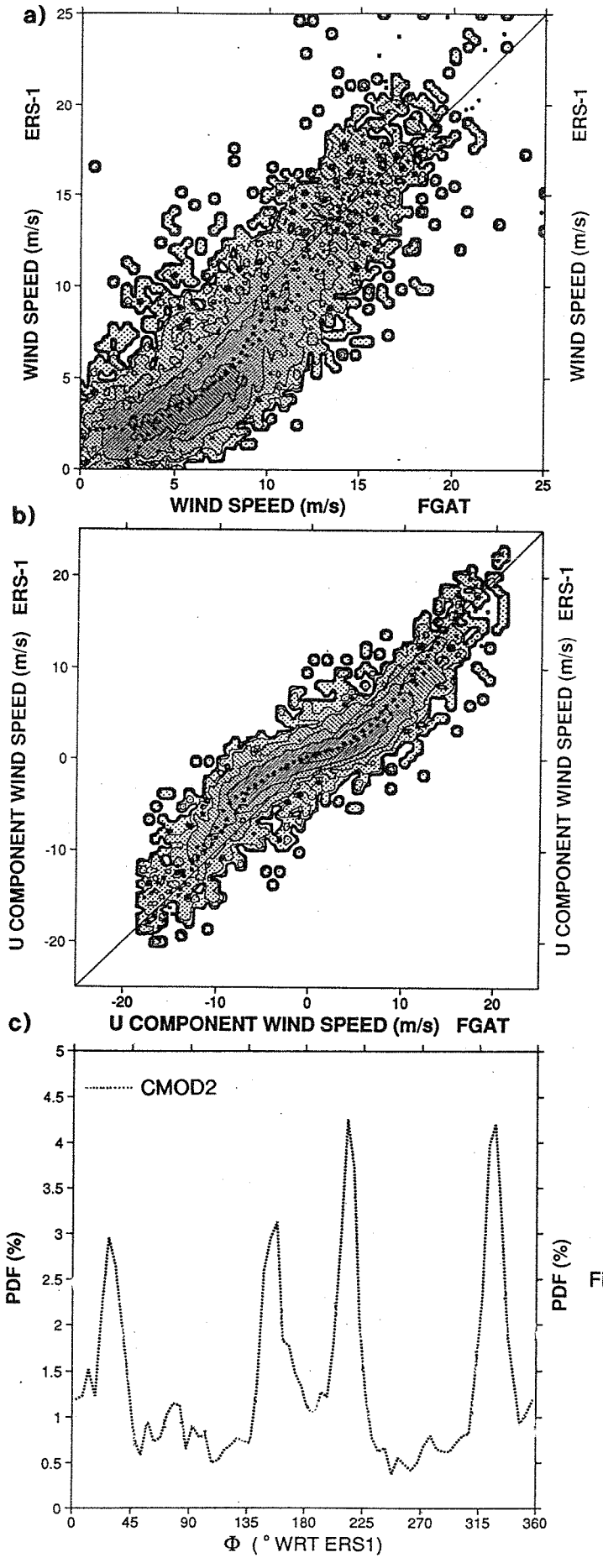

Fig 3.12 As for Fig 3.11 but for CMOD2. Panel (a) shows that there is now a speed bias at medium speeds with scatterometer speeds lower than the analysis. For high speeds, the scatterometer is biased high. This speed bias is associated with a peculiar angular distribution (panel c)), with certain directions being preferred. Panel (b) shows an S shape kink in the distribution, consistent with the problems in speed and direction.

Table 3.3 shows more detailed departure statistics of scatterometer minus ECMWF forecast winds, separately for wind speed and direction, for each odd across-swath node. The error, due to the smaller scale of representativeness of scatterometer data in comparison with the NWP model, should not vary with node number. The ECMWF model error contribution should also be the same for all nodes. However, there is a node-to-node variation in the statistics, suggesting that the scatterometer observation error contribution is now negligible for at least some nodes.

Node	Nbr.	Bias	Sd	Vrms	Nbr.	Bias	Sd	Vrms
1	9168	0.88	23.81	3.73	10883	-0.48	1.93	3.54
3	9511	0.92	21.13	3.37	11008	-0.41	1.94	3.24
5	9717	1.26	19.89	3.21	11199	-0.30	1.96	3.10
7	9783	1.46	19.17	3.16	11355	-0.28	1.97	3.05
9	9794	1.10	19.07	3.17	11472	-0.26	1.99	3.05
11	9762	1.42	18.86	3.15	11480	-0.24	1.98	3.02
13	9700	1.48	18.69	3.15	11526	-0.25	2.00	3.01
15	9656	1.29	18.71	3.15	11545	-0.25	2.05	3.02
17	9638	1.11	18.31	3.14	11564	-0.24	2.07	3.00
19	9677	0.98	18.36	3.11	11616	-0.24	2.04	2.98

Table 3.3 Departure statistics of ERS-1 minus ECMWF analysis wind speeds (columns 6-9) and directions (columns 2-5), for all odd nodes (numbered from inside swath). Direction statistics are only made when the average wind speed exceeds 4 m/s.

We can see that the departure standard deviation for wind speed increases with increasing node number, whereas for wind direction it decreases. The departure vector RMS decreases with increasing node number, indicating that the overall error of the scatterometer system is smallest at far swath. The advanced scatterometer system (ASCAT) will therefore have its swath moved to higher incidence angles.

	CMOD2	ESTEC	IFREMER	CMOD4	OREGON
Number of observations	14529	21278	21298	21298	21218
Speed bias (ms^{-1})	0.45	-0.38	0.53	0.06	0.72
Speed SD (ms^{-1})	2.20	1.93	1.71	1.65	2.21
Direction bias (deg)	0.94	0.88	-0.15	0.76	0.31
Direction SD (deg)	18.96	17.37	17.56	16.69	19.98
Vector RMS (ms^{-1})	4.28	3.25	3.36	3.18	3.60
Figure of merit	0.868	1.081	1.088	1.146	0.949

Table 3.4 Comparison between various transfer functions and RENE-91 campaign data. The transfer function labelled ESTEC is tuned on RENE-91 data, IFREMER is tuned on NOAA buoy data, OREGON is based on NMC and ECMWF analyses. The figure of merit is an attempt to measure the average performance of a transfer function. Higher values indicate a better performance.

CMOD4 was independently tested against Haltenbanken (RENE-91 campaign) data and UK Met Office analyses and compared with other transfer functions (*Offiler*, 1992). A summary of the fit to the Haltenbanken data is given in Table 3.4. This table shows that CMOD4 has the lowest speed bias, the

lowest standard deviation on speed and direction and, most importantly, the lowest vector RMS of all the models tested.

c) The difficulty in the interpretation of σ^o departures

A map of departures between measured and simulated σ^o s, using the ECMWF analysis and CMOD2 was shown in figure 2.1a. In Fig 2.1b the same plot is shown, but for CMOD4. We can see that although the average size of the departures has decreased, there are still values in excess of 10 dB. When Fig 2.1a was discussed, we noted the difficulty of interpretation of the departures. Now that we have a fair knowledge of all errors contributing to the departures, we could try to explain them. The scatter of triplets around the cone surface and the inaccuracy in the position of the cone surface as defined by CMOD4 amount to errors of ~0.3 dB, and as argued before, are not substantial (~ 3%) compared to the total wind error variance (see 3.3.4a). The interpretation of a σ^o triplet as a wind vector by CMOD4, the representativeness error, and the errors in the ECMWF analysis give a standard deviation of the departure wind speed of ~2.0 m/s and of ~19° for wind direction (Table 3.3). Given the fact that the upwind/crosswind amplitude goes up to values of 0.6, we find that a wind direction departure of 90° may amount to a 6 dB difference, and the more likely 20° departure to around 2 dB. Because of the harmonic dependency of σ^o on wind direction, a wind direction departure of 90° can also result in no difference. Equally, because of the non-linear dependency of σ^o on wind speed, a 4 m/s departure at a low wind speed could easily give a 10 dB error, while at a higher wind speed it would only result in ~ 0.5 dB. The spatial correlation in the σ^o departures in Fig 2.1b is most probably caused by the known coherence of wind error in the ECMWF analysis. Given these considerations the order of magnitude and structure of the departures in Fig 2.1b can be explained.

The statistics of wind errors are best defined in the components of the wind (see section 3.2). Because of the non-linearity, a relatively symmetric error distribution in the components (e.g. a normal distribution with a width of 2 m/s) around a hypothetical true state corresponds to "biased" and skew error distributions in σ^0. Therefore a low σ^0 departure bias and variance is not a good criterion for judging the quality of a transfer function. Furthermore, the non-linearity is wind speed and direction dependent, which makes a more correct interpretation of the σ^0 departures and computed average departure biases and variances rather complicated, and could in fact easily lead to a wrong interpretation of the quality of a transfer function.

3.3.5 *Simulation of the effect of noise on the validation*

Biases in wind speed are not necessarily caused by an offset in the level of measurent of one system with respect to the other, but may also result from different levels of noise in the systems. In this section we will illustrate this with a simulation experiment.

In table 3.4 we can see that no wind speed bias is present between CMOD4 and the RENE-91 data. But, compared to ECMWF FGAT (also compared to the analysis and FG) a bias of approximately - 0.3 m/s can be noted (table 3.3). Automatic and non-automatic SHIP data on the other hand have considerably larger biases of 0.73 and 1.43 m/s respectively. We simulated the effect of accuracy of a wind observing system on the wind speed bias, computed when compared against a reference observing system. The dotted line in Fig 3.13 shows a scatterometer wind speed probability density function (PDF) which was taken as a reference ("truth"). The scatterometer winds constituting the PDF were distorted by a random Gaussian noise with zero mean and a standard deviation of 2.25 m/s in the components of the wind. As a result the peak in the PDF, represented by the solid line, is shifted, and a wind speed bias of 0.5 m/s is created in the noisy system with respect to the reference system. The dashed line in Fig 3.13 shows the real ECMWF PDF. The resemblence of the dashed and dotted lines is remarkable. Also, the positive biases of SHIP wind speed with respect to ECMWF winds (see Table 3.2) are largely determined by the quality of the SHIP data. CMOD4 was derived from ECMWF winds, and given the above, may be considered to have the same wind speed strength scaling. A further validation of this scaling should be done taking into account the quality and representativeness of the wind observing systems used.

3.3.6 *Wind error correlation*

A σ^0 measurement is representative of an area with 50 km diameter (footprint), and therefore neighbouring measurements in the swath (at 25 km) are dependent. It is relevant to observe the wind vector variance of the departure between scatterometer wind and ECMWF model wind for a different spatial representativeness of scatterometer data. Therefore, a fixed set of scatterometer data was averaged over respectively 1, 9, 25, 49, and 81 nodes before comparing to the ECMWF model. The scatterometer wind error vector variance versus the spatial representativeness scale ("resolution") is plotted in Fig 3.14. For increasing horizontal scale the error variance decreases.

Using a wind component energy density spectrum $E = 0.0012\ (2\pi/\lambda)^{-5/3}$, with E in [m^3s^{-2}] and λ the wavelength in [m], the reduction in wind vector variance was computed by integration of E from $k_B = 2\pi/\lambda_B$ to $k_E = 2\pi/50.000$ m^{-1} and multiplication of the result by 2. λ_B is the resolution at which the comparison is done. The result plus a fixed offset is given by the dashed line in Fig 3.14. The energy density spectrum was made comparable to the range of tropospheric spectra as found by *Lilley and Petersen* (1983) and the UK Met Office (*Lorenc et al*, 1991), but decreased to 75% to account for the smaller variability close to the surface (see Fig 3.15). The spectra of Lilley and Petersen show a variance of 25% around the mean spectrum. The effect of this spread on the variance reduction in Fig 3.14 is given by the error bar on the right. The computed reduction in variance (dashed) corresponds remarkably well with the observed reduction in vector RMS error after averaging (solid).

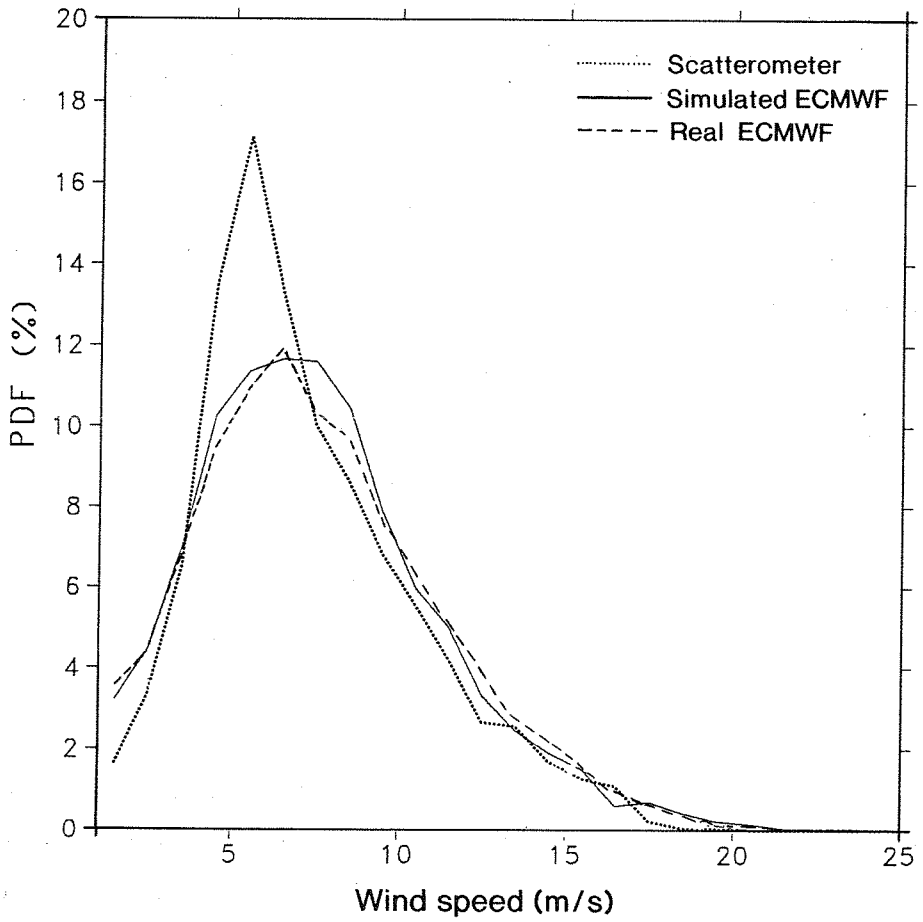

Fig 3.13 Probability density function of scatterometer winds (dotted) and simulated ECMWF model winds (solid). The latter was obtained from the former by adding a Gaussian wind component error of 2.25 m/s. The dashed line corresponds to the real ECMWF PDF.

The horizontal diffusion of momentum in the ECMWF model is very effective on scales smaller than λ = 300 km, and therefore it is expected that the ECMWF model cannot resolve much of the variability we removed by averaging scatterometer winds. In Fig 3.14 this is verified by the fact that the solid line has the same slope as the dashed line for high λ. The scale of representativeness of the model is therefore ~300 km, and quite far from the equivalent spatial resolution of ~125 km expected from a T213 spectral truncation. This means that the model will underestimate extreme wind speeds, and because the scatterometer was tuned on the ECMWF wind speeds it may also underestimate high wind speeds.

The 25 km grid sampling and the 50 km footprint cause horizontal error correlation between directly neighbouring scatterometer nodes. If the scatterometer winds had spatially strongly correlated error beyond 50 km we would expect from Fig 3.14 that at low λ the reduction in variance would be less than that explained by a $(2\pi/\lambda)^{-5/3}$ spectrum (a flat spectral response is expected in this case). We do not see significant signs of this and may conclude that the horizontal error correlation in scatterometer winds is in general not significant, which indicates that a transfer function dependency on other spatially structured geophysical parameters than wind (e.g. wave effects) is in general not likely to be substantial. It is clear that the sensitivity of the scatterometer to the wind vector is the main effect. Other geophysical parameters should, however, be investigated for correlation with the remaining departure errors in the more extreme or local conditions.

Global observation-minus-analysis departure statistics provide a good general characterisation of observation measurement error, but fail to give a complete picture of the usefulness of data. Numerous relevant and complicated synoptic weather patterns were investigated in order to gain experience in dealing with the data. In section 5 we will show some examples, used to illustrate the ambiguity removal problem.

3.3.7 *Implications of the transfer function change for inversion and ambiguity removal*

The cross-section in Fig 3.2 shows the angular variation of the transfer function, and also shows the upwind/downwind differences. The separation of the two leaves of the transfer function are closer in Fig 3.2 for CMOD4 than for CMOD2, which has implications for ambiguity removal. If these two curves were well separated then one would have a good chance of distinguishing between the two possible wind directions, on the basis of the σ^o measurements alone (i.e. 'autonomous' ambiguity removal could be satisfactory). On the other hand, if the two leaves are very close to each other, then there is no possibility of doing so. In general the leaves are rather close in CMOD4. Autonomous ambiguity removal is therefore not very likely to succeed. Furthermore, spatial correlation in the distance of measured σ^0 triplets to the cone surface (see Fig 3.10) will complicate the use of any upwind/downwind difference that exists.

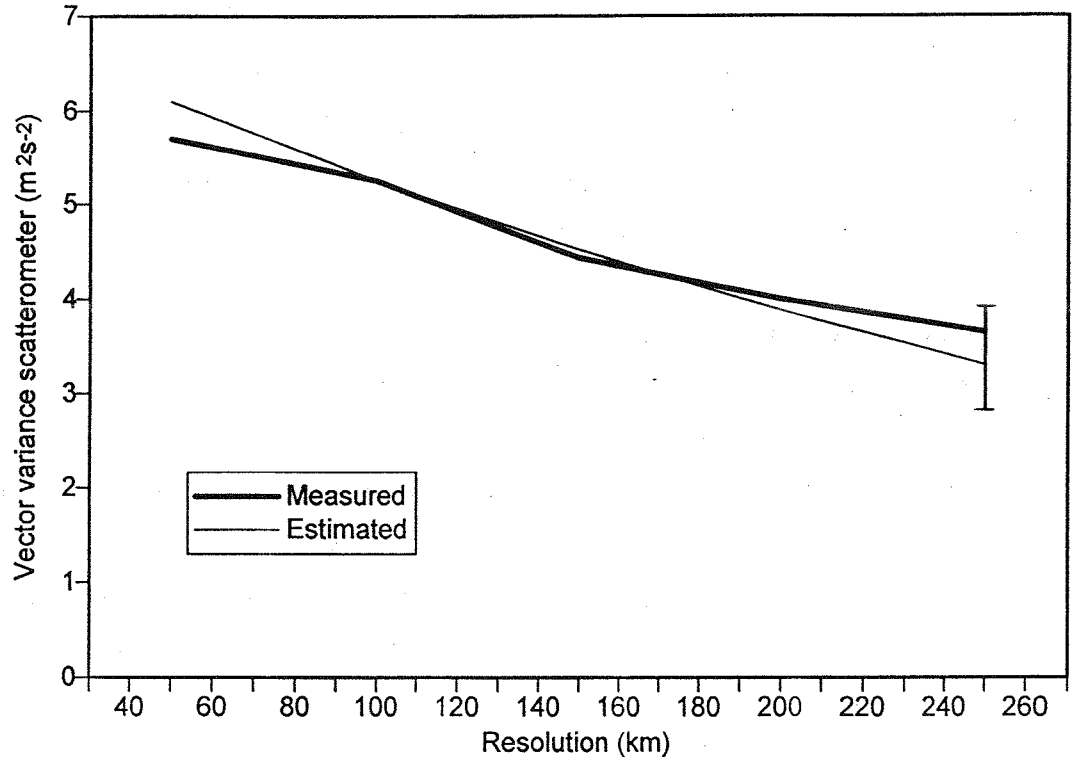

Fig 3.14 Wind vector error variance of processed scatterometer data at a fixed set of scatterometer nodes. The processing involved averaging over a square box containing 1, 9, 25, 49, or 81 nodes. The spatial scale of representativeness ("resolution") corresponds to respectively 50, 100, 150, 200 and 250 km (horizontal axis). The wind vector error variance of the ECMWF model (FGAT) was estimated to be 5 m^2s^{-2}. The thin line indicates the reduction in variance by integration of a wind spectrum (see text). The error bar indicates the spread, due to the natural variability of wind spectra (25%).

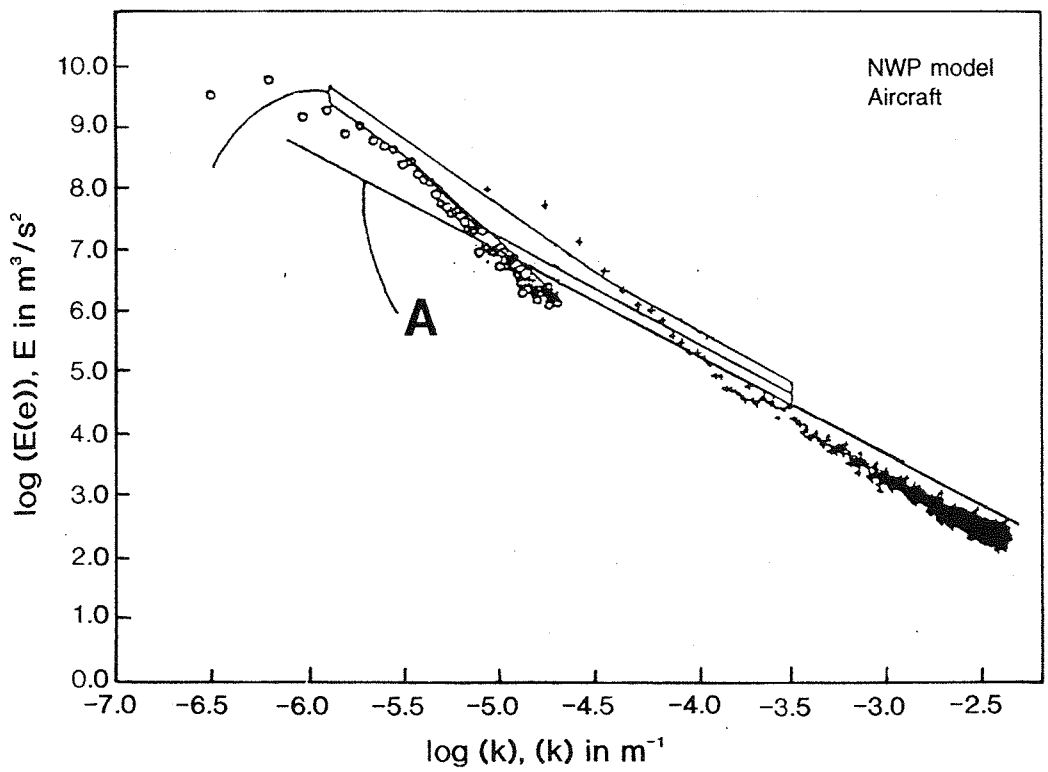

Fig 3.15 Assumed wind spectrum at 10 m height (labelled A), and wind spectra as measured by *Lilley and Petersen* (1983) (solid lines), by UK aircraft MRF (+) and the UK Met Office cyber model (0) for the free troposphere (figure adapted from *Lorenc et al*, 1991).

For nodes close to the inside edge of the swath, the extent to which the surface is well defined decreases. For node 1, noise is proportionately larger, relative to the upwind crosswind separation, than for other nodes, which implies less wind direction accuracy after inversion (see table 3.1) and therefore less skill at ambiguity removal stage. However, even for node 1, some directional skill is present except at low speeds (< 6 m/s). For node 19, the separation is favourable.

3.4 High speed comparisons

In deriving the transfer function, a uniform distribution of speed and direction was used as far as possible. Even so, winds above 15 m/s were undersampled and winds above 18 m/s were hardly present. It is therefore of interest to compare retrieved and FGAT winds in a high wind speed situation as, for example, the Braer storm at 00Z on 11 January 1993 shown in Fig 3.16. Panel (a) shows the retrieved winds and panel (b) the FGAT winds. (The retrieved winds were obtained from a procedure known as PRESCAT, described fully in sections 4 and 5.) High wind speeds are more prevalent in the FGAT than in the scatterometer retrieved winds. Nonetheless the scatterometer records speeds up to 20 m/s indicating that it has apparently not saturated up to this speed.

Another time of strong winds was the 'super-storm' which hit the east coast of the US on 14 March 1993. Fig 3.17 shows the comparison between model and scatterometer for 6Z, and again the FGAT shows higher speeds. Whether this results from a problem with CMOD4 or the analysis is unclear. Finally Fig 3.18 for 24 May 1993, 18UTC shows one example of several when scatterometer speeds up to 22 m/s are retrieved, suggesting that the scatterometer is able to detect high speeds. The retrieved speed is, however, an extrapolation from the range of validity (4-18 m/s) of CMOD4. It is therefore not surprising that we find that the average normalised distance (see section 4.2, Eqn (4.1)) is increased to values around 3 for these speeds. It is possible that the sensitivity of the transfer function decreases at higher speeds and therefore the retrieved wind speeds are noisier. However, these issues have not been explored, and are difficult to quantify firstly because other observing systems, such as SHIPs are also noisy, and the number of collocations few, and secondly because the errors in FGAT are also unknown at high speed. However, sufficient data are probably now available to allow further progress in assessing error and modifying CMOD4 if warranted. Furthermore, wave observations may help in the assessment.

3.5 Summary

In 3D σ^0 space the measured σ^0 triplets closely define a cone-type surface at each node. σ^0 scatter perpendicular to this surface is close to measurement noise specification (~5%), except at low wind speeds and at the inside swath. In general, therefore, a two parameter transfer function is sufficient to describe the σ^0 triplets. In the cases where the scatter exceeds measurement noise, the deviation from the cone's surface

may be correlated to more geophysical parameters. Such a correlation would not have a substantial effect on the global quality of the scatterometer wind product.

Problems with the transfer function formulation of CMOD2 can easily be identified in the 3D σ^0 space. New transfer functions have been derived, diagnosed and implemented (CMOD3 and CMOD4), which describe the relationship between σ^0 and the 10m wind vector considerably better than CMOD2 did. To this end, a MLE procedure (Eqn 3.1) has been posed using the components of the wind and $\ln(\sigma^0)$ as inputs. Several filters were used to prepare well-sampled input data sets.

The validation of a transfer function by the interpretation of σ^0 departures was shown to be rather complicated, but a validation of the fit of the transfer function cone surface to measured σ^0 triplets in 3D σ^0 space is a very sensitive test regarding the quality of a transfer function. Further validation of retrieved scatterometer winds results in a complete characterisation of the errors in the scatterometer wind product.

The cone surface defined by CMOD4 is shown to fit the σ^0 triplets well, relative to the scatter of these triplets. Departure statistics of scatterometer minus ECMWF model winds were used to further determine the quality of CMOD4. It was found that the retrieved scatterometer winds are superior to conventional surface wind data, and that the horizontal wind error correlation for scatterometer data is not substantial. The departure vector RMS error is lowest for low wind speeds, and increases slightly with increasing wind speed. The σ^0-to-wind speed relationship may be refined by taking into account the different quality and representativeness of scatterometer and conventional data, as well as of the ECMWF model.

There is no immediate evidence of saturation at high wind speeds as speeds up to 22 m/s are retrieved and seem reasonable, although there is a suggestion that the perceived noise, as measured by distance from the transfer function cone surface is higher at higher speed. This reduced accuracy in the transfer function could be a general misfit to the "true" cone surface or a reduced validity of the two parameter transfer function. Sufficient data have probably been gathered by now to explore these issues further. Although the general quality of the winds is very good, there may be a correlation of wind departure errors with other geophysical parameters (e.g. stability, waves, rain) in specific cases.

The 3D σ^0 space visualisation introduced in this chapter is extremely useful in considering the wind inversion problem, discussed in the next section.

a)

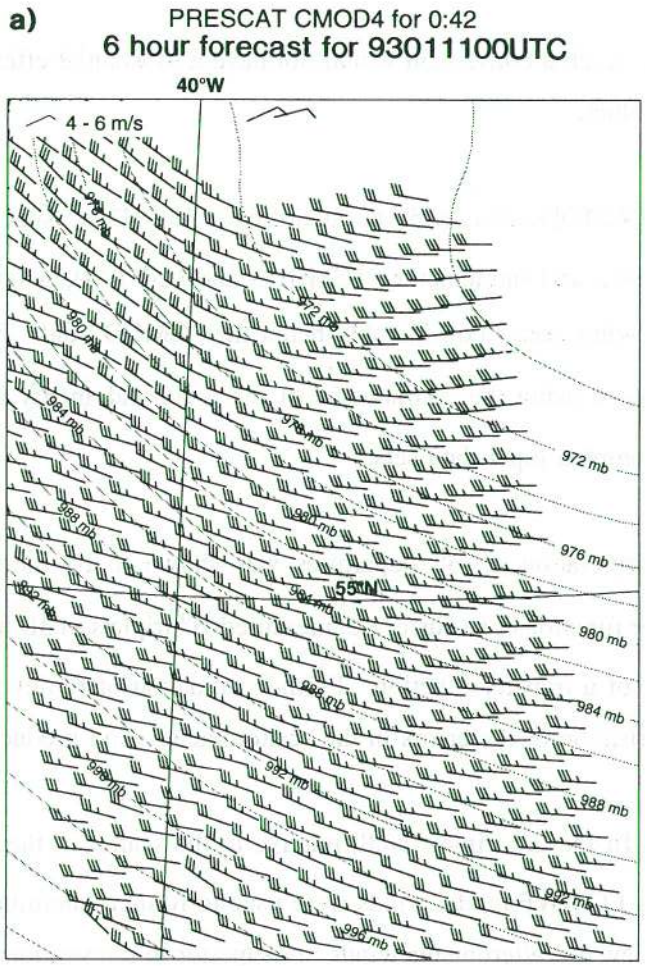

b)

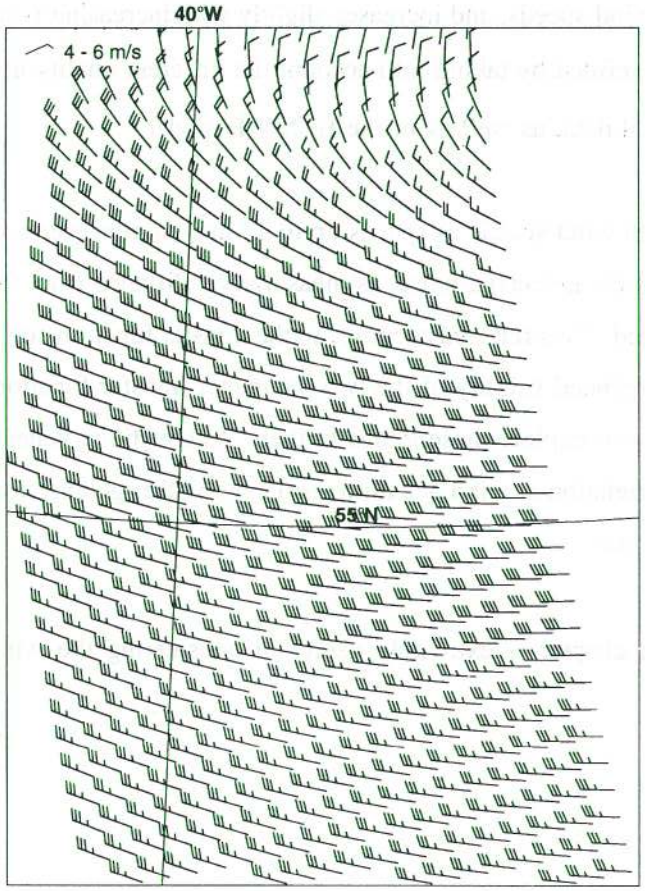

Fig 3.16 (a) PRESCAT winds to the south of Greenland at 00 UTC on 11 January 1993 showing speeds up to 20 m/s. The FGAT winds (b) are slightly higher, up to 22 ms^{-1}. One full flech indicates 10 knots and a triangle 50 knots. FG surface pressure is plotted in (a).

a)

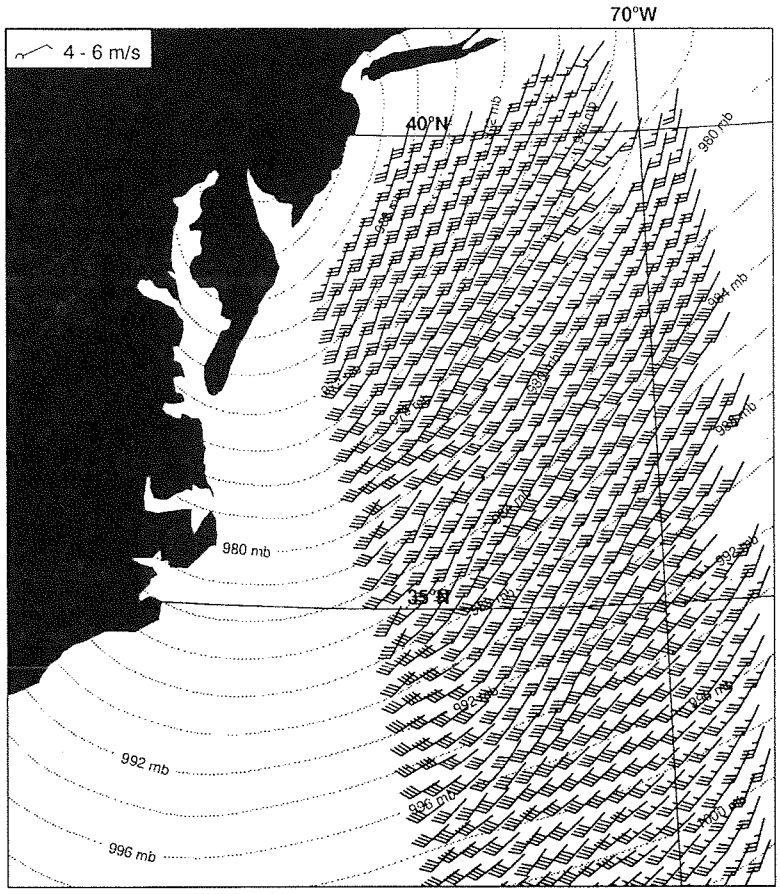

FGAT winds

b)

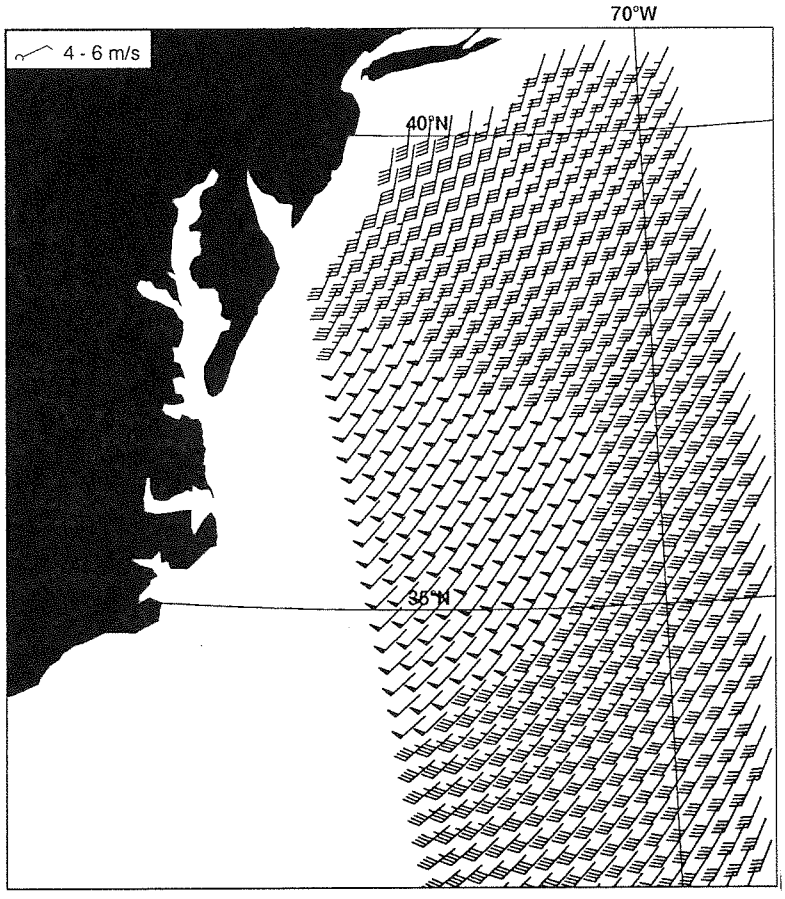

Fig 3.17 As for Fig 3.16, but for the storm which hit the east coast of the US on 14 March 1993.

a)

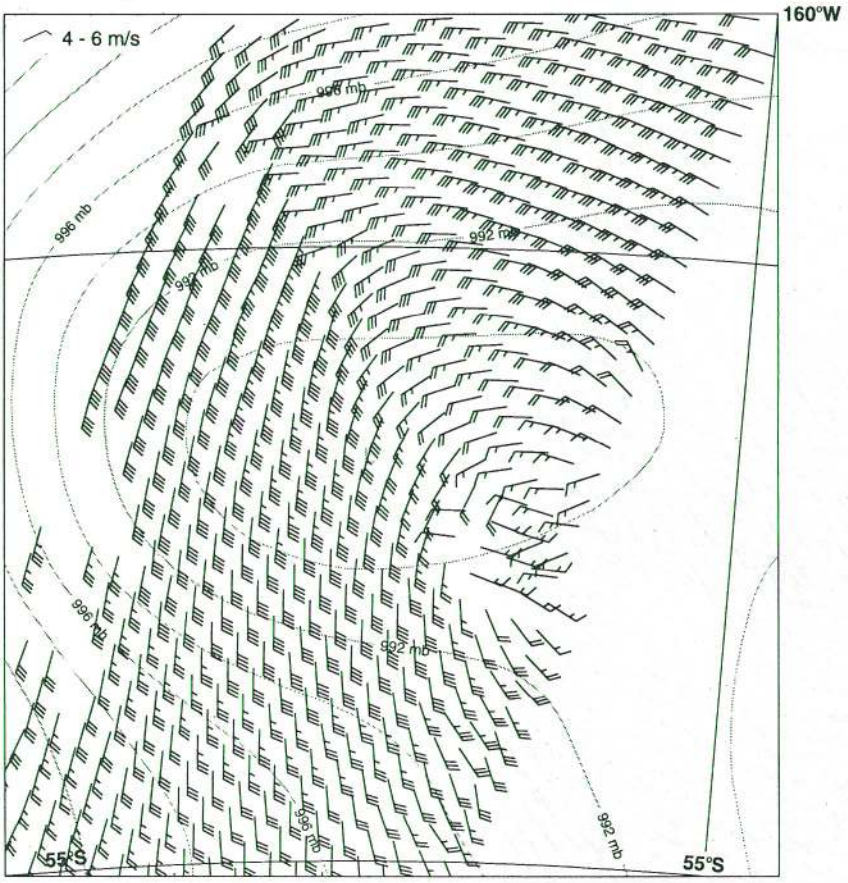

b)

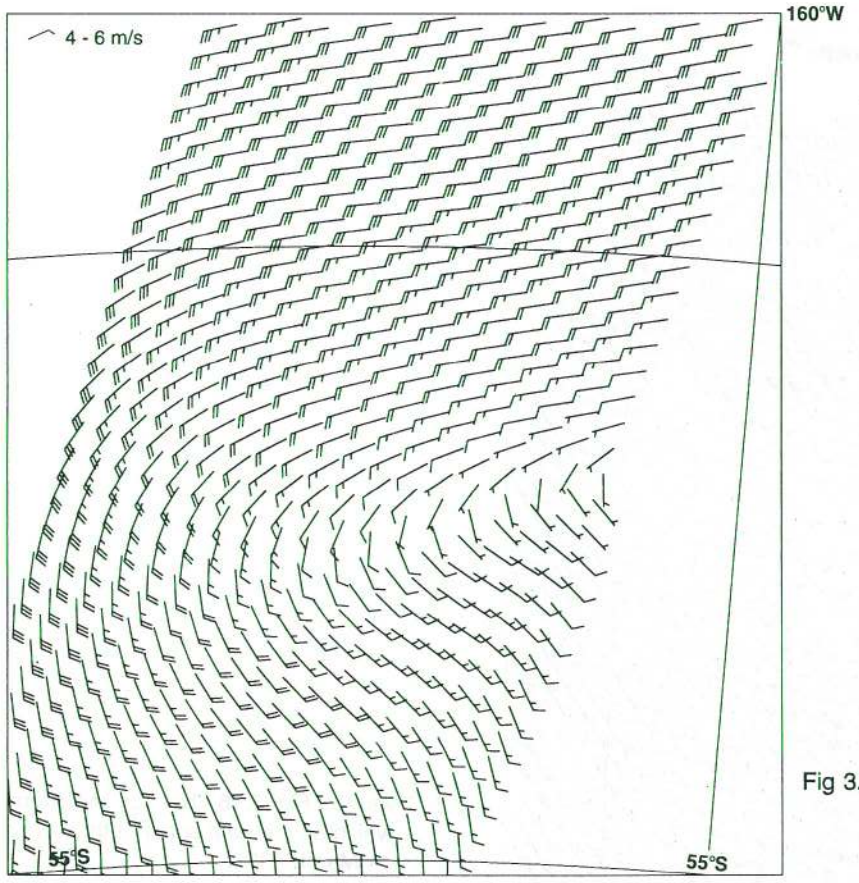

Fig 3.18 As for Fig 3.16 but for 18 UTC on 24 May 1993. PRESCAT shows speeds up to 22 m/s but FGAT winds are much weaker.

4. INVERSION

4.1 Normalisation and transformation of the MLE

A version of the CREO software was implemented and used from August 1991. Initially CMOD2 was used in the retrieval. As the transfer function improved, more attention was paid to the characteristics of the retrieved winds. An early finding was that the directional distribution of retrieved winds was not the same as that of the ECMWF winds. This does not of itself imply the retrieved winds are wrong: it could be that the ECMWF winds are wrong. However, the distribution of retrieved winds showed minima roughly every 90° (Fig 4.1a, dotted curve), which indicates that there is a problem with the retrieved directions (all directions are relative to the direction of the sub-satellite track). A similar feature had been noted for SASS data from SEASAT (*Anderson et al*, 1991) but no explanation was offered.

We investigated this problem and found it was related to the way distances in 3D σ^0 space were measured in the MLE of Eqn (1.4). To find possible solutions, minima in the MLE are sought by varying trial values of wind speed and direction. The normalisation used in the MLE changes the measure of distance in 3D σ^0 space. CREO uses normalisation by trial solution. Other possibilities were to use normalisation with the measurement, or to use constant normalisation. The MLE estimator generally has two local wind minima when constant normalisation is used and generally four, but sometimes up to six when normalisation by solution is used. (See *Graham et al*, 1989). It is desirable that the function being minimised should have as few local minima as possible. The two primary minima, corresponding to the two most likely solutions are approximately 180° different in direction but differ for different normalisations. The occurrence and location of the other minima depend much more strongly on the normalisation, making one doubt their validity. Normalisation can be loosely thought of as a distortion of the space shown in Fig 3.1.

We investigated the effect of normalisation through visualisation of differently scaled 3D measurement spaces. Fig 4.2 shows cross-sections for which $\sigma_1^0 + \sigma_3^0$ are constant. Panel (a) shows no normalisation, and panel (b) shows a scaling of each axis with the σ_i^0 value at the centre of gravity of the plot. The latter scaling visualises approximately the space used to compute a distance, for a normalisation of Eqn (1.4) by either $SD(\sigma_{Oi}^0)$ or $SD(\sigma_{Si}^0)$. In order to be able to obtain accurate wind directions and a realistic wind direction probability density function (PDF) after inversion, it is desirable that equal portions of the σ^0 triplets are thrown onto equal wind direction intervals. This is the case if the solution surface has no sharp curvature and is circular rather than elliptic. Normalisation by solution or measured σ^0 looks unfavourable for achieving this goal, whilst no normalisation appears favourable. Furthermore, the effects of a misfit of the surface (defined by the transfer function) with the measured σ^0 triplet distribution are more serious in the inversion for a sharply curved solution surface.

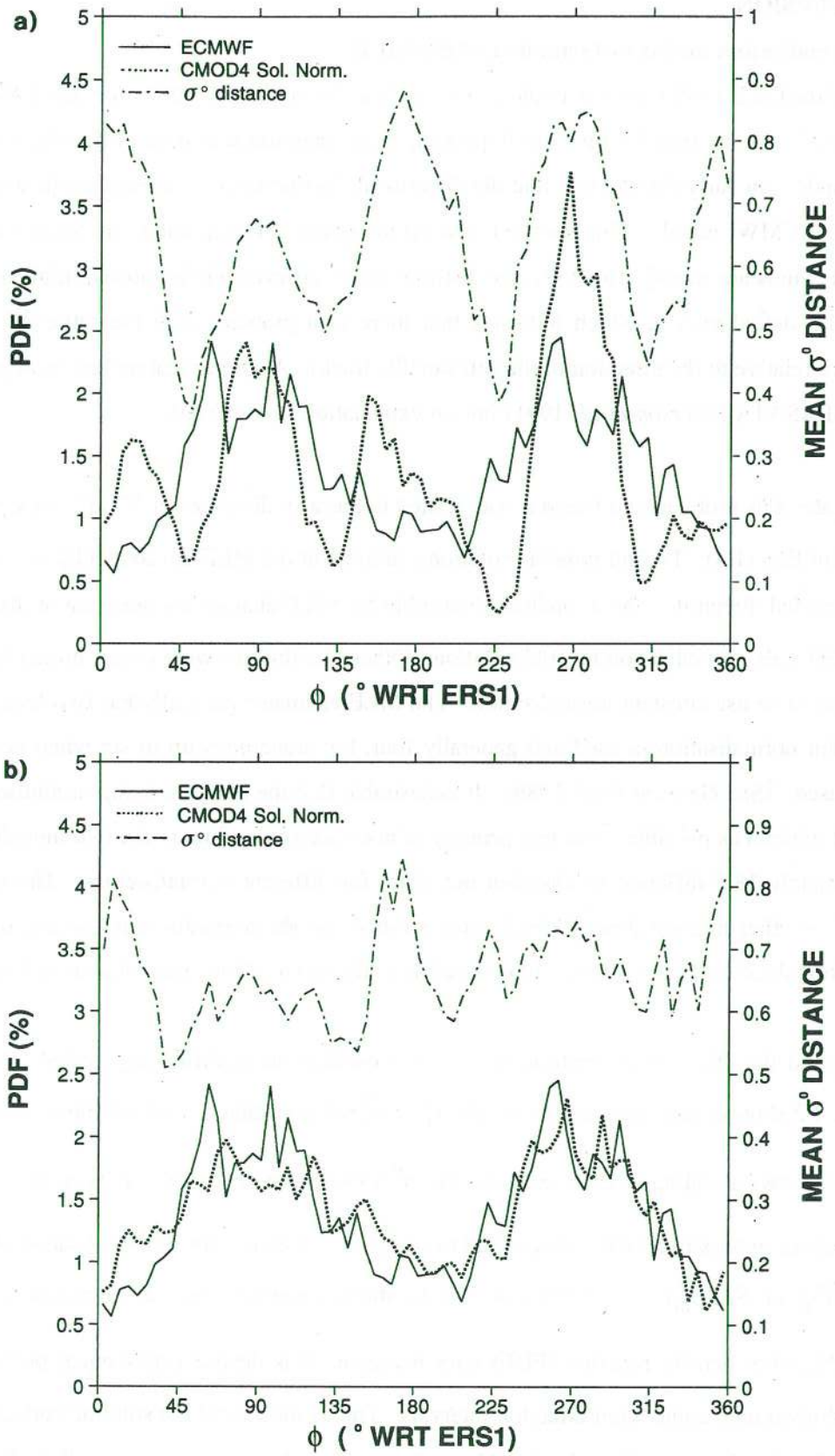

Fig 4.1 Comparison of scatterometer wind direction distribution (a) when using inversion with normalisation by solution and (b) when using equation (4.1) for the inversion. Wind direction is with respect to the sub-satellite track. The solid line represents the ECMWF direction distribution and the dotted line the scatterometer distribution. The dash-dotted curve describes the mean distance to the cone in arbitrary units (the square root of the residual). Data are for node 3 for average wind speeds above 4 m/s and from 13/2/94 21 UTC to 16/2/94 9 UTC.

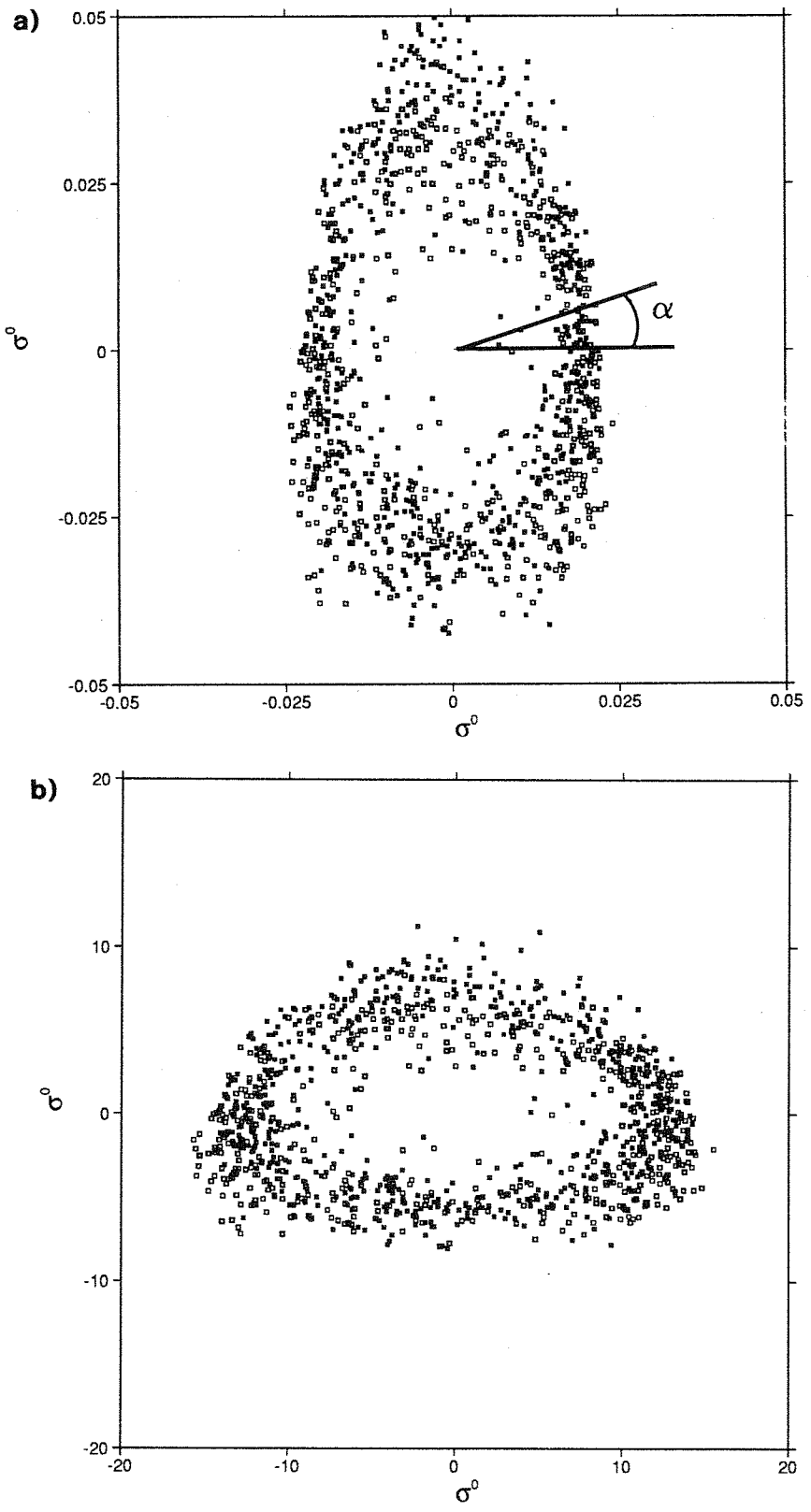

Fig 4.2 Cross-section through 3D measurement space for $\sigma_1^0 + \sigma_3^0 - 2\sigma_{av}^0$, with a thickness of $0.05\sigma_{av}^0$ for node 7. The centre of the plot represents $(\sigma_1^0,\sigma_2^0,\sigma_3^0)$ - (0.031, 0.11, 0.031) and σ_{av} is equal to 0.031. In (a) no scaling is used, and in (b) σ_1^0, σ_2^0, and σ_3^0 values are scaled by their centre of plot value. Data from september 1993. As in Fig 3.2 "upwind" and "downwind" triplets are represented by respectively open and solid squares.

From a theoretical point of view a non-quadratic MLE should be used for this estimation problem involving a non-linear surface, but because of the complexity of the cone surface, the computation of this MLE is not easy. Instead, we sought an optimal but still practical solution by transformation of σ^0 space derived as follows:

Provided we have an accurate mathematical description of the cone surface indicated by S, then given a measured vector σ^0_O, we may be able to analyze the most probable value of the "true" vector σ^0_t lying on the cone's surface. According to Bayes probability theorem we may write:

$$p(\sigma^0{}_S \,|\sigma^0{}_O) \;=\; p(\sigma^0{}_O \,|\sigma^0{}_S) \cdot p(\sigma^0{}_S) \,/\, p(\sigma^0{}_O)$$

where $p(\sigma^0_S|\sigma^0_O)$ is the conditional probability density for σ^0_S given a fixed σ^0_O. This equation can be maximised for varying σ^0_S. The a priori probability density $p(\sigma^0_O)$ is a constant in this process, since σ^0_O is given. The analysis equation requires a description of $p(\sigma^0_S)$, the a priori probability density of having a "true" triplet somewhere in the 3D σ^0 space. Since we have assumed a perfect description of the cone surface, we have $p(\sigma^0_s) = 0$ for $\sigma^0_s \notin S$. Therefore, we only need to search trial values $\sigma^0_s \in S$. For convenience we may assume:

$$p(\sigma^0{}_S) \;=\; \begin{cases} p(\sigma^0{}_{S1} + \sigma^0{}_{S3}) \cdot p(\alpha \,|\, \sigma^0{}_{S1} + \sigma^0{}_{S3}) \,, & \sigma^0_s \in S \\ 0 \,, & \sigma^0_s \notin S \end{cases}$$

Here $\alpha \in [0,2\pi)$ is a cylindrical angular variable as depicted in Fig 4.2a (the exact choice of the two parameters describing the surface is not significant at the moment, but later we will use wind speed and direction), and $\int p(\alpha \,|\, \sigma^0_{S1} + \sigma^0_{S3})\, d\alpha \;=\; 1$. Given the low measurement noise we now make the assumption that $p(\sigma^0_{S1} + \sigma^0_{S3})$ is constant, for $|\sigma^0_S - \sigma^0_0|$ close to or smaller than the measurement noise, without any significant impact on the retrieved σ^0_t. Fig 4.2a shows a cross-section through 3D measurement space, in the plane of the angular variable α. We can observe a distinct elliptical or triangular shape. Given this geometry of the surface the probability of finding a certain number of σ^0 triplets in an angular sector $\Delta\alpha$, depends on α, and therefore $p(\alpha|\sigma^0_{S1}+\sigma^0_{S3})$ is not constant.

Fig 4.3 shows the same cross-section in 3D z-space after the transformation $z_i = g(\sigma^0_i) = (\sigma^0_i)^{0.625}$. Now the data lie on a conical surface $\sum = g(S)$, with an approximately uniform distribution in α. Therefore, the assumption $p(\alpha)$ is constant is appropriate in this space. We may assume that the conditional

probability density $p(z_O|z) = N(z,\varepsilon)$, where N is a 3D normal distribution with mean z and standard deviation ε. The assumption of normal error distribution was verified a posteriori by considering the distribution of triplets over the different cross-sections introduced in section 3.1.

Now we can reformulate the MLE as:

$$\text{MLE} = \frac{1}{SD^2} \sum_{i=1}^{3} (z_{Oi} - z_{Si})^2 \qquad (4.1)$$

where SD is the standard deviation of the scatter in z_O. SD contains the estimated scatter normal to S. When S is not perfectly known, it can be shown that the uncertainty in the location of S may be accounted for in SD. We will discuss the form of SD in section 4.2, but for the present it is sufficient to note that it is a constant, i.e. independent of i. Therefore, the normalisation in Eqn (4.1) represents only a scaling, not a distortion of distance as in Eqn (1.4). Eqn (1.4) is obtained when the term $p(\sigma_S^0)$ is neglected altogether, and consequently no account is taken of the fact that it is known a priori that the occurrence of certain σ_S^0 in 3D σ^0 space is more likely than others (*Stoffelen and Anderson*, 1993 a).

To test the different normalisations statistically, we compared ECMWF velocities with those retrieved with the different normalisation functions. The number of possible solutions differs for each normalisation, but to make a fair comparison one should make the number of solutions the same. This was done as follows. For each scheme we selected at each node the most probable solution (i.e. the solution with the lowest MLE). Then we selected from the other plausible minima (i.e. those which pass the '3 σ' test discussed below in section 4.2), the one which is closest to a 180° difference in wind direction. We then pick from those two the solution that is closest to the ECMWF wind direction. A direction distribution obtained by using equation (4.1) is shown in Fig 4.1b and may be compared to the distribution obtained by using normalisation by solution in Fig 4.1a. The gaps in the PDF present when using solution normalisation disappear when using equation (4.1). We note that, at the direction gaps, the average distance to the cone is relatively small; points relatively far from the cone surface are always projected onto other directions. The improvement in direction accuracy when using eq. (4.1) rather than the other schemes discussed here is most significant at the inside swath, but present over the whole swath. A synoptic consequence of the CREO normalisation is a granularity in the resulting wind fields. (An example of this is shown in *Stoffelen and Anderson* (1993).) Instead of winds turning smoothly with position, they would all point in one direction and then jump abruptly to a new direction. With the constant normalisation this problem has been removed and the winds show no abrupt unmeteorological jumps in direction.

The transformation has a beneficial though less pronounced effect on the wind direction distribution than normalisation.

4.2 Quality tests based on distance from the cone

During inversion we also assign quality indicators based on normalised distances, $d = \sqrt{\text{MLE}}$, from the measurement point to the solution cone, where MLE is as given in Eqn (4.1) with:

$$SD = 0.625 \left(\sum_{i=1}^{3} \sigma_{0i}^{1.25} \right)^{1/2} g \tag{4.2}$$

The normalising factors have been obtained by characterisation of the noise in σ^0 space as a function of incidence angle and wind speed (see Fig 3.3). Fig 4.4 shows the estimated scatter normal to the cone, and the functional form, g, chosen to represent it, where g is the equivalent of K_p used in Eqn (1.4). The form of g is:

$$g = 2\left(1+\frac{45-\theta_m}{27}\right)\left(1+\frac{5}{V}+\frac{1}{V^2}+\frac{5}{V^3}\right)h(V) \tag{4.3}$$

where θ_m is the incidence angle of the mid beam, measured in degrees and V is in m/s. $h(V)$ represents an additional σ^0 scatter contribution for winds above 15 m/s and has the form:

$$h = \begin{cases} 1 & , for\ V \le 15\ m/s \\ 1 + (V-15)^2/100, & for\ V > 15\ m/s \end{cases}$$

The minimum normalised distance is denoted d_1. The normalisation used in Eqn (4.1) and defined in Eqn (4.2) is such that the expectation value of d_1^2 is 1 in case of a perfect transfer function. For winds above 15 m/s it is unclear whether the σ^0 scatter increases by the amount specified in h. h has been determined empirically as a threshold for which the wind retrieval is just not effected by the σ^0 scatter. A test is then implemented to reject points for which d_1 is greater than 3, i.e. to reject points lying more than 3 standard deviations away from the cone.

The values of the residuals (the minima in d^2) are also used to decide which solutions will be considered for a given node in the ambiguity removal procedure. Generally if points lie outside the cone then there will be two minima approximately 180° apart. There may be other minima but they are not likely to be meaningful and will correspond to large distances from the cone, i.e. large values of d. On the other hand, points near the central axis of the cone may have several solutions, all about the same distance from the

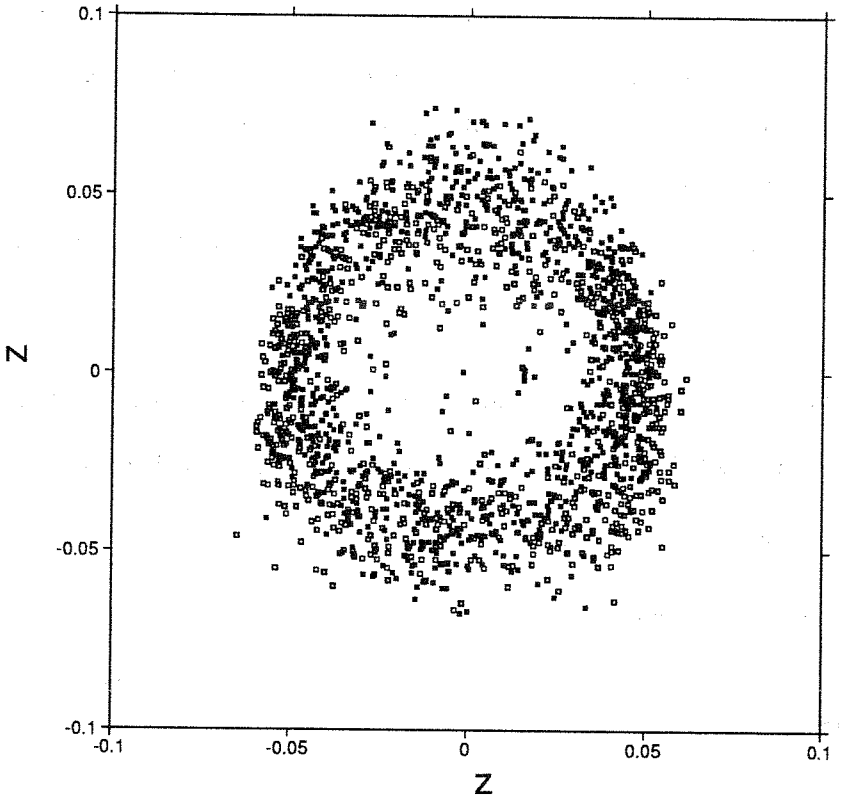

Fig 4.3 As Fig 4.2, but through a cone in a transformed space where the axes are $z = (\sigma^0)^{0.625}$, showing that the cone is much more circular in this space than in the space plotted in Fig 4.2 a). The centre of plot corresponds to Fig 4.2 and is (0.114, 0.245, 0.115).

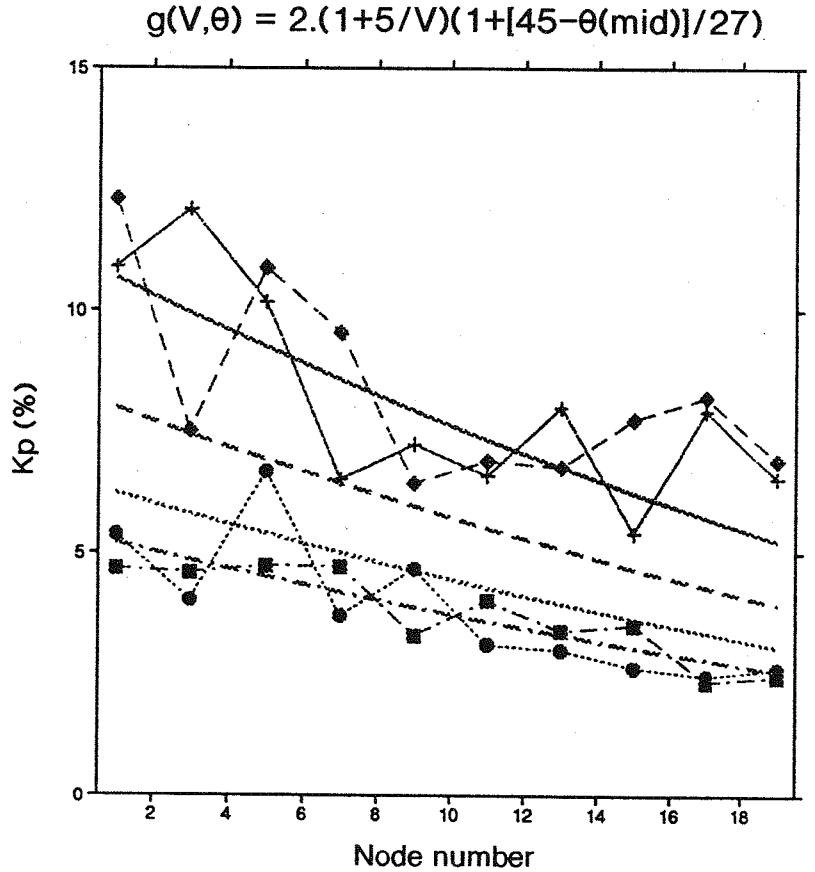

Fig 4.4 Plot of the estimated scatter in σ^0 triplets normal to the cone surface (as a % of $|\sigma^0|$) as a function of node number. The functional form of g used to represent noise is also shown.

surface therefore all equally probable, but not representative of the real wind direction. A '3σ' test was used to decide when to include the third or fourth solution. Solutions 3 or 4 were included in approximately 5% of cases but including up to four solutions did not improve wind departure statistics. In cases with low directional skill, we smooth d^2 over a wind direction interval, in order to obtain fewer but more realistic minima, the width of the interval depending on the skill. This procedure leads to a marginal improvement in performance.

The probability information in d is used further to assign a quantitative skill index. For a given triplet we calculate a mean normalised distance to the surface, averaged over all wind directions, denoted $\overline{d^2}$, and give each point a skill rating based on the closest (rank 1) distance d_1 and the mean distance $\overline{d^2}$. Specifically, the skill index is calculated from

$$I = \frac{\sqrt{\left(\overline{d^2} - d_1^2\right)}}{\max(d_1, 1)} \tag{4.4}$$

According to this formula, directional skill will increase monotonically from the centre of the cone outwards, reaching a maximum just outside the cone, and will then decrease for points far outside the cone. Fig 4.5 shows a section through the cone for node 7, along the plane $\sigma_1^0 = \sigma_3^0$, with skill colour coded. It is seen that the test works well in that points in the centre of the cone have low skill ratings, while those near the cone have high skill values.

In principle, the skill index, I, could be used to reject points just as d_1 was. Several threshold values of I, denoted T, were tried as the basis for rejecting points for ambiguity removal. We looked at the sensitivity of T with respect to global wind departure statistics, and found no sensitivity for $T > \sqrt{10}$. Comparing retrieved wind maps for different T, the cut-off $T = \sqrt{10}$ was confirmed to be adequate to exclude points with low directional skill. This test had the effect of rejecting many low speed points and points near the inside edge of the swath, however. At NWP centres, the quality of wind data is usually measured by its vector RMS error. This is a much more useful measure than one based on wind direction alone, especially for low wind speed. Since the vector RMS error for scatterometer data is estimated to be lowest for low wind speeds, we chose not to reject points on the basis of our skill index but instead use it to calculate a weighting which is used in the ambiguity removal procedure, described in the next section.

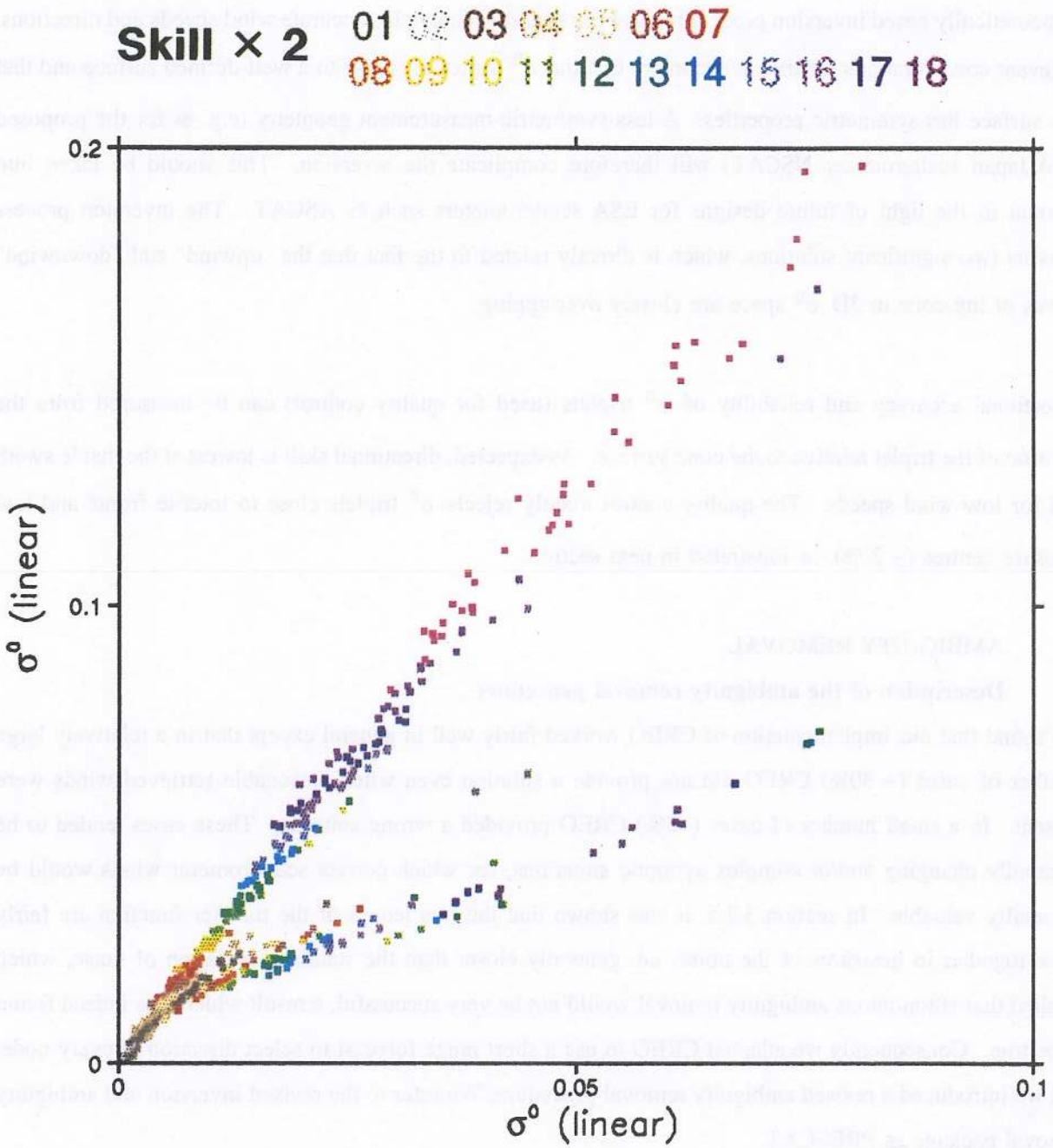

Fig 4.5 Section through the cone along the plane $\sigma_1^0 - \sigma_3^0$ for node 11. The wind direction skill multiplied by two is colour coded and given on top.

4.3 Summary

A theoretically based inversion procedure has been found which yields accurate wind speeds and directions. Relevant considerations for the inversion are that the σ^0 triplets lie close to a well-defined surface and that this surface has symmetric properties. A less symmetric measurement geometry (e.g. as for the proposed USA/Japan scatterometer NSCAT) will therefore complicate the inversion. This should be taken into account in the light of future designs for ESA scatterometers such as ASCAT. The inversion process delivers two significant solutions, which is directly related to the fact that the "upwind" and "downwind" leaves of the cone in 3D σ^0 space are closely overlapping.

Directional accuracy and reliability of σ^0 triplets (used for quality control) can be measured from the position of the triplet relative to the cone surface. As expected, directional skill is lowest at the inside swath and for low wind speeds. The quality control mainly rejects σ^0 triplets close to intense fronts and low pressure centres (~ 2 %), as illustrated in next section.

5. AMBIGUITY REMOVAL

5.1 Description of the ambiguity removal procedure

We found that our implementation of CREO worked fairly well in general except that in a relatively large number of cases (~ 30%) CREO did not provide a solution even when reasonable retrieved winds were present. In a small number of cases (~5%) CREO provided a wrong solution. These cases tended to be in rapidly changing and/or complex synoptic situations, for which correct scatterometer winds would be especially valuable. In section 3.3.5, it was shown that the two leaves of the transfer function are fairly close together in measures of the noise, i.e. generally closer than the standard deviation of noise, which implied that autonomous ambiguity removal would not be very successful, a result which was indeed found to be true. Consequently we adapted CREO to use a short range forecast to select direction at every node, and we introduced a revised ambiguity removal procedure. We refer to the revised inversion and ambiguity removal package as PRESCAT.

A first selection of direction is made by choosing the retrieved solution with direction closest to the background wind field. This selection is made from the two solutions provided by the previous inversion step. Experience has shown that the field so produced is reasonable most of the time but there are local regions, i.e. ~ 5% of cases, where the solution appears unmeteorological. It is therefore useful to apply a filter to try to increase meteorological consistency. The implementation of the selection filter used here is based on SLICE (*Offiler*, 1987), but differs from it in a number of ways. These differences are discussed below.

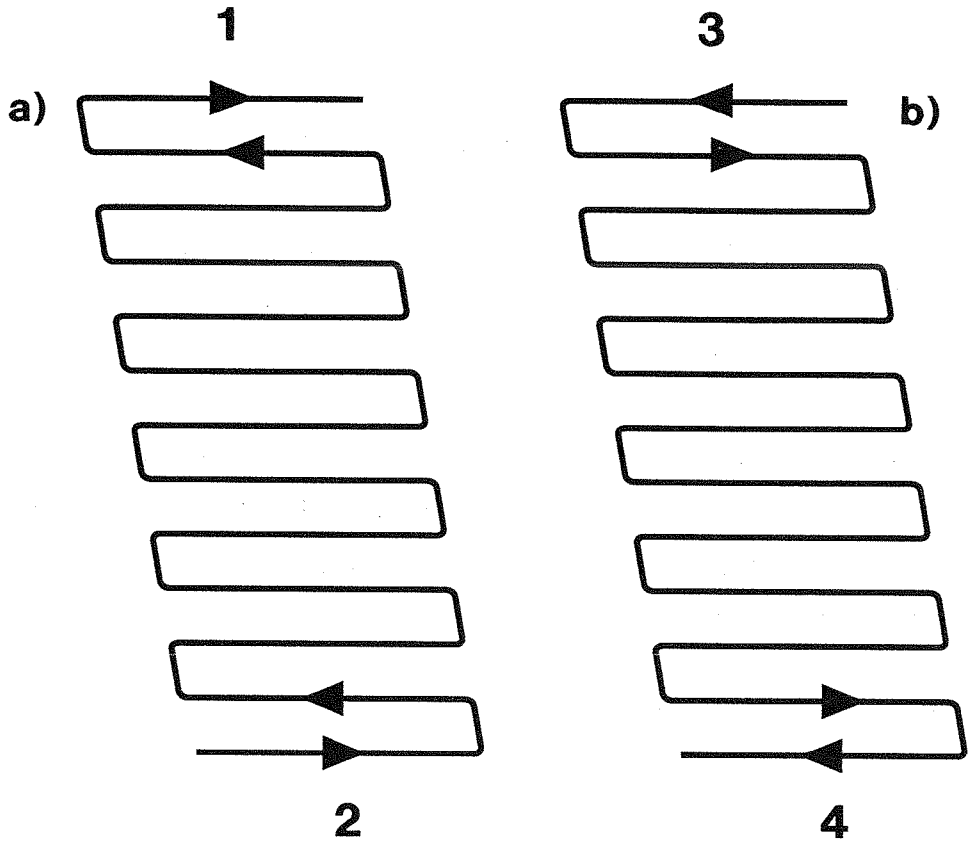

Fig 5.1 Schematic of the way the filter slides along an ascending orbit in (a) the first two iterations and (b) the second two iterations.

The filter consists of a 5X5 box which slides over the wind field, up to 114 rows at a time. The box first slides in the opposite direction to the satellite propagation direction, starting at the inside edge of the swath and proceeding as in Fig 5.1a. When it reaches the end of the sector, the direction is reversed and it exactly retraces its track. On the third pass it starts at the outside edge of the swath and proceeds as in Fig 5.1b. On the fourth pass it exactly reverses the trace of the third pass. In PRESCAT there are always four passes. In SLICE the scheme finishes processing when there are less than a certain number of points changed in a pass. However, it was found that even if there were no changes made on one pass there could be changes on the next pass and that these changes were in general beneficial.

Within a 5X5 box, the direction at the centre of the box is chosen, based on a weighted average of the differences from the N surrounding points, of which there are usually 24, but there may be less near the edge of the swath, if part of the box is over land, or if some points have been rejected by the distance check on d_1. At the central point, a mean likelihood, L_i, is calculated for each solution i where

$$L_i = \frac{\sum_{j=1}^{N} C_j \exp\{.5[(u_i-u_j)^2+(v_i-v_j)^2]/q^2\}}{N} \qquad (5.1)$$

and the summation on j is over the N surrounding points in the box. The solution, i, with the highest probability L_i is then selected. The parameter q^2 should represent the wind component variability within a box. Currently a value of q=2.5 m/s is used. When a lower value of 2.0 m/s was used, the filter was unable to influence neighbouring points sufficiently. In PRESCAT the computed likelihood of a solution depends on the wind vector (Eqn (5.1)) rather than just direction as in SLICE, since we found several cases (near fronts) where speed as much as direction indicates the consistency between neighbouring points.

The parameter C_j represents the confidence in the solution at node j. The initial value of C is:

$$C = \frac{P A.NN}{4} \qquad (5.2)$$

where P is derived from I (Eqn (4.4)). As I can range from zero to quite high values for high speeds and outer nodes, it is necessary to map it to the range 0 to 1 in order to use it as a probability index of skill. The mapping $P = I'(2-I')$ where $I' = \min(I/\sqrt{10},1)$, has the property of being 0 for $I = 0$, increasing monotonically with increasing I, to a value of 1 at $I = \sqrt{10}$ and is constant for $I > \sqrt{10}$. At the end of the last section we empirically determined that adequate directional skill exists for $I > \sqrt{10}$, as is reflected in the above mapping. A is defined according to $A = \exp\{-0.5[(u-u_b)^2+(v-v_b)^2]/q^2\}$, where A

determines the probability that the selected solution is the correct one, and (u,v) is the closest of the two scatterometer wind vectors to the ECMWF model FGAT, denoted (u_b,v_b). The factor NN is the number of nearest neighbours to the node under consideration and therefore has a value between 1 and 4.

The confidence of a point is updated on a pass of the filter according to: $C = C + (1-C)L$ where L is defined in eq. 5.1. Points for which C is low are given low weight, and will not have a strong influence on the selection of a solution at neighbouring points: the opposite is true for points for which $C \approx 1$. Thus, the filter propagates information with high confidence to areas where confidence is low.

In the next section we will give a few examples of PRESCAT to both show its power and also highlight remaining problems. The examples chosen emphasise important meteorological situations.

5.2 Examples of PRESCAT ambiguity removal

Fig 5.2a shows a plot of the winds resulting from PRESCAT inversion and ambiguity removal for 27 March 2:17 UT. The appropriate FGAT field used in PRESCAT is shown in Fig 5.2b. The blank areas in the swath in Fig 5.2a are regions in which data have been rejected by the quality tests in the inversion procedure because the triplets lie too far from the cone. Of most interest is the region close to the front. This is an area in which the winds change rapidly in space and by implication time, and our hypothesis is that there are confused sea state conditions. However, in some areas rain may also be a disturbing factor on the sea surface. The high normalised residuals arise from the σ^0 measurements themselves, not from a realisation that there is a front. Nevertheless, the front is well delineated by this test.

Fig. 5.2a also shows how well the scatterometer can see sharp features. The front is pinpointed to within 50 km with 90° changes in wind direction across it. By contrast FGAT (Fig. 5.2b) shows a much more gentle turning of the wind and no sharp front. A sharp front is present in the CREO (ESA) solution also (Fig 5.2c), but a block of winds has a wrongly selected direction. The cause of this error lies in a wrongly selected solution in the south west of the area at the location of the front. It is obvious from the observed speed gradient that wind speed information is also useful for ambiguity removal.

A second example is of a complex double-centred low pressure system which developed in the Australian Bight on 26 March 1993, 00Z. The PRESCAT solution is shown in Fig 5.3a. Again a region of highresiduals is present in and around the southern-most low pressure system. These points are towards the outside of the swath where wind direction accuracy is generally higher. This figure is selected to show that complex systems exist where it is hard to choose the correct wind pattern. The pattern chosen in Fig 5.3a looks unmeteorological in the area east of the southernmost low because there are sharp shear zones with

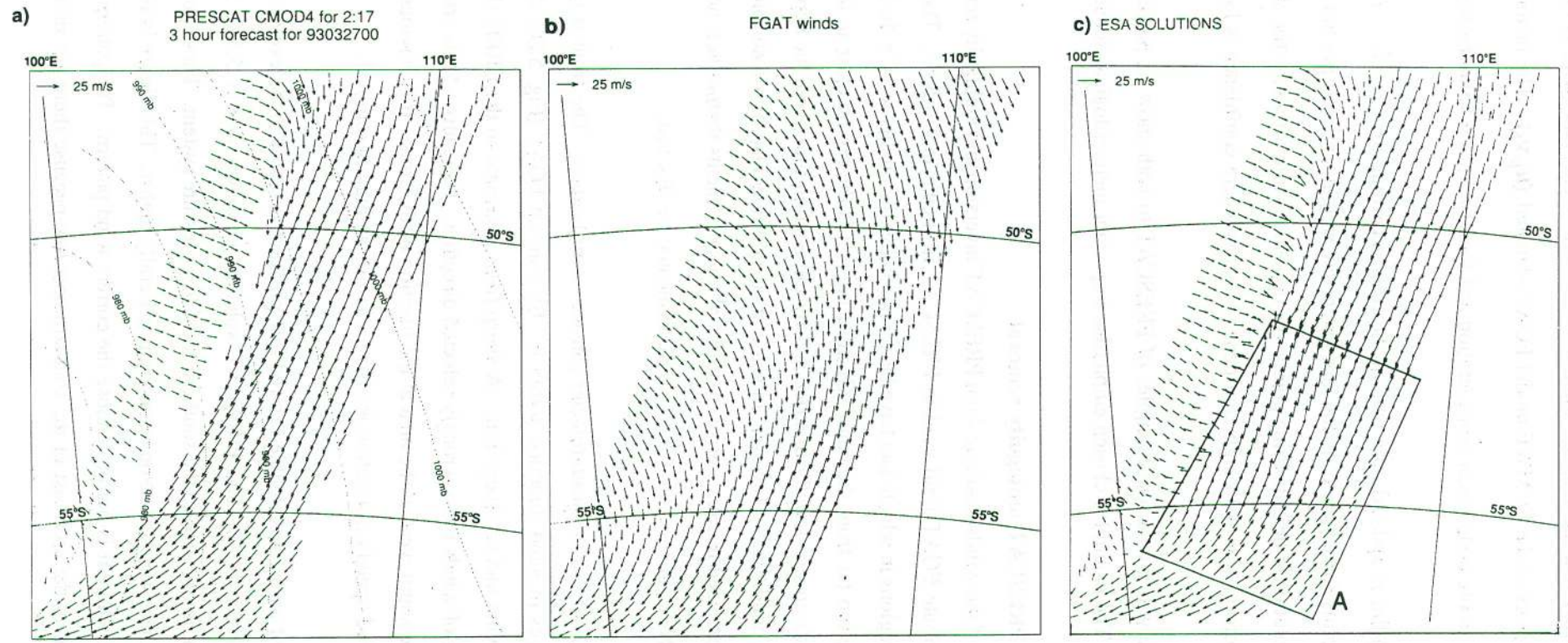

Fig 5.2 a) Winds inverted and with ambiguities removed by PRESCAT for 02 UTC on 27 March 1993. Contours are ECMWF 6 hour forecast of mean sea level pressure verifying at 00 UTC.
b) FGAT winds
c) Winds inverted and with ambiguities removed by CREO.
In a) winds with a low confidence rating are not plotted. These lie mainly along the line of the front, which is very sharp in the UWI but much less so in FGAT.

a large shift in direction, but, disregarding phase shifts, the main pattern fits the forecast surface pressure. Part of the difficulty in selecting the best wind pattern arises because the scatterometer can see much smaller scale features than are present in the FGAT winds (Fig 5.3b), which shows only a single depression. A possible interpretation is to have a shear line joining the centres of the two lows. Finally Fig 5.3c shows the CREO (UWI) solution which is clearly wrong in region A.

Errors in PRESCAT can arise when the FGAT directions are roughly along the direction of the wrong solution. In these cases the initially wrongly selected solutions compare relatively well to FGAT and are assigned high confidence (Eqn (5.2)). If the FGAT is close to 180° wrong only for a few isolated points, then the filter can correct for this. If the area is large, then the filter is unable to make a satisfactory correction. Errors also arise if the FGAT directions are nearly orthogonal to the pseudo-streamline. (The notation pseudo streamline is used rather than streamline since the rank 1 and 2 directions are not exactly antiparallel.) Such points would be given low confidence and would be corrected by PRESCAT provided they are surrounded by areas of higher confidence. However, if higher confidence areas are not present then errors can occur. The above directional errors can arise when the FGAT winds are light and the wind direction therefore not very meaningful or when there is a mispositioning of a meteorological system in the first guess. The next two examples provide illustration.

Fig 5.4a shows the retrieved winds in a polar low at 12Z on 26 March 1993 and Fig 5.4b the corresponding FGAT winds. Fig 5.4a shows an intense polar low which is completely absent in FGAT. Although PRESCAT has delineated this structure very well in general, there is a patch to the south west of the depression in which the winds are obviously wrong. The main cause of error in Fig 5.4a arises because FGAT winds over a significant part of the area are nearly orthogonal to the pseudo streamline defined by the scatterometer, making the direction selected very sensitive to errors in FGAT. There is also a smaller area in which FGAT is closest to the wrong solution. A small difference in FGAT could tip the selected winds to ~10° different, as illustrated in Fig 5.4c. In this case FGAT is taken from an experiment in which scatterometer data are assimilated (see next section). This FGAT is very similar to Fig 5.4b, but it compares slightly better to the circulation indicated by the scatterometer in the south west sector of the low (not shown). This is just enough to tip the initial selection at a few nodes. The subsequent filter is then able to converge to the correct solution. This example illustrates the sensitivity of our ambiguity removal to the quality of the input forecast data. It is also a very nice example of mesoscale features which can be seen by the scatterometer but are not detected by the ECMWF analysis/forecast system, as there are no other useful observations available in this area of the Southern Hemisphere.

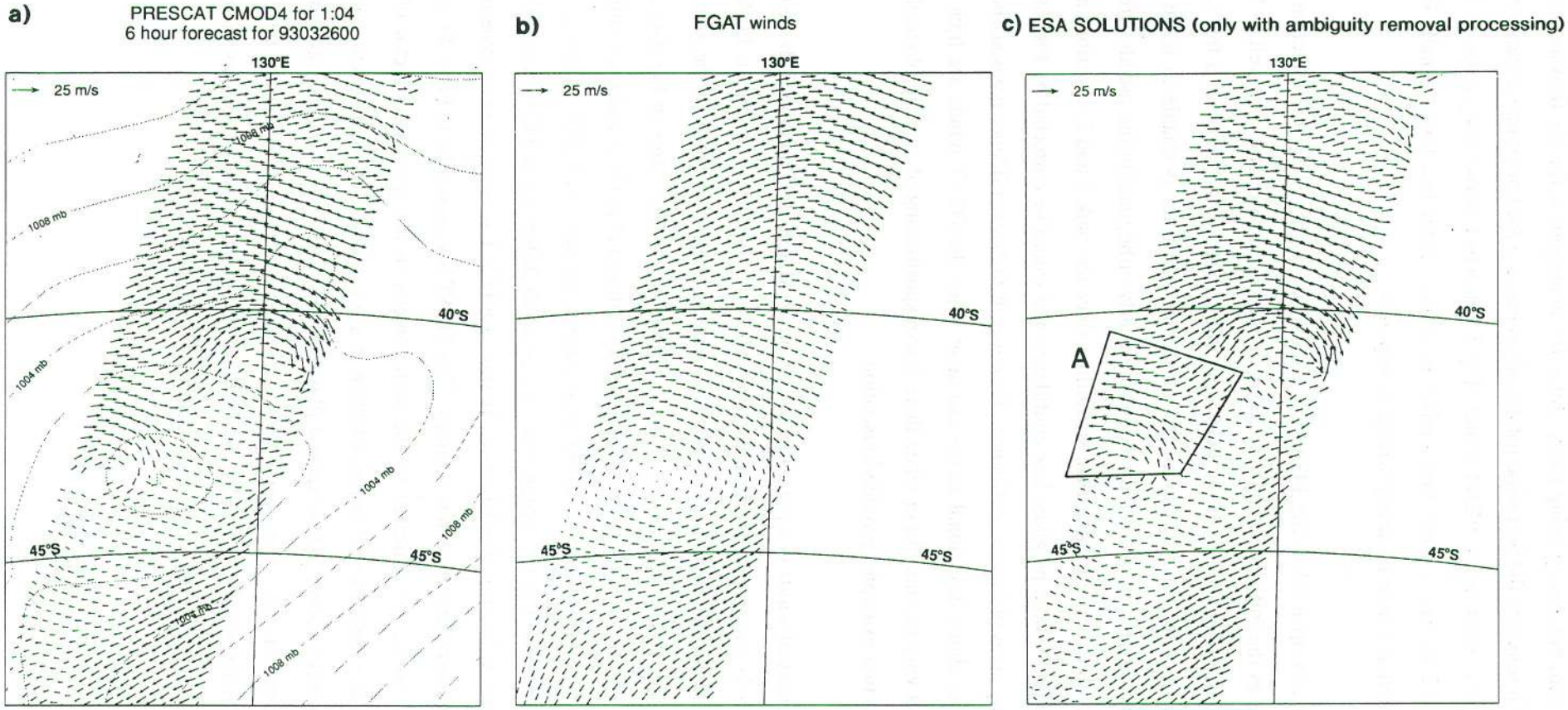

Fig 5.3 Similar to Fig 5.2 but for 00 UTC on 26 March 1993. This figure shows a complex double low structure in the PRESCAT winds (a), but only a broad feature in FGAT (b). A shear line is needed somewhere. Its position is unclear, but probably should join the centres of the two lows. Panel (c) shows the ESA solution. Here, the area marked "A" is obviously wrong.

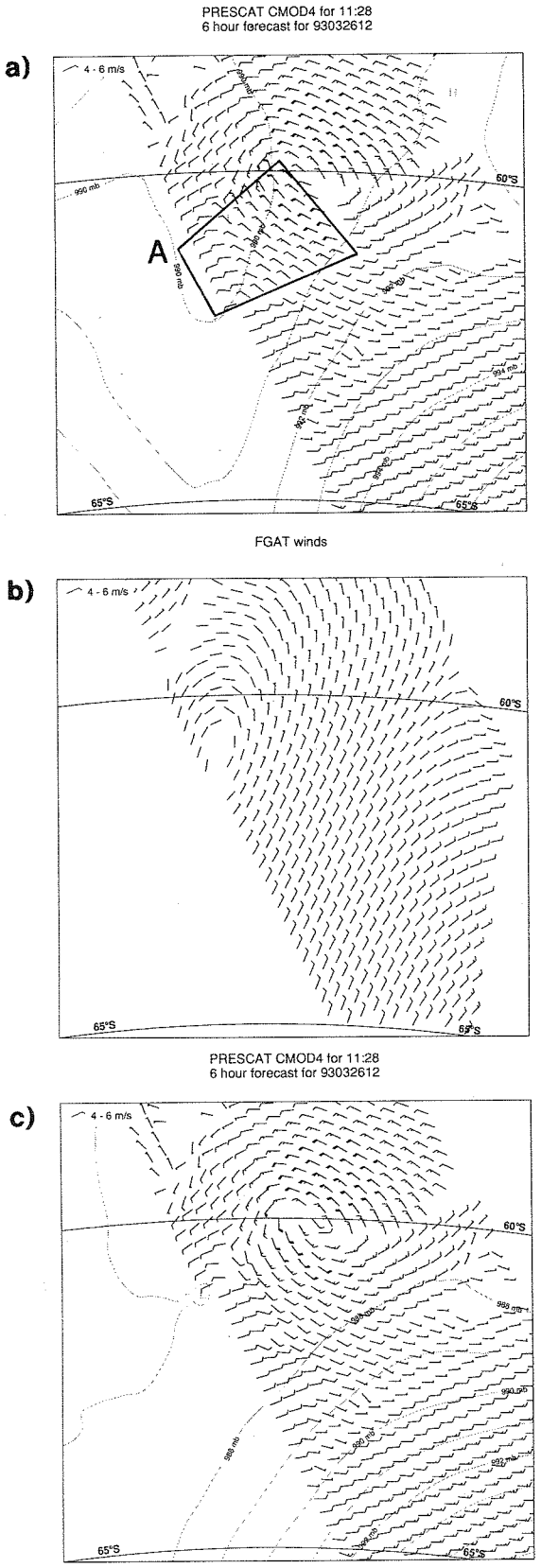

Fig 5.4 Plots of a low pressure system for 12 UTC on 26 March 1993 with ambiguities removed using a) the FGAT from the ECMWF operational analysis system shown in b). c) Winds with ambiguities removed by using FGAT obtained from an experiment in which PRESCAT data were assimilated. The latter FGAT was visually close to b) but just marginally different, leading to improved winds in the sector south west of the depression. The pseudo streamline is close to orthogonal to FGAT directions at many nodes in this example. This means that the solutions are very sensitive to small changes in FGAT, and prone to error as in area "A" in panel (a).

Finally, we show an example of a tropical storm in Fig 5.5. In this case the FGAT shows a tropical feature with wrong position and weak winds near the centre, while the scatterometer shows an active tropical storm.

The reason for including this example is two-fold: first to show that PRESCAT can represent tropical storms not present in the FGAT, but secondly there can still be correlated error resulting from large phase errors in FGAT. The patch of winds labelled A is almost certainly in error. In the next section we will describe a quality control procedure which can effectively remove wrongly selected ambiguities, called "buddy" checking.

When developing PRESCAT, a 6 hour forecast was originally used. However, it was found beneficial to use a FG appropriate to the satellite measurement time (FGAT). For slow moving, large-scale features, this was not necessary, but for rapidly moving systems it was essential. Fig 5.6 shows the scatterometer winds to the east of the deepest ever recorded low pressure system which later hit the Shetland islands (and the grounded oil tanker Braer) in January 1993. In the case when a 6 hour FG was used rather than FGAT, the winds in the area marked A and B looked unmeteorological and were very likely wrong. By using FGAT and therefore a more appropriate comparison between the background winds and the scatterometer winds, a correct wind selection was made. Obviously, using a forecast with a lead time of between 18 and 36 hours (as is currently done in ESA operations) would degrade the performance of the PRESCAT scheme (or any other procedure using meteorological forecast information as background for the ambiguity removal procedure).

5.3 Summary and conclusions

We developed an alternative ambiguity removal scheme to CREO and SLICE, called PRESCAT, based on the assumptions (a) that information on wind direction retrieval skill is an important input to ambiguity removal, (b) that wind vector filtering is beneficial compared to wind direction filtering and (c) that meteorological forecast information already enables us to remove correctly ~95% of all ambiguities. The scheme is able to remove a large percentage of the remaining ambiguities. The performance of the scheme is sensitive to the quality of the forecast wind information used and we found FGAT, based on a 3-9 hr is sensitive to the quality of the forecast wind information used and we found FGAT, based on a 3-9 hr forecast, to give the best results. A necessary further check on horizontal consistency will be explained in the next section.

As noted already in section 3, and as illustrated above, the scatterometer contains more synoptic and subsynoptic detail than the ECMWF model. We did not find evidence of large-scale systematic error in the scatterometer (except ambiguity removal errors which are difficult to describe statistically).

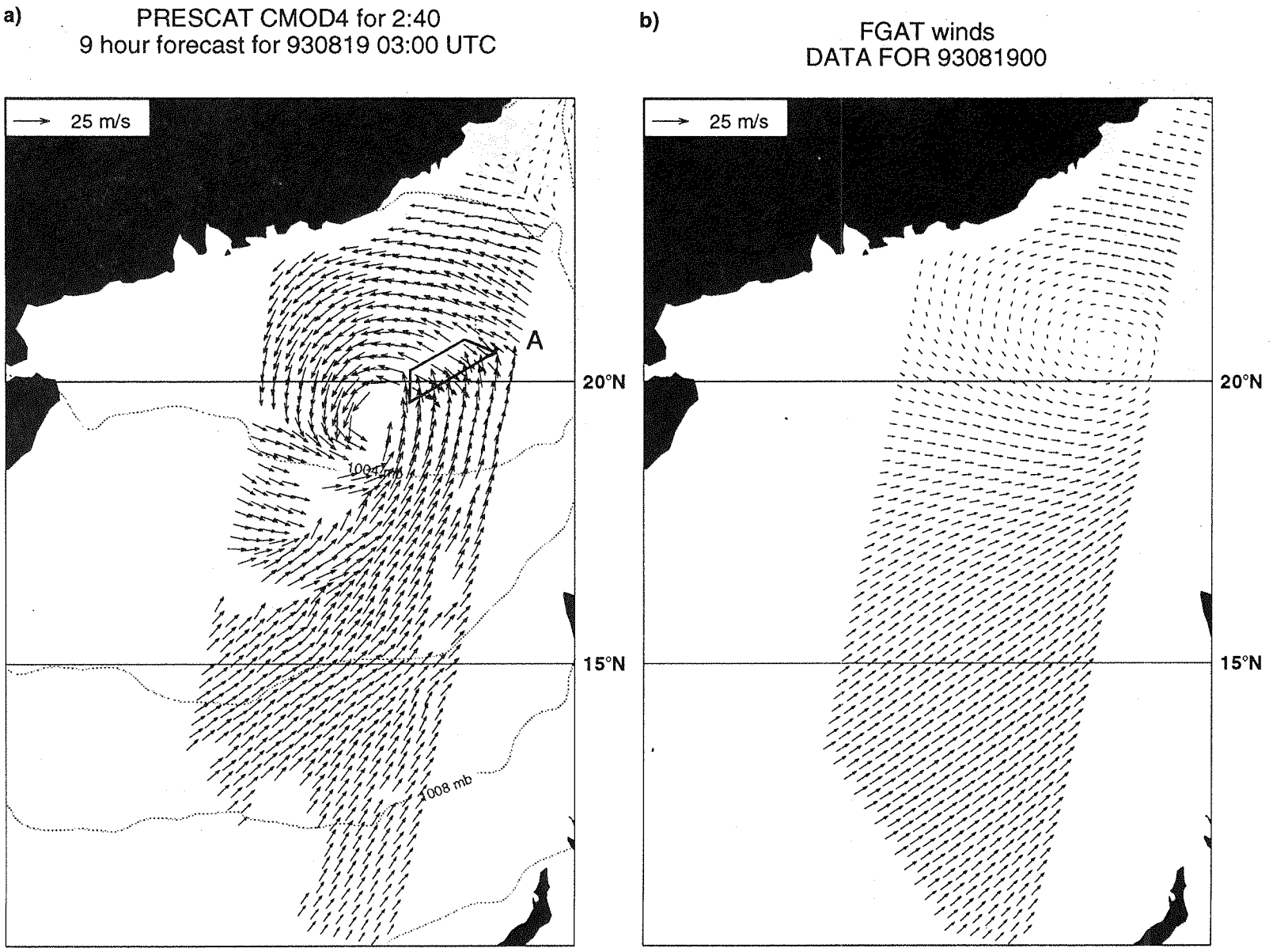

Fig 5.5 a) Plot of winds with ambiguity removed using PRESCAT and b) of the FGAT field used in the ambiguity removal. An important tropical cyclone is shown for 19/8/'93. The system is present in a), but only a weak feature is present in b). Mispositioning of the cyclone in the ECMWF short-range forecast has led to some erroneous vectors marked A.

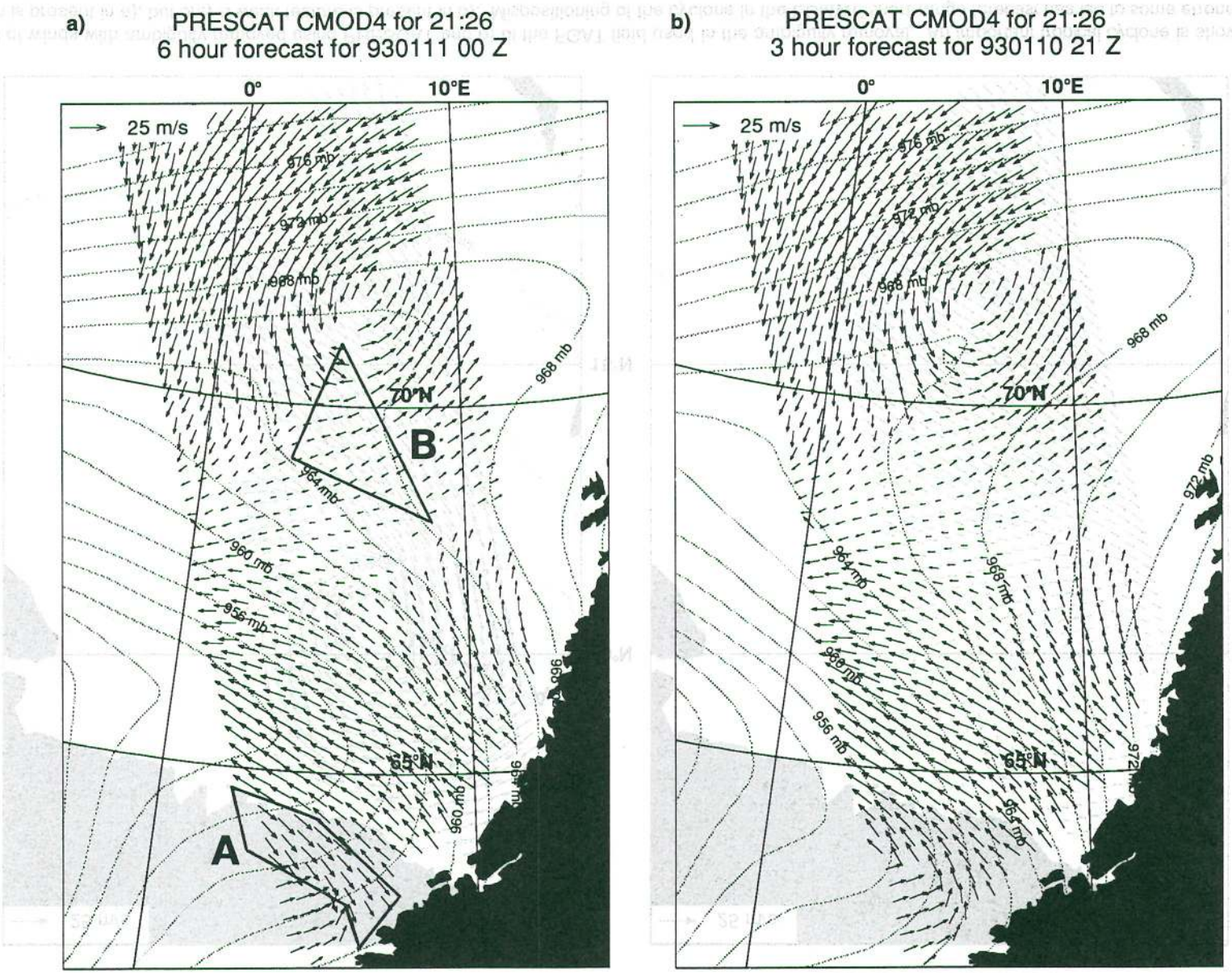

Fig 5.6 a) Plot of winds close to the "storm of the century" with the lowest ever recorded pressure. The general PRESCAT circulation is good except to the NW of Norway. In this application of PRESCAT, the winds are selected using a forecast valid for the central time (FG), i.e. 00 UTC on 12 January 1993. The winds are probably wrong in the areas marked "A" and "B". b) Winds after ambiguity removal using FGAT.

PRESCAT only uses wind vector consistency in filtering the data. The use of background error covariance structures to obtain the most likely wind field structure should lead to a meteorologically more consistent analysis and thus more accurate ambiguity removal. In a variational procedure these structure functions can be used to correct errors in the background field with the information provided by the scatterometer σ^0 triplets. Thus a meteorologically balanced analysis will result, to be used for the benefit of the ambiguity removal. The 3D- and 4D-Var procedures (see section 6.5) currently being developed at ECMWF are a sensible framework for further investigation of a 2D-Var approach (*Stoffelen*, 1994; *Courtier et al*, 1993).

6. DATA ASSIMILATION AND FORECAST IMPACT

Given the high quality of the retrieved scatterometer winds, it is important to assimilate the data into NWP models. For many years, ECMWF has used a statistical interpolation (OI) scheme to perform the analysis. To test whether the data could be used to modify the ECMWF analyses using the current OI analysis scheme, various experiments in which winds from PRESCAT are assimilated into the ECMWF model analysis were performed. Ten-day forecasts from these assimilations were made and compared with the appropriate analyses to test for impact of the scatterometer data on the forecast. Since scatterometer data have not yet been used operationally at the ECMWF, they can be used to verify operational ECMWF surface wind analyses and forecasts as discussed in section 6.4. Variational procedures are being developed to replace the statistical interpolation scheme. It was anticipated before launch that scatterometer data were best assimilated in a variational scheme by using σ^0 directly. We will show in section 6.5, however, that it is in fact more practical to assimilate retrieved ambiguous scatterometer winds. An example of variational assimilation of scatterometer winds will be given.

Earlier assimilation experiments with SEASAT scatterometer data in the T106 spectral resolution ECMWF model have shown a neutral impact in both Southern and Northern Hemispheres (*Anderson* et al, 1991). In contrast, for the case of the rapidly developing QEII storm the KNMI Limited Area Model (LAM) gave a better forecast than ECMWF did (*Stoffelen and Cats*, 1991), and the use of SEASAT scatterometer data had a further substantial and beneficial effect on the forecast. Preliminary tests with ERS-1 scatterometer data in the ECMWF T106 model showed neutral impact (*Hoffman*, 1993). However, the quality of the SEASAT data mentioned above and the preliminary ERS-1 scatterometer data used by Hoffman is substantially less than the current quality of ERS-1 scatterometer data. Assimilation experiments at the UK Meteorological Office showed a beneficial impact of ERS-1 scatterometer winds in a day 5 forecast in the southern hemisphere (*Bell*, 1994). *Breivik et al* (1993) showed a small beneficial impact in the Norwegian 50 km resolution LAM.

6.1 The analysis system

The analysis uses a statistical filter, called optimum interpolation or OI, in which data and model FG are combined into a coherent, balanced analysis. Differences between model and observation are used to alter the FG. Although the OI is carried out at discrete 6 hour intervals, the differences between observation and model are calculated at the correct observation time of the measurement (FGAT). Data are separated into 6 hour windows.

Since the analysis used is multivariate, measurements of wind will not only influence the wind analysis (as in a uni-variate scheme where each variable is analysed separately), but will also influence the mass field (i.e. temperature at a given height or, as in the model, the height of a given pressure surface) through a latitude dependent application of geostrophy. Near-surface data adjust not only the surface layers but have an influence in the vertical also. Differences between the PRESCAT winds and the FGAT are projected in the vertical as in Fig 6.1. This projection is strictly vertical. This is good for mature systems, but probably not so for young developing baroclinic systems. An adaptive assimilation scheme (4D-Var) is being tested and found beneficial for baroclinic projection (*Thépaut et al*, 1992), but this is still in development. Therefore, the test on the potential impact of the PRESCAT winds is carried out using the more mature OI scheme.

Since the background error is assumed to have a horizontal structure, the difference between a datum and the FGAT influences an area around the observation with influence decreasing with increasing distance from the observation. This is defined by the horizontal weighting functions shown in Fig 6.2. As shown in Section 5, the scatterometer can see mesoscale features very well. In order to allow the best possible use of this data in the current analysis system, the highest possible model spectral resolution of the ECMWF model was used viz T213, which corresponds to about 60 km spatial resolution, i.e. comparable with the resolution of the scatterometer. However, the effective analysis resolution is likely to be considerably poorer than this, being set by the weighting functions shown in Fig 6.2. Analysis is a costly procedure, so some assimilation experiments were carried out at the reduced model spectral resolution of T106 (~ 125 km spatial model resolution).

Although there are typically 40,000 scatterometer measurements in a 6 hour period, the data presented to the analysis are thinned to 100 km resolution. This is done because the resolution of the analysis is lower than that of the UWI and so cannot resolve the structure seen in the UWI. To avoid horizontal correlation in the data used for assimilation we perform thinning rather than averaging to achieve 100 km resolution.

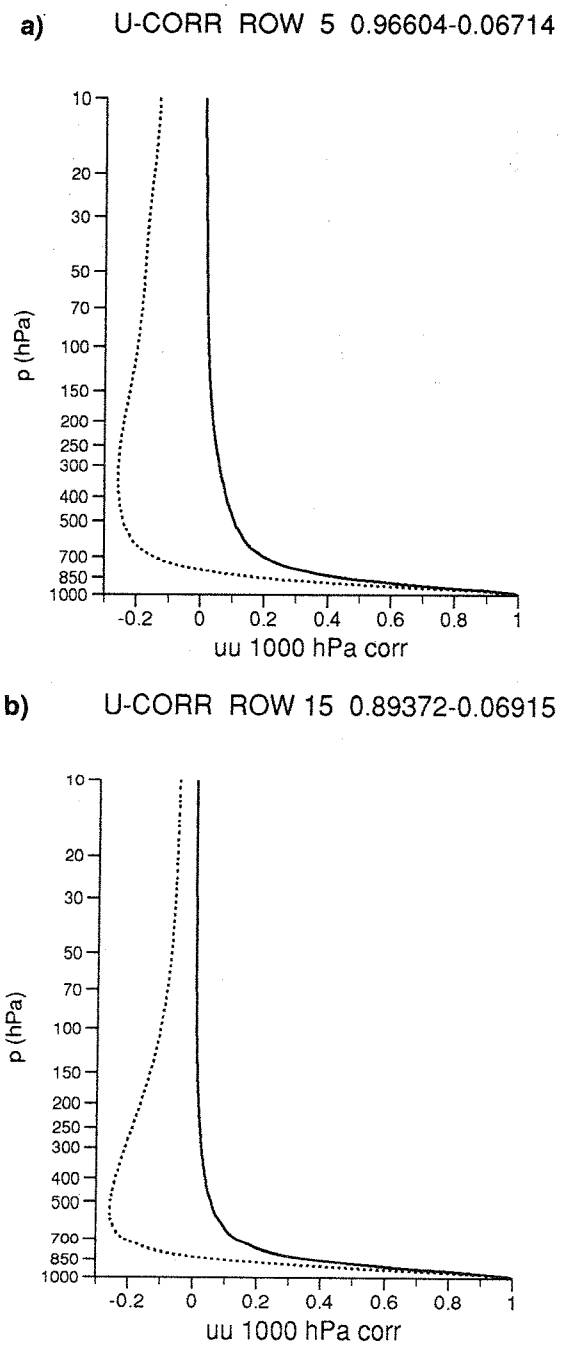

Fig 6.1 Vertical correlation function in the OI system used to extend surface forecast errors in the vertical.
a) Mid-latitudes (60°),
b) Tropics.
Solid line: nondivergent wind component covariance. Dotted line: divergent covariance (from Undén, 1989).

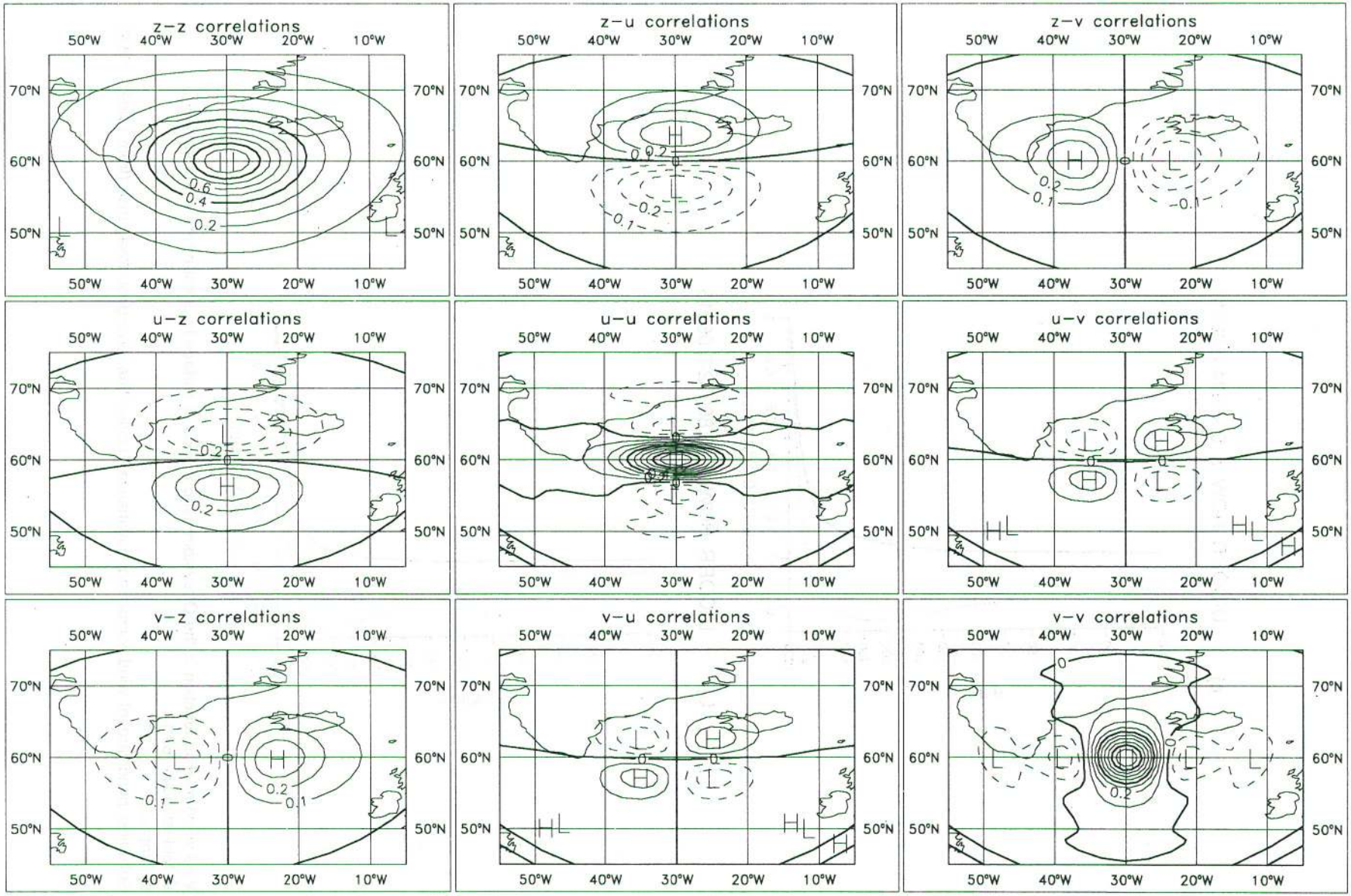

Fig 6.2 The horizontal correlation function used to extend forecast error in the horizontal. From theECMWF Research manual 1: Data Assimilation, P Lönnberg and D Shaw. Forecast error is computed for both components of the wind (U,V). The U component error is correlated not only to a U component error in a nearby location, but also to a V component error and a height error (by geostrophy). The correlation functions depend on latitude by a similarity transformation (the spatial scale for the Tropics is double that shown here, and in the Southern Hemisphere a factor 1.2 larger).

One stage in the analysis procedure consists of a buddy-check. For every datum, an analysis is done without that datum and the value of the analysis then compared with the measurement. If the difference is large, the datum is rejected. Thus any datum which passes the retrieval quality control described in section 5 might still be rejected in the analysis if it is judged of dubious validity. Typically about 4 PRESCAT winds are rejected per analysis from about 3000 presented to the analysis. Thus, the most serious ambiguity removal errors are removed.

6.2 Analysis differences resulting from assimilation of PRESCAT winds

Several analysis periods have been considered and forecasts performed from these analyses. We will consider here only the periods March 18 12Z to March 28 12Z 1993 and 26 April 12Z to 2 May 00Z 1993 (see Table 6.1). Fig 6.3a shows the differences in the control and assimilated analyses for 18 March, 12Z i.e. after a single 6 hour assimilation of scatterometer winds from PRESCAT. Differences in the 1000 mb height are typically of order 10 m (approximately 1 mb in surface pressure) although, in the southern hemisphere, larger differences of ~ 30 m i.e. 4 mb occur. Speed differences at the 10 m level can be up to 10 m/s. From other experiments, not shown, we found these numbers to be typical. These differences now evolve with time to the next analysis, 6 hours later, when new data are assimilated and consequent changes are made. After a few days of assimilation, differences grow in magnitude and need not be confined to the satellite orbit but in the southern hemisphere cover the storm track belt around Antarctica. However, the differences do not grow indefinitely. Fig 6.3b shows the differences between the control (NoSCAT) and SCAT assimilation after 10 days of assimilation. Typical differences are a few tens of metres, (a few mb) and maximum differences are ~140 m, i.e. ~ 18 mb.

Experiment	Dates	Resolution	Levels	PRESCAT	SATEM/ SATOB	Code
SCAT	18.3.93-28.3.93	T213	31	YES	YES	BYL
NoSCAT	18.3.93-28.3.93	T213	31	NO	YES	OPS
SCAT/SAT	26.4.93-1.5.93	T106	19	YES	YES	BWU
NoSCAT/SAT	26.4.93-1.5.93	T106	19	NO	YES	BXP
SCAT/NoSat	26.4.93-1.5.93	T106	19	YES	NO	BZM
NoSCAT/NoSAT	26.4.92-1.5.93	T106	19	NO	NO	CAR

Table 6.1 Analysis experiments. PRESCAT=YES means scatterometer winds are assimilated, and similarly for SATEM/SATOB.

An important question is whether these changes are beneficial. This is not easy to determine. Possible methods of assessment are to compare (a) the fit of the FGAT from the SCAT and NoSCAT runs to the SCAT data, (b) the fit of other data to the FGAT with and without SCAT, or (c) to compare meteorological or wave model forecasts started from the analyses. The latter approach has been tried using meteorological forecasts (see 6.3) but wave forecasts have not yet been performed.

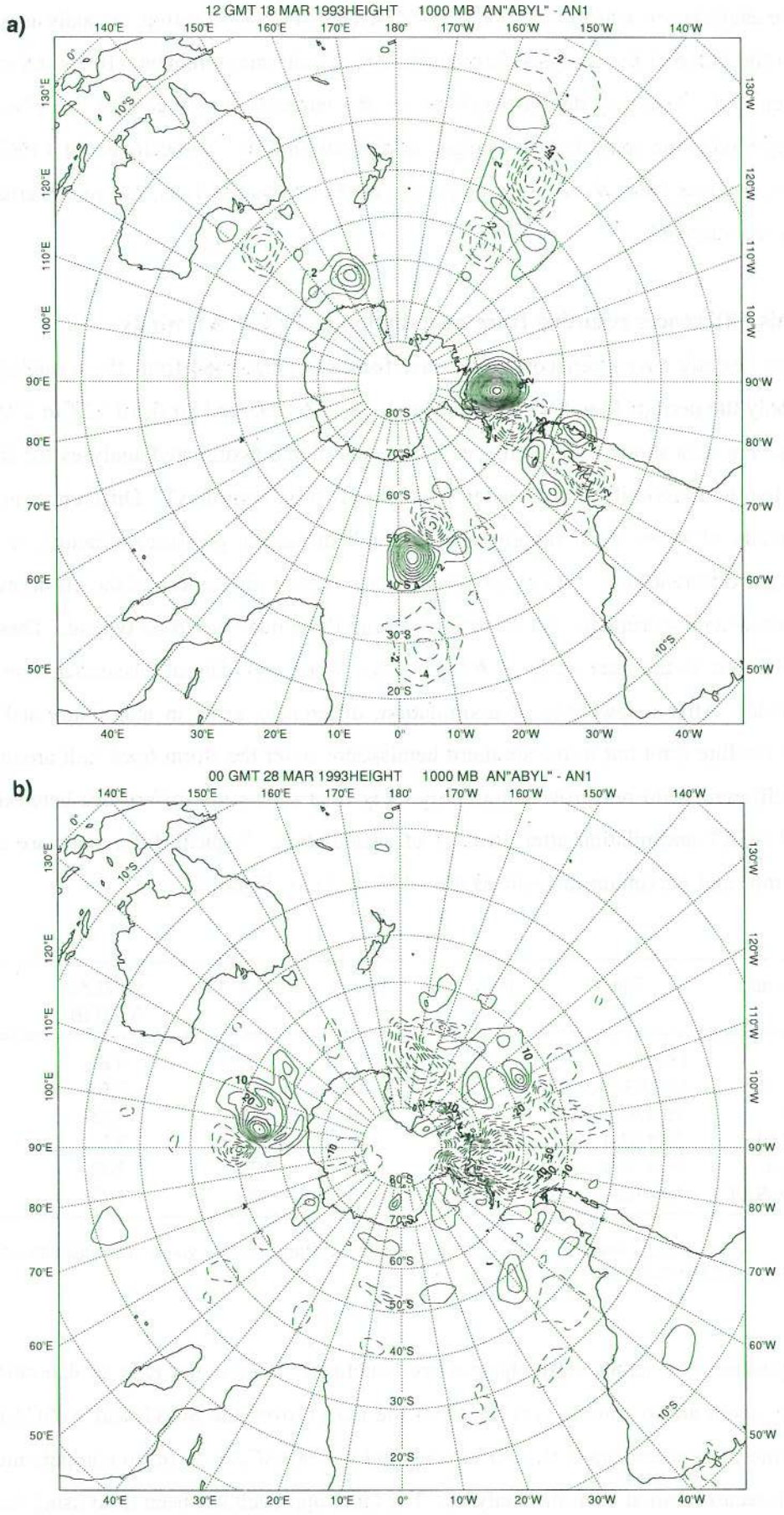

Fig 6.3 Differences between an analysis in which PRESCAT winds are assimilated (BYL) and a control (OPS) in which they are not used a) after the first assimilation, b) after 10 days of assimilation. Field shown is the height of the 1000 hPa surface. In a) the contour interval is 2 m and in b) 10 m.

6.3 Results of forecasts

For the period 18 to 28 March, ten day forecasts were made every day and compared with the corresponding operational forecasts (denoted control). All model parameters were the same in these two sets of experiments. The only differences were the analyses from which the forecasts were made: one was the control without scatterometer data (NoSCAT) and the other had assimilated scatterometer data (SCAT). Height anomaly correlations were then made for the two forecasts, with the operational (i.e. control) analyses. Anomalies are calculated by subtracting a seasonal climatology from the forecast and analysed height fields before the correlation is made. An ensemble average, over the 11 forecasts is given in Fig 6.4 which shows that assimilation of scatterometer data has had no beneficial impact on the forecasts in the sense that the anomaly correlations are, on average, the same in forecasts initiated from NoSCAT and SCAT. On the basis of forecast height anomaly correlations there is no advantage for medium-range forecasts in assimilating scatterometer data. A measure of the scatter of these forecasts is shown in Fig 6.5, for the forecast lead time of 72 hours. From the 11 forecasts for this period, we found examples when SCAT was slightly better, not much different or slightly worse. The differences were mainly in the southern hemisphere.

The neutral medium-range forecast impact of scatterometer data in the ECMWF forecasting system contrasts with the clear beneficial impact obtained with the UK Met Office forecasting system (*Bell*, 1994). However, the ECMWF 5-day forecasts without scatterometer data had approximately 10% better verifications of 500 hPa height against ECMWF analyses than the UK Met Office forecasting system not using the data. The average improvement of 4% of the Met Office 5-day forecasts when using scatterometer data is therefore insufficient to match the quality of the ECMWF 5-day forecasts over this particular period. It is therefore harder to show a positive impact in the ECMWF system. Such a situation has occurred frequently in the past in comparative studies of observation system impact.

We investigated the impact of scatterometer data in a degraded data assimilation system in a second series of experiments. Four separate analyses were made and forecast experiments performed from them. The first two analyses are NoSCAT/SAT, the control without PRESCAT winds, and SCAT/SAT, which assimilated PRESCAT winds. These are similar experiments to those for March discussed above (NoSCAT and SCAT) except for a different time period. Moreover, the horizontal sampling of the model is reduced to T106 spectral truncation (125 km) and has 19 rather than 31 levels in the vertical. Satellite temperature data, called SATEM, from the TOVS sounder (*Smith et al*, 1979) contribute positively to the southern hemisphere forecast scores. SATEM mainly define the larger scales of the analysis. SATOBs are made by tracking clouds on geostationary satellite imagery. They have much less impact in the southern hemisphere than SATEM. Two further analyses were performed, removing both SATEM and SATOB. In

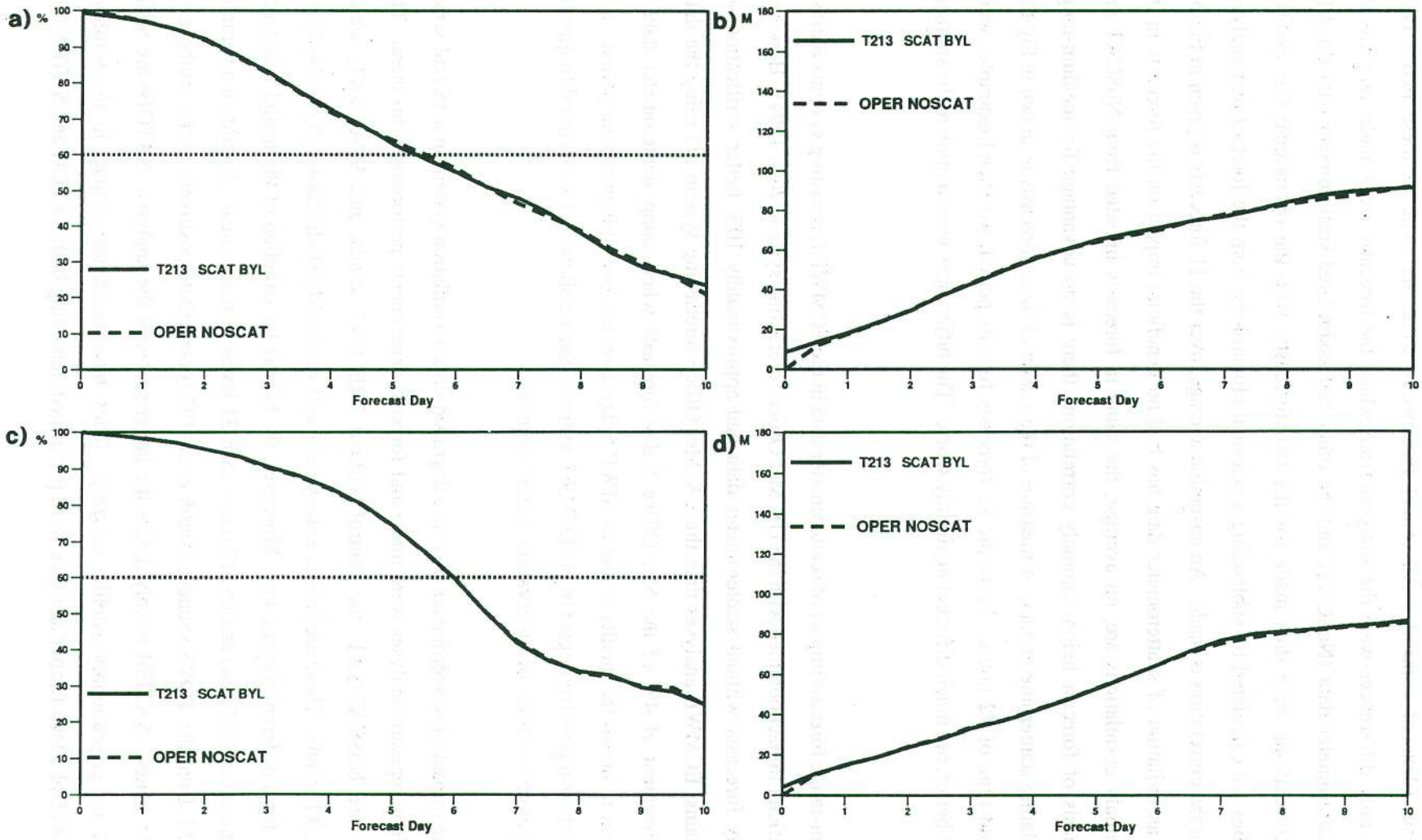

Fig 6.4 a) Anomaly correlation and b) RMS errors in the northern hemisphere for an average over the 11 forecasts initiated from BYL analyses. Similarly, c) and d) are for the southern hemisphere. The statistics are derived from the operational analysis.

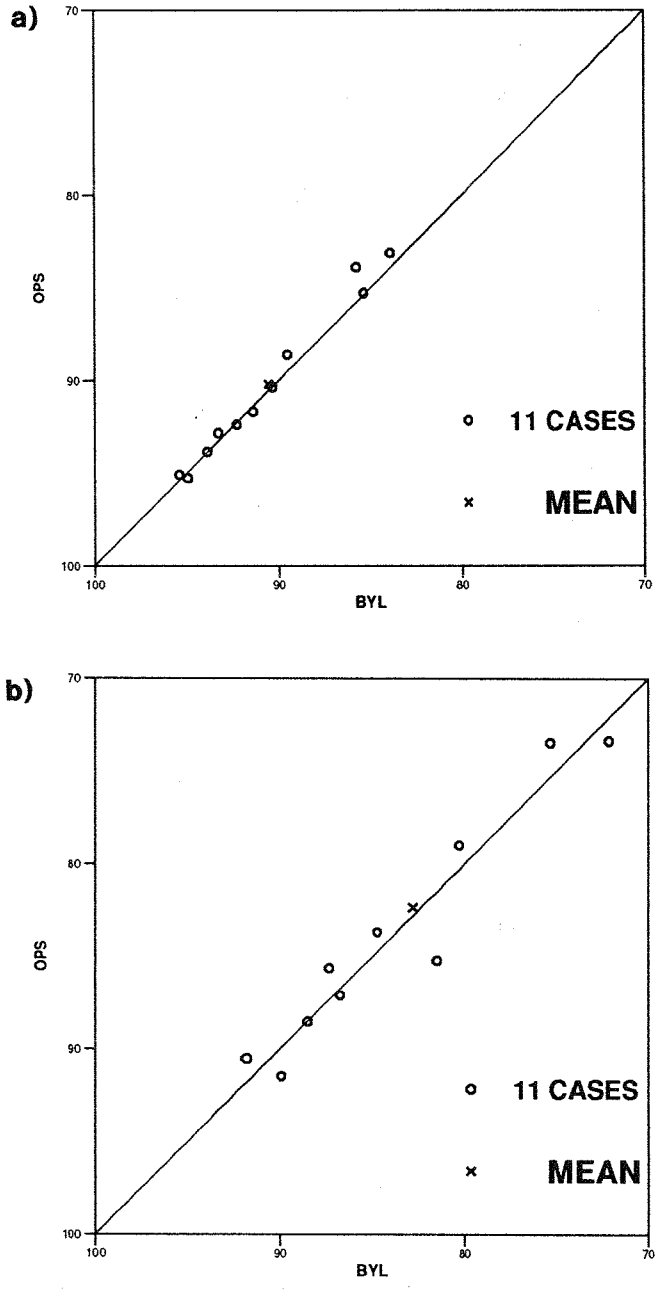

Fig 6.5 a) Scatter plot of the 11 individual anomaly correlations for 72 hour forecasts initiated from BYL analyses. a) Northern Hemisphere, b) Southern Hemisphere.

one of them scatterometer winds were assimilated (SCAT/NoSAT) and in the other not (NoSCAT/NoSAT). The analyses are listed in table 6.1.

Average anomaly correlations for the 6 forecasts from these analyses, one for each day from 26 April to 1 May are shown in Fig 6.6a for NoSCAT/SAT and SCAT/SAT and in Fig 6.6b for SCAT/NoSAT and NoSCAT/NoSAT. Again the figures show comparisons at 1000 hPa i.e. near the surface, but the results at 500 hPa are similar. In the case of NoSCAT/SAT and SCAT/SAT, the results are consistent with experiments NoSCAT and SCAT in that, on average, the PRESCAT winds do not lead to improved medium-range forecasts. In the case of SCAT/NoSAT and NoSCAT/NoSAT, however, the assimilation of the PRESCAT winds does lead to a significant improvement in the southern hemisphere forecasts. Thus, part of the lack of impact of the scatterometer in SCAT and SCAT/SAT is that there is significant redundancy between the scatterometer and the other observing systems. If the normal observing system is degraded, for example, by the removal of SATEMs (SATOBs are probably not so important), then the scatterometer can play a useful role although, as might be expected, it is not able to compensate fully for the loss of thermal data throughout the atmosphere provided by SATEMs.

In the above a height anomaly correlation skill index is used for interpretation of the impact of scatterometer data in the ECMWF analysis/forecasting system. Most of the energy in the atmosphere is in the larger spatial scales and it is these scales to which this skill index is most sensitive. We would expect, however, that the impact of scatterometer data is on the smaller spatial scales and, therefore, also the shorter temporal scales. To measure the improvement on these scales (important for severe weather prediction) in the ECMWF analysis/forecasting system, the same experiments have been verified by direct comparison with observations.

As illustrated in the previous sections, scatterometer data possess significantly more synoptic detail than the ECMWF model fields. Further, on a 100 km scale, scatterometer errors are random rather than correlated (see section 3). In table 6.2 we show a comparison between departure statistics of scatterometer minus FGAT winds for the experiment SCAT and the control NoSCAT averaged over 12 x 6 hr windows. Vector RMS departures are improved by ~5%. Because of the orbit geometry, passes 6 hours apart are generally well separated geographically. Passes 12 hours apart fall in a similar geographical area i.e. it is approximately 12 hours before an area can be resampled. The departure statistics are therefore a verification of scatterometer data assimilated at least 12 hours earlier.

approximately 12 hours before an area can be resampled. The departure statistics are therefore a verification of scatterometer data assimilated at least 12 hours earlier.

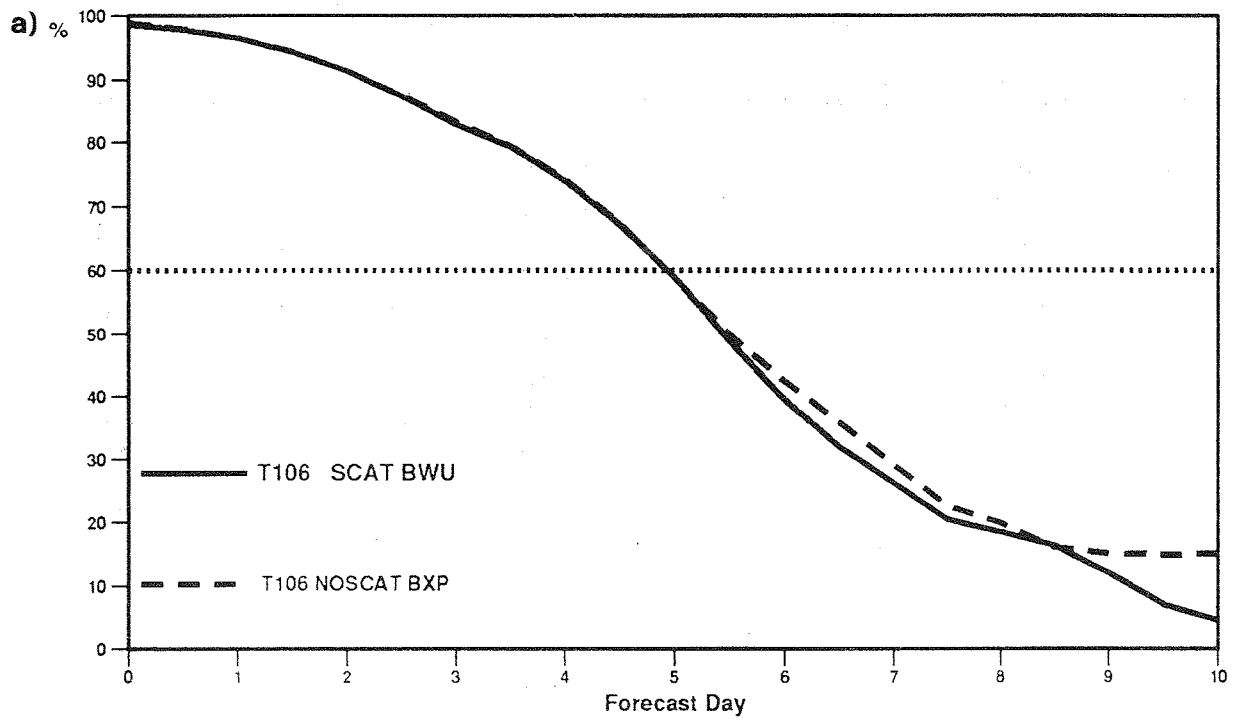

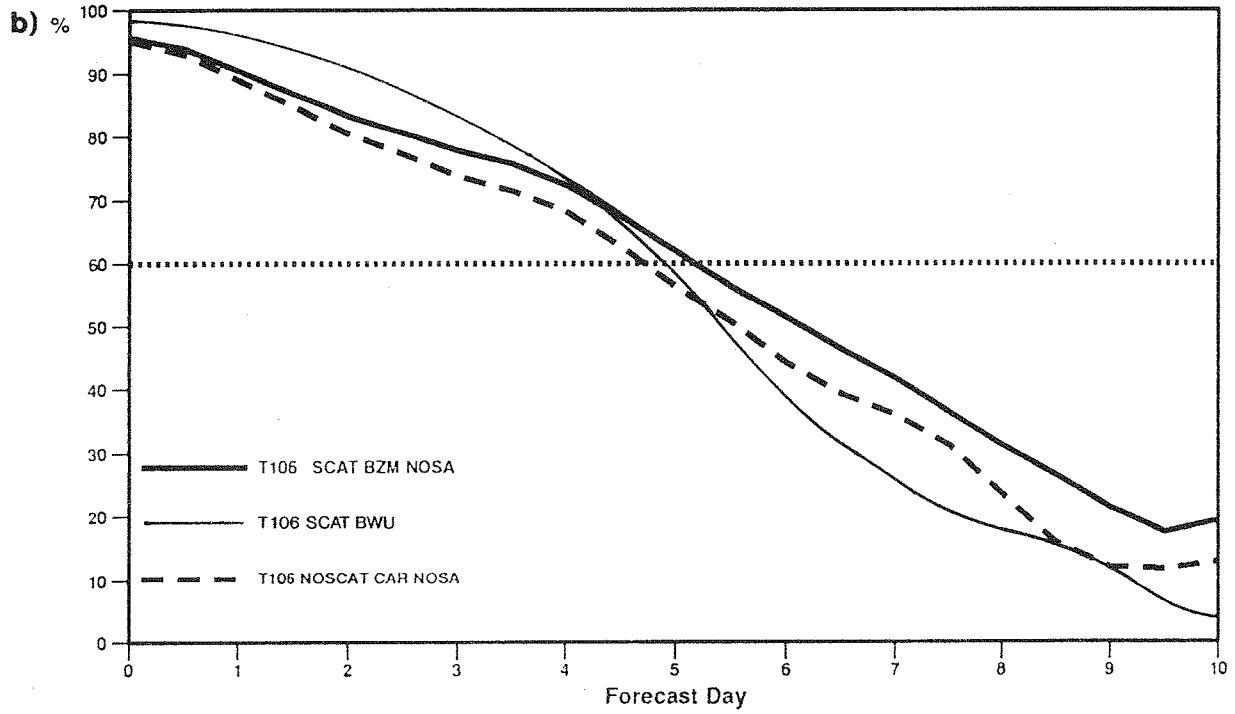

Fig 6.6 a) As for Fig 6.4, but the averages are over the 6 forecasts from 26 April to 1 May, for experiments BXP and BWU. b) As for a), but for experiments BZM and CAR. In this case, assimilation of the scatterometer winds from PRESCAT leads to improved forecasts. For comparison BWU is shown again.

FGAT SCAT 930324:12, 12 06-Hr steps							
Node	Number	Bias	SD	Number	Bias	SD	VRMS
1	10089	-0.41	31.15	13203	-0.61	1.77	3.92
3	10109	0.42	24.49	13398	-0.59	1.72	3.30
5	10137	0.73	21.90	13560	-0.48	1.72	3.10
7	10008	1.01	20.48	13627	-0.39	1.77	3.04
9	9849	1.13	19.76	13547	-0.30	1.81	3.05
11	9722	1.47	19.10	13462	-0.26	1.83	3.04
13	9546	1.28	18.96	13291	-0.29	1.83	3.02
15	9306	1.69	18.65	12986	-0.32	1.84	3.01
17	9118	1.87	18.52	12680	-0.32	1.86	3.02
19	8963	2.37	19.62	12316	-0.33	1.85	3.03

FGAT NoSCAT 930324:12, 12 06-Hr steps							
Node	Number > 4 ms^{-1}	Bias (degrees)	SD (degrees)	All speeds	Bias (ms^{-1})	SD (ms^{-1})	VRMS (ms^{-1})
1	10040	-0.89	32.14	13203	-0.64	1.88	4.06
3	10054	-0.11	25.75	13398	-0.61	1.83	3.46
5	10097	0.34	22.79	13560	-0.51	1.83	3.24
7	9971	0.80	21.47	13627	-0.42	1.87	3.19
9	9833	0.99	21.06	13547	-0.34	1.91	3.20
11	9743	1.37	20.60	13462	-0.30	1.94	3.20
13	9564	1.40	20.48	13291	-0.33	1.93	3.18
15	9310	1.70	20.08	12986	-0.36	1.93	3.17
17	9078	1.94	19.91	12680	-0.36	1.95	3.19
19	8941	2.33	20.59	12316	-0.37	1.94	3.20

Table 6.2 Comparison of PRESCAT winds with experiment SCAT and NoSCAT averaged over 3 days near the end of the experiment. For all nodes, the bias between the FGAT and scatterometer winds and the vector rms differences are all smaller in SCAT than in NoSCAT, indicating that the SCAT FGAT fit the data more closely.

SCAT	NoSCAT
VRMS 4.41 ms^{-1}	VRMS 4.46 ms^{-1}

Table 6.3 Vector rms departures of SATOB winds - FGAT for experiments SCAT and NoSCAT.

To verify the improvement in the upper air we made similar comparisons between SCAT and NoSCAT for SATOB winds (mainly in the sub-Tropics and Tropics), as in table 6.3. Again an improvement in the vector RMS departure is found, >1%. The improvement was largest in the southern hemisphere, and of similar magnitude below and above the 700 mb level. Furthermore, we found that in general using FGAT from experiment SCAT in the ambiguity removal generally gave a better wind field than FGAT from NoSCAT

(one specific example is shown in Fig 5.4). Further diagnosis could be done to interpret the effects of scatterometer data on a short forecast lead (1 or 2 days). Wave model forecasts are sensitive to different input wind fields, and could be used as a diagnostic.

6.4 Validation of the ECMWF data assimilation system

When data are not used actively in the analysis they can be used to verify the analysis and subsequent forecasts, as will be shown in this section for scatterometer winds. Fig 6.7 shows the wind vector variance of the error of the ECMWF model as computed over the oceans using a fixed set of scatterometer data. We have assumed that approximately half of the variance of the departures is due to the scatterometer (5 m^2s^{-2}) and this has been subtracted from the departure variances to give the ECMWF model error shown in Fig 6.7. The operational ECMWF model (with no scatterometer information included) is verified at different forecast times. The first point to note is the large increase in variance when a 6 hour forecast is interpreted as being valid at a time 2.5 hours earlier or later, compared to using a forecast at the appropriate time (FGAT) (open square). This means that using FGAT is important both for ambiguity removal (as was illustrated in section 5), and for data assimilation. If FGAT is not used for the latter, approximately 15% of the variance of the increments will be due to a timing error and is incorrect as such. Obviously, these errors made in the analysis will be spatially coherent for timely consistent data such as from the scatterometer.

A second point to note is that the observations used in the analyses adversely effect the FG 10 m wind field over the oceans; the vector error variance of the FG is 0.5 m^2s^{-2} lower than the vector error variance of the analyses, verified at the same locations. The average analysis minus FG difference (increment) over the oceans is 2.3 m^2s^{-2}. So, on average a part of 0.9 m^2s^{-2} (40%) of this increment verifies to be correct and a part of 1.4 m^2s^{-2} does not verify. After the OI procedure an initialisation procedure is run to filter out noise generated by OI (gravity waves). The initialisation filter has no effect on the verification of the analyses. In the previous section we demonstrated the positive effect of the assimilation of SATEM, SATOB and scatterometer data. Here we see that the positive effect in the analyses does not extend to the full analysis domain. However, during the 6 hour forecast the 10 m winds are again properly balanced (baroclinically) with the upper air dynamics and become more realistic.

The balance of the analysis increments is determined by flow-independent structure functions that specify a mass-wind coupling, a vertical structure and a horizontal structure. Both upper air and surface, and mass and wind observations effect the 10 m wind analyses. From the experiments done it is difficult to explain the adverse effects, but since fixed structure functions are used to assimilate scatterometer data, which are not optimal for each particular case, it is very likely that the scatterometer data will also adversely effect some parts of the analysis domain. Conversely, scatterometer data will inhibit increment structures that

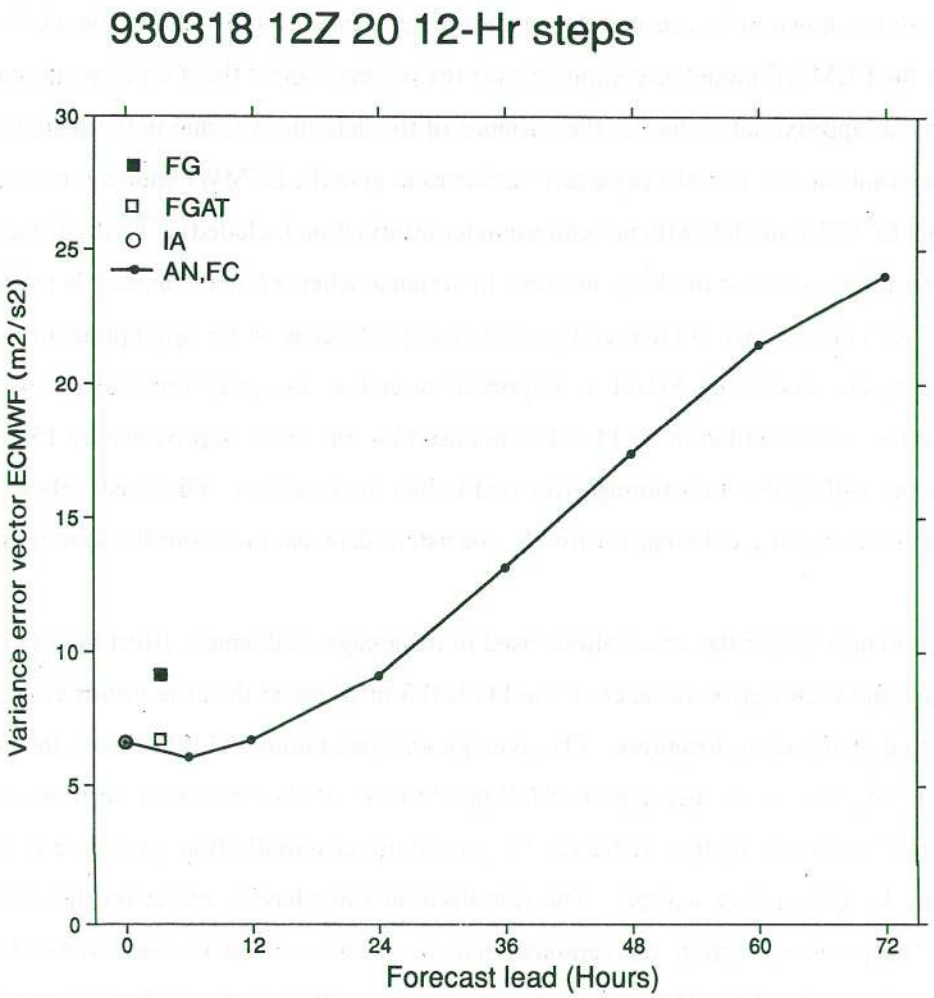

Fig 6.7 Wind vector error variance of the ECMWF model at a fixed set of scatterometer nodes. The wind vector error variance of the scatterometer observations was estimated to be 5 m^2s^{-2}. The solid line represents from left to right the forecasts at different lead times. (Lead time 0, corresponds to the analysis and lead time 6 hours to the FG.) The symbol O is the initialised analysis. The time difference between scatterometer observations and the corresponding field values is less than 1 hour. The squares represent verification against another set of scatterometer winds that are between 2 and 3 hours from the verification time; solid FG and open FGAT.

adversely effect the 10 m wind. It is therefore worthwhile to further investigate these effects in order to make observational systems more complementary.

Recent studies show that in a 4D-Var system baroclinic structures can be enforced by assimilating surface (i.e. scatterometer) data (*Thépaut et al*, 1992), by using the time trajectory of the forecast model. The fact that in a 6 hour forecast the surface balance is restored, indicates that this is a promising technique which potentially can overcome a weakness in 3D methods.

6.5 Variational methods

In a variational assimilation scheme (*Le Dimet and Talagrand, 1986*) one minimises a cost function:

$$J = J_O + J_B \tag{6.1}$$

where J_O is a weighted quadratic term which measures the differences between the estimated control variables and the observations, and J_B is a quadratic term measuring the difference between the estimated control variables and the background field. An implicit ambiguity removal for scatterometer data would be helped by meteorological balance constraints on differences between the control variables and the guess field, incorporated in the penalty term J_B. Following *Lorenc* (1988), we may specify the contribution of scatterometer data to the cost function as:

$$J^{SCAT}_O = -2 \ln[\, p(\sigma^0_O \mid \boldsymbol{V}) \,] \tag{6.2}$$

where V is the estimate for the local wind vector. Further:

$$p(\sigma^0_O \mid \boldsymbol{V}) = \int_{\sigma^0_S} p(\sigma^0_O \mid \sigma^0)\; p(\sigma^0 \mid \boldsymbol{V})\; d\sigma^0 \tag{6.3}$$

The integral is over σ^0_S, i.e. the cone surface as described by the transfer function. The first term in the integral should express the scatter observed perpendicular to the cone's surface, which was discussed earlier (uncertainty about the cone's location should also be included in this expression). The second term should express knowledge of the errors made when interpreting σ^0_S as the "true" wind vector and of the misrepresentation of the NWP model spatial and temporal scales by the retrieved wind.

One could attempt to assimilate σ^0_O directly in a NWP model, and project the transfer function and representativeness error, which have their only contribution along the surface S and are therefore well characterised by the wind parameters, onto σ^0_S. Because the σ^0 to wind relationship, as represented by the curved cone surface, is highly non-linear, the projection of wind errors onto the cone is a complex problem. Certainly plane approximations using only $\partial\sigma^0_S/\partial V$ will be inappropriate. Using the curvature, i.e. $\partial^2\sigma^0_S/\partial V^2$ should be better, although still not perfect, and will certainly result in an algorithm of

substantial mathematical complexity and computational cost. Moreover, in an attempt to strive for mathematical elegance, one would forget that the uncertainties in our knowledge of $\partial^2\sigma^0_S/\partial V^2$ may be of a limiting adequacy.

Alternatively, one could try to formulate the problem in terms of wind. For this purpose, we will have to make some approximations concerning Eqn (6.3). As discussed in section 4, we can accurately identify the most likely "true" position of a measured σ^0 triplet on the cone's surface, and we have shown in Table 3.1 the uncertainties it introduces in the wind domain. When discussing Table 3.3, we argued that since measurement "noise" is low, it may be neglected. Therefore, replacing $p(\sigma^0_O|\sigma^0_S)$ by $p(\sigma^0_R|\sigma^0_S)$, with σ^0_R as derived from the retrieval (section 4) is a valid approximation. The retrieval has multiple solutions $\sigma^0_{R,i}$ because of the 180° ambiguity, and therefore the first term in the integral will be a sum of $p(\sigma^0_{R,i}|\sigma^0_S)/n$ with $i = 1, \ldots, n$ the solution index where $n = 2$. In section 4 we found that limiting ourselves to just two solutions has no impact on the departure statistics and the quality of the retrieved wind fields. Furthermore, autonomous ambiguity removal skill is difficult to use (section 5) and therefore we have assumed no skill in the distinction of the different $\sigma^0_{R,i}$, i.e. all solutions have probability $1/n$.

Assuming negligible σ^0 measurement errors in 3D σ^0 space, then a further replacement of $p(\sigma^0_{R,i}|\sigma^0_S)$ with a Kronecker δ -function of the form $\delta(\sigma^0_{R,i}-\sigma^0_S)$ is a valid assumption. Now, after integration and using the transfer function to map $\sigma^0_{R,i}$ onto the retrieved winds $V_{R,i}$, Eqn (6.3) reduces to $p(\sigma^0_O|V) = p(V_{R,1}|V)/2 + p(V_{R,2}|V)/2$. Therefore, the formulation of the problem in wind space only needs a proper characterization of the sum of transfer function error and the representativeness error in wind space, which was addressed in section 3. We may assume $p(V_A|V) = p(V|V_A) = N(V_A, \varepsilon_R)$ for an unambiguous scatterometer wind V_A, where N is a normal distribution around the components of V with error ε_R. Similarly, for the ambiguous solutions we may write $p(\sigma^0_O|V) = N(V_{R,1}, \varepsilon_R)/2 + N(V_{R,2}, \varepsilon_R)/2$. From Eqn (6.2) we can derive the scatterometer cost function, which will not be quadratic particularly when $(|V-V_{R,1}| - |V-V_{R,2}|) \leq |\varepsilon_R|$. Moreover, in these cases we find only one minimum at $V = 0$.

An alternative analytic formulation can be found, that describes a conditional functionality in terms of the penalty function J_O^{SCAT}:

$$J^{SCAT}_{O} = \left[\frac{\prod_{i}^{2} K_i}{\sum_{i}^{2} K_i} \right]^{\frac{1}{P}} \tag{6.4}$$

with $K_i = \{J^S_{O,i}(V_{R,i})\}^P$, and e.g. $P = 4$. $J^S_{O,i}$ characterises the estimated scatterometer wind error for one single solution, and is assumed quadratic as before. For low wind speeds this J^{SCAT}_O cost function also has two minima located at $V_{R,1}$ and $V_{R,2}$, and a quadratic dependency on V in almost the entire speed domain, except where $V - V_{R,1} = V - V_{R,2}$. Therefore, this formulation has more symmetry around its minima. For $P < 4$ we have a weaker gradient towards the minima, or in other words, exact ambiguity removal will be less of a constraint and intermediate solutions more likely. From our experience with ambiguity removal we believe that a strong constraint is more appropiate, but this needs to be tested.

To investigate the statistical consequence of the cost function formulation, we performed Monte Carlo simulations. $V_{R,1}$ and $V_{R,2} = -V_{R,1}$, and a background wind V_B were simulated for a given V, using respectively a Gaussian wind component error of ε_R and ε_B for the scatterometer and background wind (in fact ε_B characterises the accuracy of all available information, except the observation under investigation). Fig. 6.8a shows a result when minimising Eqn (6.1) with the above scatterometer cost function for 2000 trials. Ambiguity removal is generally successful for a speed as low as 3.5 m/s. Fig. 6.8b shows the distribution of solutions for 2000 simulations, but in this case $\varepsilon_B = 4$ m/s and $V = 7$ m/s. As expected, it can be seen that ambiguity removal is less successful with reduced supporting wind direction information. The statistical difference between the two proposed cost functions is marginal, and therefore, because of the more symmetric and quadratic behaviour, the functionality in Eqn (6.4) may be more desirable to use in a minimization. With this equation, we have arrived at a practical and accurate solution for the variational assimilation of scatterometer observations. Preliminary results with a 3D-Var analysis system show that ambiguity removal is done accurately, and a large scale compromise is easily found in complicated situations as illustrated in Fig 6.9 (*Stoffelen et al.*, 1993).

6.6 Summary and conclusions

The OI analysis system "buddy" check is used effectively to identify and remove the few (~ 0.1%) solutions wrongly selected by PRESCAT. Assimilation of PRESCAT scatterometer winds has a beneficial impact on short-range forecasts (Table 6.2 and 6.3), probably mainly from improvements on the sub-synoptic scales. On the larger temporal and spatial scales a significant forecast impact has been found when a 'reduced' observing system (without SATEM (satellite temperature soundings) and SATOB (cloud tracked winds)) is used, but in a 'full' observing system the scatterometer could not provide information beneficial for medium-range forecasts. observing system (without SATEM (satellite temperature soundings) and SATOB (cloud tracked winds)) is used, but in a 'full' observing system the scatterometer could not provide information beneficial for medium-range forecasts. This implies that scatterometer winds and SATEMs are not complementary on the large scales. Also, combining our results with the results obtained by *Bell* (1994) indicates that the impact of scatterometer data depends on assimilation system method and performance: in comparing data impact in two assimilation systems it is more difficult to show impact from the system which is performing better.

Surface data are difficult to use in meteorological analysis. In most current data assimilation schemes no account is taken of the special meteorological conditions (Ekman spiral) in the planetary boundary layer (PBL). Further, the structure functions are defined in a climatological sense and do not take into account the fact that the structure of error in the FG will depend on meteorological conditions. The spatial structures used to update the background to fit e.g. surface observations will therefore partly be inappropriate to change the upper air, and conversely upper air observations may have adverse effects on the surface analysis. In particular, it was shown that the global ECMWF analysis of surface wind is of slightly lower quality than the FG winds, as measured by scatterometer data. When scatterometer data are used they will oppose such increment structures that deteriorate the surface wind. Further investigations are needed to make the different observational systems more complementary and useful.

The above is a weakness of 3D-Var as well, but in a 4D-Var assimilation scheme the sensitivity of the time trajectory of the forecast model to external forcing will mainly determine the structure of change in the model due to an observation at a particular time and location. This will make the 4D-Var analysis meteorologically better balanced than its 3D equivalent and should lead to a more beneficial modification of upper air fields in response to changes in the PBL.

The problem of surface data assimilation becomes especially relevant in future planned coupled atmosphere/ocean data assimilation and forecasting systems.

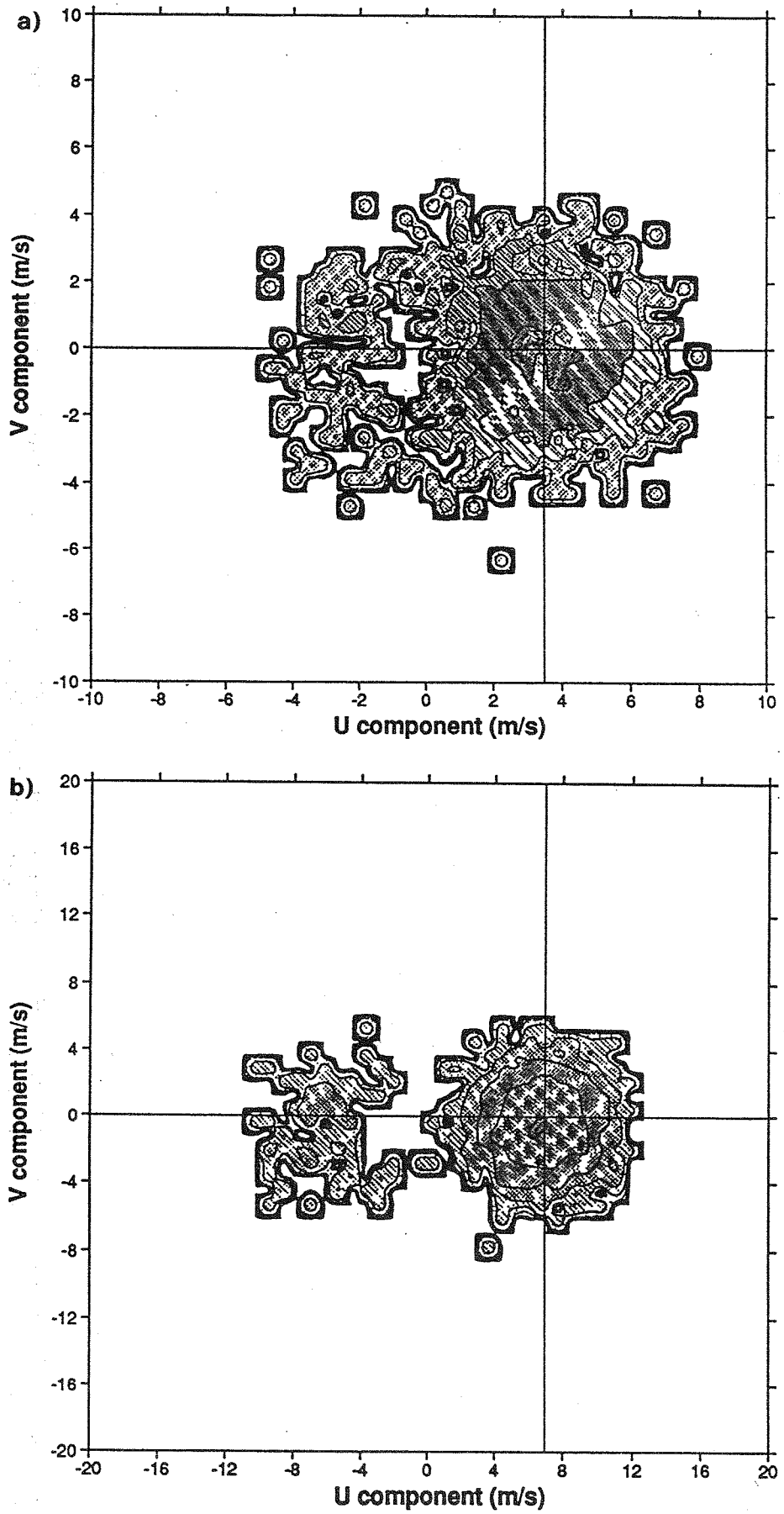

Fig 6.8 Monte Carlo simulations as explained in the text. The solution points are calculated with $J_O^{SCAT} - J_{O,1}^S J_{O,2}^S / [(J_{O,1}^S)^4 + (J_{O,2}^S)^4]^{1/4}$. In (a) the true wind vector V = (3.5, 0), and noise ε_R - 2 m/s and ε_B - 2m/s. The mean retrieved U-component is 3.25 m/s (a). (b) is for V = (7, 0), and the anomalously high noise of ε_B - 4 m/s. The mean retrieved u is 6.44 m/s with standard deviations of 3.29 m/s for u and 1.84 m/s for the v component. 2000 simulated scatterometer and background winds are used.

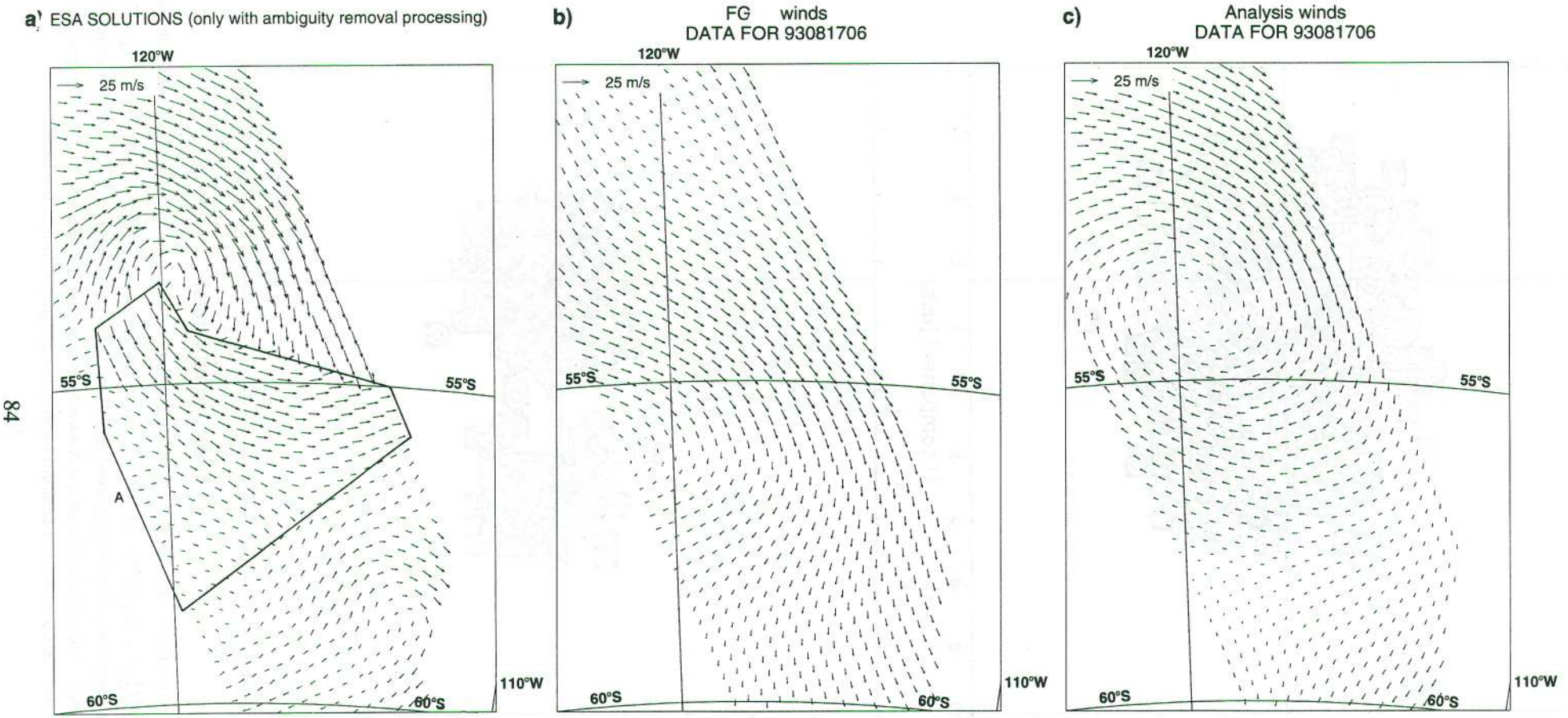

Fig 6.9 (a) ESA winds for 930817 at 08 UTC over the South Pacific, (b) ECMWF forecast winds and (c) the 3D-Var analysis using information from the scatterometer and the forecast as shown in (b). The analysis in (c) illustrates amongst other things the ambiguity removal capability of 3D-VAR.

7. SUMMARY AND CONCLUSIONS

It has been shown that an operational weather centre is an excellent place in which to quality control the data from any satellite instrument making meteorological observations. Checks can be made between the satellite measurements and the meteorological analysis, allowing near-real time monitoring of the instrument performance. For the UWI, files of collocations between the scatterometer measurements, σ^0, retrieved vector winds and other observations can be made, provided the data are received within 7 hrs. The collocation files can be analysed off-line by any number of investigators. In this report, we have used mainly comparisons between the scatterometer data and the ECMWF analysis or a short-range forecast (FGAT). Collocations with other instruments e.g. ships, island stations and buoys were made, but are difficult to interpret, partly because those measurements are local and are not representative of the scatterometer footprint.

The real time monitoring of average σ^0s with the ECMWF analysis was useful in the calibration of the scatterometer and in the removal of the interbeam biases. To avoid problems arising from retrieval and ambiguity removal, the initial product validation was done by direct σ^0 comparison. This showed significant differences between the measured and simulated σ^0, obtained using CMOD2. These differences are however difficult to interpret due to the non-linear relationship between wind and σ^0. However, we also noted a poor validation of the UWI winds against ECMWF analyses. Eventually, plotting CMOD2 in 3D σ^0 space together with measured σ^0 triplets showed their mutual inconsistency and confirmed the need to reformulate and retune the transfer function. The (σ^0_1, σ^0_2, σ^0_3) plots of the cone shaped transfer function together with plane slices through it were not only extremely useful in characterising the geophysical interpretation of σ^0, but also in validating the behaviour of the instrument. The ability to interpret σ^0 triplets as 10 m horizontal winds requires the existence of a solution surface in 3D σ^0 space around which the σ^0 triplets are scattered. We confirmed the existence of such a cone-shaped surface, and quantified the scatter of σ^0 triplets around this surface. This scatter can generally be explained by instrumental noise and contributes in general to only an insignificant part of the estimated wind error. The information on the scatter in σ^0 space was used in deriving a new transfer function (denoted CMOD4) and for quality control of the σ^0 triplets.

Since differences between measured and simulated σ^0s are difficult to interpret, due to the non-linear mapping of wind errors onto the simulated σ^0s, alternative transfer function validation methods were developed. Because of the low σ^0 scatter, a very sensitive test for a transfer function is its fit to the distribution of measured σ^0 triplets in 3D σ^0 space. The interpretation of the σ^0 triplets as a wind vector can further be tested by comparing to other wind observations or model winds.

After the transfer function was tuned, attention was directed to inversion. Several issues associated with the normalisation of the 'cost' function to be minimised were identified. Constant normalisation and a transformation $z = (\sigma^0)^{0.625}$ were derived to be optimal using a Bayesian method. This further gave wind directions which were closest to those of the ECMWF analyses. The probability distribution function for the retrieved winds does not show spurious spikes and gaps indicative of preferred or unattainable directions, as occurred with other normalisation and no z transformation. The symmetric geometry of ERS-1 is essential in the retrieval. A less symmetric design (e.g. as NSCAT) will complicate the retrieval.

The cone in 3D σ^0 space consists of two closely overlapping sheaths, one corresponding to winds with a component along the direction of the mid beam towards the satellite, and the second with winds having a component in the opposite direction. Interpretation of σ^0 triplets should therefore result in only two possible wind solutions. This restriction to two solutions is validated to have no adverse effects on the quality of the wind product when using our inversion method.

Problems with the CREO ambiguity removal software were identified. A revised scheme, called PRESCAT, which makes greater use of prior information was developed. More specifically, a short-range forecast is used at every node with the forecast interpolated to the measurement time. The velocity is initially chosen to be the one closest to the forecast velocity in a vector RMS sense. A spatial filter is then applied to correct unmeteorological features. The scheme seeks to select the field with the highest wind vector consistency. Points where the forecast wind vector is close to one of the two scatterometer solutions, and where the scatterometer wind directions are relatively accurate, are given initially high confidence. The filter propagates information from areas where confidence is high to areas where the confidence is low.

The wind fields obtained from PRESCAT were generally of high quality and showed relevant small scale features in meteorologically important situations. No other observing system can provide such a consistent view of mesoscale features. Statistics of differences between PRESCAT and ECMWF model winds show that the scatterometer winds are more accurate than operationally available conventional surface wind observations, and that the scatterometer wind error is not correlated over distances larger than 100 km. (This excludes ambiguity removal errors, when correlations can be of larger scale, but occur infrequently). The PRESCAT product meets the scatterometer design specifications of 2 m/s or 10 % in speed and 20 degrees in direction, at least over the speed range 4-18 m/s. For speeds below 4 m/s the design specification for speeds is also met.

For low wind speeds and low incidence angles, the scatter of σ^0 triplets around the cone surface may be correlated with other geophysical parameters than wind. When such a correlation is found it is expected to have no substantial effect on the general quality of the wind product. Rejected σ^0 triplets are generally

close (~100 km) to fronts, lows and tropical cyclones. Given the expected representativeness error and ECMWF model wind error, the scatterometer wind error is very small. Therefore, it will be difficult to further improve the general quality of the scatterometer wind product. In specific cases (the less common geophysical conditions) however, substantial improvement may be achieved.

Following ambiguity removal, the winds can be passed to an OI scheme for further quality control using "buddy" checking. The winds may then be assimilated into the analysis. A series of assimilations was performed at both T213 and T106 spectral truncation. The PRESCAT winds lead to changes in the analyses which were generally small in the northern hemisphere. In the mid-latitudes of the southern hemisphere, however, surface pressure changes were typically ~ 5 mb, but could be as high as 20 mb. In the tropics, pressure changes are small and wind changes were ~ 2 m/s.

Several forecasts were made from the analyses produced with and without scatterometer winds to assess whether the assimilation of these winds had been beneficial. By comparison to scatterometer and SATOB winds, a significant improvement in the short-range forecasts (up to 12 hours) has been found when using scatterometer data. However, on average, the impact of the scatterometer winds was neutral for the medium-range in the current observational system as measured by height anomaly correlations. When this system was degraded by withholding SATEMs and SATOBs, then the scatterometer winds were beneficial and lead to an enhanced medium-range forecast skill. Also, by comparison to forecast results obtained by *Bell* (1994) over the same period, it was found that the sensitivity to scatterometer data depends on assimilation system and performance. It was further shown that the surface wind field is adversely affected during the analysis when scatterometer data are not used. It is thought that the use of flow-independent structure functions and the absence of information on the special meteorological conditions in the PBL in the structure functions, contribute to this effect. To make observational systems more complementary and useful for Numerical Weather Prediction the effects of the structure functions have to be investigated more precisely. It is expected that surface wind data can be used meteorologically more consistently in a 4D variational assimilation system than in the current OI scheme. Also, in high resolution forecast models wind data are expected to have more impact. However, the improved surface wind analyses are important in themselves for ocean forecasting and climate modelling.

8. RECOMMENDATIONS

i. The impact of the validation campaign off Norway on developing a revised transfer function to CMOD2 was minimal. Instead we developed the transfer function based on ECMWF analyses. The fit to Haltenbanken campaign data was checked only a postiori. For the purpose of tuning a transfer function there seems to be no case for any extensive future campaign. There was a danger that bias in the ECMWF analysis was built into the transfer function, but this seems not to have been the

case based on validation against Haltenbanken winds (*Offiler*, 1993). Further, at ECMWF, monitoring against other GTS wind observation systems provides a quantification of systematic errors in the ECMWF winds. None-the-less there is a case for continued monitoring against high quality measurements such as from oceanographic research ships.

ii. Monitoring the performance of the instrument should continue throughout its lifetime, but this need not be a major activity. Monitoring the average normalised residual after inversion is very effective and should be implemented.

iii. CMOD4 gives a good general description of the cone surface around which σ^0 triplets are distributed in 3D σ^0 space. This is the most sensitive requirement for the quality of a transfer function. For low wind speeds and incidence angles and e.g. close to fronts and vigorous lows and tropical cyclones, the 2 parameter model is less adequate, however, and other geophysical information may be present in the σ^0 triplets. But, we do not expect that alternative proposals for the transfer function will in general substantially improve the quality of the scatterometer wind product. Systematic biases in wind speed against the ECMWF model are not significant. However, the effect of the different representativeness of the ECMWF model, the scatterometer and conventional wind data should be further investigated to refine the relationship between σ^0 and wind speed. For high wind speeds it has been shown that CMOD4 performs reasonably well and that speeds up to 22 m/s are obtained. Validation at high speeds is difficult, but it could be done more systematically with the currently available data than has been done in this report. The vector RMS departure from the ECMWF model is lower for scatterometer data than for conventionally available surface wind data.

iv. An optimal inversion procedure based on Bayesian probability theory was derived, and should be adopted by ESA, together with its quality control on normalised residual.

v. A revised ambiguity removal scheme, PRESCAT, was developed, which has some advantages over CREO and SLICE. This scheme makes heavy use of NWP model forecast information and benefits from time interpolation of the forecast field to the measurement time of the UWI. At ECMWF a forecast between 3 and 9 hours, i.e. the shortest possible lead, is used. At ESA, the forecast lead is between 18 and 48 hrs. Since, the use of such a long-range forecast will degrade the quality of the ambiguity removal, it would be useful to provide users with the two possible solutions, and a package for ambiguity removal, rather than a single solution as is done at present. Smaller centres could benefit from not having to do the inversion and therefore from receiving say two winds. But some centres use regional scale models with short cut-off times. If including winds would delay

the product delivery time, then it is likely that it would be better to send the σ^0 with minimum delay for use by short-range forecast centres. Centres could then produce their own winds in their area of interest if ESA supplied inversion and ambiguity removal software, for which we recommend PRESCAT.

iv. Offline users could obtain wind fields from the PAFs. The PAFs could base their product on a 3 to 9 hour forecast from ECMWF, using FGAT and PRESCAT software. (The collocation files at ECMWF are extended to include the two wind solutions and FGAT information.)

vii. The OI buddy check in the ECMWF statistical interpolation analysis scheme flags the most serious ambiguity removal problems (0.1% of cases), and could be used to correct them. This check could be developed inside PRESCAT to improve performance. However, we expect a 2D-Var ambiguity removal scheme to perform better than such a PRESCAT. We recommend this be developed, analogous to the existing 3D-Var, for use by other centres. The performance of 3D-Var should be further assessed in this respect.

viii. Most current data assimilation schemes use horizontally and vertically fixed structure functions to estimate the forecast error covariances. We suggest that this is a severe limitation in the assimilation of surface data and that research should be initiated to improve the modelled covariances. However, it is expected that in a 4D-Var analysis procedure the detrimental effect of fixed structure functions is much less severe. Assimilation experiments at higher resolution are also recommended, since the wind information provided by the scatterometer is most important on the smaller scales.

ix. A wave model response to surface wind data can be verified with wave observations. As the wave model response is a sensitive test of wind stress, it is recommended that the impact of assimilated scatterometer data in the ECMWF model be tested by using the assimilated fields to force the WAM model.

x. The availability of σ^0 triplets for descending passes between 40°N and 60°N in the North Atlantic is limited. Information on surface wind is however essential in this area for the prediction of weather and waves in and around Europe. The increase of data availability and timely release of the data in the specified area are therefore of major interest.

ACKNOWLEDGEMENTS

It is a pleasure to acknowledge the constructive discussions we have had with Evert Attema (ESA-ESTEC), Alf Long (ESA-ESTEC), Pascale Lecomte (ESA-ESRIN), David Offiler (UK Met Office) and other members of the ESA analysis team, and with P Woiceshyn (JPL) and Ross Hoffman (AER). Alf Long, Pascale Lecomte and David Offiler provided software which we adapted for model tuning and ambiguity removal. The use of the ECMWF operational analysis/forecast system involves support from many ECMWF staff members, too many to name in full, but A Hollingsworth, J Eyre, G Kelly and P Undén were especially helpful. C Gaffard is currently implementing our ideas on variational assimilation of scatterometer data.

REFERENCES

Anderson, D L T, A Hollingsworth, S Uppala and P M Woiceshyn, 1991: A study of the use of scatterometer data in the ECMWF operational analysis - forecast model Part I. Quality assurance and validation. J Geophys Res, 96, 2619-2634.

Anderson, D L T, A Hollingsworth, S Uppala and P M Woiceshyn, 1991: A study of the use of scatterometer data in the ECMWF operational analysis - forecast model Part II: Data impact, J Geophys Res, 96, 2635-2647.

Bell, R S, 1994: Operational use of ERS-1 products in the Meteorological Office. In proceedings of 2nd ERS-1 symposium - Space at the service of our environment. Hamburg 11-14 Oct 1993, ESA SP-361, pp 195-200.

Breivik, L-A, 1993: Assimilation of ERS-1 scatterometer wind information in a limited area model, Technical Report No.104, DNMI, P.B.43 Blindern, 0313 Oslo, Norway.

Britt, H I and R H Luecke, 1973: The estimation of parameters in non-linear, implicit models, Technometrics, 15, 2, 233-247.

Cavanié, A and P Lecomte, 1987: Vol 1 - Study of a method to dealias winds from ERS-1 data. Vol 2 - Wind retrieval and dealiasing subroutines, Final report of ESA contract No 6874/87/CP-I(sc), ESA publications division, ESTEC, Postbus 299, 2200 AG Noordwijk, The Netherlands.

Courtier, P et al., 1993: Variational assimilation at ECMWF, Research Department Tech Mem 194, ECMWF, Shinfield Park, Reading, RG2 9AX Berkshire, UK.

Donelan, M A and W J Pierson Jr, 1987: Radar scattering and equilibrium ranges in wind-generated waves with application to scatterometry, J Geophys Res, 92, C5, 4971-5029.

ECMWF Research Department, Ed 1993: ECMWF data assimilation scientific documentation. ECMWF Research Manual 1, 3/92 3rd revised edition.

Graham, R, D Anderson, A Hollingsworth and H Böttger, 1989: Evaluation of ERS-1 wind extraction and ambiguity removal algorithms: meteorological and statistical evaluation, ECMWF report.

Guignard, J-P et al, 1992: AMI Performances, Proceedings of the ERS-1 commissioning phase mid-term review held at ESA/ESTEC from 24-25 September 1991.

Hoffman, R N, 1993: A preliminary study of the impact of C-band scatterometer wind data on global scale numerical weather prediction. J Geophys Res., 98 (C6), pp. 10233-10244.

Lecomte, P, 1993: Wind scatterometer processing requirements for ice detection,Doc. No.: ER-SA-ESA-SY-1122, Issue 2.1, 21 september 1993, ESRIN DPE/OM, Via Galileo Galilei 5, I-00044, Frascati, Italy,

Le Dimet, F-X and O Talagrand, 1986: Variational algorithms for analysis and assimilation of meteorological observations, Tellus, 38A, 97-110.

Lilley, D K and E L Petersen, 1983: "Aircraft measurements of atmospheric kinetic energy spectra", Tellus 35A, 379-382.

Long, A E, 1985: Towards a C-Band radar sea echo model for the ERS-1 scatterometer, Proceedings of a conference on spectral signatures, Les Arcs, France, December, ESA SP-247.

Lorenc, A C, 1988: Optimal non-linear objective analysis, Q.J.R. Meteorol. Soc., 114, 205-240.

Lorenc, A C, R J Graham, I Dharssi, B Mcpherson, N B Ingleby and R W Lannon, 1991: Study of preparation for the use of Doppler Wind Lidar information in meteorological assimilation systems. Draft final report on ESA study contract 9063/90/HGE-I, UK Met Office, Bracknell, UK.

Offiler, D, 1987: ERS-1 wind retrieval algorithms, UKMO MET O 19 Branch Memorandum No 86.

Offiler, D, 1992: CMOD model tuning (Phase III), report to the ERS-1 analysis team meeting, Frascati, Italy, 9 November.

Offiler, D, (1994): The calibration of ERS-1 Satellite Scatterometer Winds, Journal of Atmospheric and Ocean Technology, in Press for October 1994.

Roquet, H and A Ratier, 1988: Towards direct variational assimilation of scatterometer backscatter measurements into numerical weather prediction models, IGARSS 88 Proceedings.

Smith, W L, H M Woolf, C M Hayden, D Q Wark and L M McMillin, 1979: The Tiros-N operational vertical sounder, Bul Am Met Soc, 60, 1177-1187.

Stoffelen, A C M and G J Cats, 1991: "The impact of SEASAT-A scatterometer data on high-resolution analyses and forecasts: The development of the QEII storm", Mon Wea Rev, 119, pp 2794-2802.

Stoffelen, A C M and D L T Anderson, 1992: ERS-1 scatterometer calibration and validation activities at ECMWF: A. The quality and characteristics of the radar backscatter measurements. Proc European 'International Space Year' Conference, Munich, Germany, 30 March - 4 April 1992. ESA publication.

Stoffelen, A C M, D L T Anderson, and P M Woiceshyn, 1992: ERS-1 scatterometer calibration and validation activities at ECMWF: B. From radar backscatter characteristics to wind vector solutions. Proc European 'International Space Year' Conference, Munich, Germany. ESA publication.

Stoffelen, A C M and D L T Anderson, 1993: "ERS-1 scatterometer data characteristics and wind retrieval skill", in proceedings of the First ERS-1 Symposium held in Cannes, France, 4-6 November 1992. ESA publication.

Stoffelen, A C M, D L T Anderson and C Gaffard, 1993: From measurement to model: ERS-1 scatterometer data assimilation. IGARSS 93 proceedings.

Stoffelen, A C M and D L T Anderson, 1993: ERS-1 scatterometer data characteristics and wind retrieval skill. IGARSS 93 proceedings.

Stoffelen, A C M and D L T Anderson, 1993: Wind retrieval and ERS-1 scatterometer radar backscatter measurements. Adv Space Res, 13, 53-60.

Stoffelen, A C M, C Gaffard and D Anderson, 1993: "ERS-1 scatterometer data assimilation", in proceedings of the second ERS-1 Symposium held in Hamburg, Germany, 11-13 October 1993. ESA publication.

Stoffelen, A C M, 1994: "From measurement to model: ERS-1 scatterometer data assimilation", to appear in ECMWF proceedings "Developments in the use of satellite data in Numerical Weather Prediction" of seminar held at ECMWF from 6-10/9/'93, Reading, UK.

Thépaut, J-N, P Courtier and R N Hoffman, 1992: "Use of dynamical information in a 4D variational assimilation". Proceedings of ECMWF workshop on variational assimilation with emphasis on 3-dimensional aspects, Reading, UK, 9-12 Nov, pp 237-270.

Thépaut, J-N, R N Hoffman and P Courtier, 1993: Interactions of dynamics and observations in a four-dimensional variational system. Mon Wea Rev, 121, No. 12, 3393-3414.

Undén, P, 1989: Tropical data assimilation and analyses of divergence. Mon Wea Rev, 117, 2495-2517.

APPENDIX A: DEFINITION OF BINARY FILE FORMATS FOR THE ERS-1 UWI VALIDATION FILES TO BE SUBMITTED TO ESA

1. INTRODUCTION

At ECMWF a project was carried out to give technical support for global validation of ERS-1 wind scatterometer data. In this context ECMWF agreed to transmit model information and conventional observations collocated with ERS-1 measurement nodes to ESA. This note describes the transmission file formats.

It was agreed to collocate at a resolution of 50 km rather than 25 km in order to reduce the amount of information generated and be compatible with model resolution. Thus of all incoming UWI node BUFR subsets we will only process ~ 25 %, i.e. in each second node starting at 1 and each second row starting at 1 for all UWI products. However, with the formats described underneath it is still possible to collocate at the full resolution.

The scatterometer data are time ordered before they go into the collocation program. This results in a time ordered collocation with the ECMWF model. The collocation with conventional surface data is not necessarily chronological. All UWI nodes and conventional surface data are rejected if interpolation from land grid points would occur. The number of data rejected was a few per cent prior to September 1991, but was significantly reduced after the T213 resolution ECMWF model was implemented (September 1991). The procedure excludes ships while in harbour.

Four files are prepared:

a) SC_MD_YYMMDDHH in FM94 BUFR code,

b) CL_CO_YYMMDDHH in FM94 BUFR code,

c) CL_SC_YYMMDDHH in FM94 BUFR code, and

d) the operational analysis of mean sea level pressure and 10m wind on a Gaussian grid in FM92 GRIB code; AN_SS_YYMMDDHH.

YYMMDDHH indicates date and time e.g. 91051506 represents 15 may 1991 6:00 am. The observation files contain data observed between 3:00 am and 9:00 am on that day, and the next files will be for 6 hours later. The GRIB coded file is standard, available from ECMWF, and thus needs no format extensions. The other three files are a mix of model and observational information, for which no BUFR formats currently exist, and will be described here. These files a), b) and c) will have BUFR type 12 and BUFR subtype of respectively 200, 201 and 202. The file mentioned first needs only a collocation of model fields and observational information, the second and third files also include collocation of ERS-1 winds with conventional observations and are the most complex ones. The structure of the files is given in table 1.

Tables 2-9 show the BUFR descriptors present in files a), b) and c). The field number refers to the positioning in the sequence of data values present in BUFR section 4. Decoded (real) BUFR values are in predescribed S.I. units. In the tables the precision in which the values are stored as binaries is given, and the maximum number of bits used for storage in binary.

The CL_CO_YYMMDDHH file contains those conventional observations (SHIP, BUOY, and Island reports), here called CONVOBS, which are collocated (within 300 km and 3 hours) with a ERS-1 UWI observation at 50 km resolution, and the CL_SC_YYMMDDHH file contains the CONVOBS collocated with ERS-1 UWI reports. Further, model information on 10 m wind from analysis and time interpolated forecast, on wave state from the WAM model, and on the Atmospheric Boundary Layer (ABL) from time interpolated forecasts, are included for both conventional and ERS-1 observations. A list of more than one collocated UWI report can be provided. For simulated CONVOBS back-scatter values the geometry of the first (nearest) collocated node is chosen in that case. ERS-1 nodes and CONVOBS which have positions that give rise to more than 1% model land contamination during interpolation are excluded from the BUFR data sets.

For ease of handling of the CL_CO_YYMMDDHH file, a standard CONVOBS BUFR data subset is developed, including the relevant (the cloud section is omitted) observational information present in SHIP, BUOY, drifting BUOY, and Island reports. The data descriptors of this subset are given in table 2. The total number of items n in the UWI and CONVOBS BUFR subsets is defined in table 3.

The SC_MD file contains the ERS-1 wind subsets (at 50 km resolution as mentioned above), the weather model information shown in table 4, and the wave model information shown in table 5 appended to each of those.

In the collocation software, the items in tables 4, 5 and 6 are appended to FM94 BUFR subsets of the conventional observations, and the ERS-1 wind scatterometer product UWI, to include the collocation model information agreed to be submitted to ESA. Table 5 shows a table of items which are appended to include information about the sea (swell) state at all observational points, extracted from the WAM model. Since the WAM model does not (yet) run operationally, the table is preliminary and BUFR values are set to "missing" at the moment.

Table 6 contains information on the boundary layer from the guess field of the ECMWF model. For all levels below 850 mb, pressure, height, wind, temperature and humidity are given. The number of levels changed (from 5 to 6) when ECMWF operations went from the 19-level model to the 31-level model in September 1991.

The actual collocation information calculated is given in table 7. These items are appended to table 6 for all the collocated UWI subsets.

Table 8 shows the locally or recently defined BUFR descriptors and the values, which are used in the BUFR subsets mentioned before. Table 9 explains the sequence descriptors used in earlier tables.

REFERENCES

WMO, Commission for basic systems, Expert meeting of the working group on data management, sub-group on data representation, final report (rev. 11-90), Geneva, 15-19 October 1990.

ECMWF, Binary Universal Form for data Representation, FM 94 BUFR, collected papers and specification, February 1988.

Offiler, D, B Edkins, C Long and C Brüning, The transmission and storage of ERS-1 data using FM94 BUFR, Met. Office, S (Nowcasting) Image Processing Group,Technical note no. 8.6, 20-11-90.

Offiler, D, FM94 BUFR Encoding and Decoding: A software implementation for ERS-1 data, Met. Office, S (Nowcasting) Image Processing Group,Technical note no. 12.1, 27-11-90.

WMO, Manual on codes volume I; international codes, WMO no. 306, Secretariat of the WMO, Geneva, Switzerland, 1988.

a)

SC_MD_YYMMDDHH (FM94 BUFR)		
1st UWI subset	interpolated model wind information	interpolated WAM wave information
....	....	....
last UWI subset	interpolated model wind information	interpolated WAM wave information

b)

CL_CO_YYMMDDHH (FM94 BUFR)			
1st collocated conventional subset	interpolated model wind information	interpolated WAM wave information	interpolated model ABL information
....	....	....	....
last collocated conventional subset	interpolated model wind information	interpolated WAM wave information	interpolated model ABL information

c)

CL_SC_YYMMDDHH (FM94 BUFR)				
1st collocated UWI subset	interpolated model wind information	interpolated WAM wave information	interpolated model ABL information	collocation information
....	....	....	....	....
last collocated UWI subset	interpolated model wind information	interpolated WAM wave information	interpolated model ABL information	collocation information

d)

AN_SS_YYMMDDHH (FM92 GRIB)		
wind direction at 10m	wind speed at 10m	pressure at mean sea level

Table 1: File structure of files transmitted to ESA: (dots denote the intermediate sequence between first and last subset):

Field number	BUFR descriptor	Parameter name	(Precision) Unit	Bits Table
1	0 01 001	WMO block number	numeric	7
2	0 01 002	WMO station number	numeric	10
3	0 01 011	Ship call sign	CCITT IA5	72
4	0 01 005	Buoy/platform ident.	numeric	17
5	0 01 012	Direction of motion	deg.true	9
6	0 01 013	Speed of station mot.	m/s	10
7	0 02 001	Type of station	code table	2
8	0 04 001	Year	year	12
9	0 04 002	Month	month	4
10	0 04 003	Day	day	6
11	0 04 004	Hour	hour	5
12	0 04 005	Minute	minute	6
13	0 05 002	Latitude	(0.01) deg.	15
14	0 06 002	Longitude	(0.01) deg.	16
15	0 07 001	Height of station	m	15
16	0 10 004	Pressure	(10) Pa	14
17	0 10 051	Pressure reduced to mean sea level	(10) Pa	14
18	0 10 061	Pressure change (3 h)	(10) Pa	10
19	0 10 063	Tendency character.	code table	4
20	0 11 011	Wind direction at 10 m	deg.true	9
21	0 11 012	Wind speed at 10 m	(0.1) m/s	12
22	0 12 004	Dry bulb temp. at 2 m	(0.1) K	12
23	0 12 006	Dew point temp. at 2 m	(0.1) K	12
24	0 13 003	Relative humidity	%	7
25	0 20 001	Horizontal visibility	(10) m	13
26	0 20 003	Present weather	code table	9
27	0 20 004	Past weather (1)	code table	5
28	0 20 004	Past weather (2)	code table	5
29	0 22 042	Sea surface temperature	(0.1) K	12
30-31	3 01 200	QC sequence[1]	see table 9	10
32	0 01 193	Sigma_0 simulation method	see table 8	4
-	1 01 003	Replication factor	-	-
	Next item appears 3 times and will be in field 33 to 35 for fore, mid and aft beam.			
33	0 21 192	Sigma_0	(0.01) dB	13

Table 2: BUFR format for conventional observations (CONVOBS).

[1] Conventional observations are checked against a very strict "black-list" developed to improve the possibility for estimating an accurate model function. Black-listed stations do not fulfil the constraints on statistical behaviour concerning wind data over a period of month(s), and on number of monthly reports.

Observation type	Value of n
CONVOBS	35
UWI	29

Table 3: Length of CONVOBS and UWI BUFR subsets

Field number	BUFR descriptor	Parameter name (comment)	(Precision) Unit	Bits table
n + 1	0 01 031	Generating centre	see table 8	16
n + 2	0 01 192	Model version number	see table 8	8
n + 3	0 04 024	Time or displacement[2]	hour	11
-	1 05 002	Replication factor	-	-
	Next 5 items will be repeated 2 times, for the analysis and subsequently for the forecast from n + 9 to n + 13.			
n + 4	0 01 032	Generating application	see table 8	8
n + 5	0 04 003	Day of field (base)	day	6
n + 6	0 04 004	Hour of field (base)	hour	5
n + 7	0 11 012	Wind speed at 10 m	(0.1) m/s	12
n + 8	0 11 011	Wind direction at 10 m	deg.true	9
n + 14	3 01 201	Analysis QC sequence[3]	see table 9	9
n + 17	0 01 193	Sigma_0 simulation method	see table 8	6
-	1 01 006	Replication factor	-	-
	Next item will be repeated 6 times; for the analysis from n + 18 to n + 20 and for the forecast from n + 21 to n + 23, i.e. respectively for fore, mid and aft beam.			
n + 18	0 21 192	Sigma_0	(0.01) dB	13

Table 4: Interpolated ECMWF model winds and their estimated quality at the observation spot.

[2] If for forecast data (0 01 032) = 62 (see n + 4) then time difference between forecasts else forecast period of field. The actual forecast period for forecast data in the first case is observation time minus base time (see n + 5 and n + 6).

[3] This is the standard Q.C. performed on observations fed into the analysis procedure. Ships which have produced low quality reports for the last few days will have analysis quality flag 3 (see table 9) set, but might have an acceptable wind report in this issue.

Field number	BUFR descriptor	Parameter name	(Precision) Unit	Bits table
n + 24	0 01 032	Generating application	see table 8	8
n + 25	0 01 192	Model version	see table 8	8
n + 26	0 22 001	Direction of waves	deg.true	9
n + 27	0 22 011	Period of waves	second	6
n + 28	0 22 021	Height of waves	(0.1) m	10

Table 5: WAM wave model information at the observation spot.

Field number	BUFR descriptor	Parameter name	(Precision) Unit	Bits table
n + 29	0 01 032	Generating application	see table 7	8
n + 30	0 01 192	Model version	see table 7	8
n + 31	0 22 042	Sea temperature	(0.1) K	12
n + 32	0 12 004	Dry bulb temp. at 2 m	(0.1) K	12
-	1 06 005	Replication factor	-	
Next 6 items will be repeated 5[4] (or 6) times: i.e. from n + 33 up to n + 62 (68).				
n + 33	0 10 004	Pressure	(10) Pa	14
n + 34	0 07 002	Height or altitude (above surface)	(10) m	16
n + 35	0 11 002	Wind speed at level	(0.1) m/s	12
n + 36	0 11 001	Wind direction at level	deg.true	9
n + 37	0 12 001	Temperature at level	(0.1) K	12
n + 38	0 13 001	Specif. humidity at level	(10^{-5}) g/g	14

Table 6: ECMWF weather model ABL information at the observation spot for to the wind measurement related quantities.

Field number	BUFR descriptor	Parameter name	(Precision) Unit	Bits table
m + 1	0 01 032	Generating application	see table 8	8
m + 2	0 08 200	Number of observations[5]	see table 8	8
-	2 01 131	Change data width	-	-
m + 3	0 06 021	(collocation) Distance	(10) m	16
-	2 01 000	Reset data width to default	-	-
m + 4	0 04 025	Time displacement (C - E)	minute	12

Table 7: CONVOBS with ERS-1 wind scatterometer collocation information to be appended to table 6 only for UWI. m equals the last field number of table 6.

[4] The operational change from the T106 19-level model to the new T213 31-level model at the beginning of september 1991 involved a change in the number of model levels generally below 850 mb. This number, encoded here is for the T213 system, 5 for the T106 version of the model.

[5] This number indicates the total number of ERS-1 UWI collocations with the particular CONVOBS concerned.

Descriptor	Bits	Value	Meaning
0 01 031	16		Generating centre
	All	98	ECMWF
		65535	Missing value
0 01 032	8		Generating application
	All	1	Preprocessing consistency check
		41	Optimum interpolation (OI) analysis scheme
		61	Guess field (6 hour forecast)
		62	Guess field (time interpolated)
		81	Wave model (WAM) forecast
		201	Collocation with surface data
		206	Collocation with ERS-1 scatterometer winds
		210	Writers black-listing program
		242	OI guess field check
		243	OI neighbour observations check
		255	Missing value
0 01 192	8		Model version number
	All	31	Forecast model T106L19
		40	Forecast model T213L31
		201	WAM model cycle 3
		255	Missing value
0 01 193	4		sigma_0 simulation method
	All	1	CMOD2_1
		2	CMOD2
		3	CMOD3
		4	CMOD4
		5 - 14	Reserved
		15	Missing value
0 33 193	3		ECMWF QC descriptor
		0	Data considered correct
		1	Data probably correct
	All	2	Data probably unfit for use
		3	Data considered unfit for use
		4-6	Reserved values
		7	Missing data
0 33 001	2		Quality indicator
		0	Not suspect
	All	1	Suspect
		2	Reserved value
		3	Missing data
0 08 200	8	8	Number of observations

Table 8: Description of local or recently developed BUFR data descriptors.

Sequence descriptor	Expansion	Meaning
3 01 200		QC sequence
	0 01 032	Generating application
	0 33 194	Data quality indicator
3 01 201		Analysis QC sequence
	1 01 003	Replication factor
Replication of next item for resp. preprocessing, and guess field and observational check within the analysis		
	0 33 193	ECMWF QC descriptor

Table 9: Expansion of sequence descriptors.

APPENDIX B: TUNING CONSIDERATIONS: EXAMPLES OF POSSIBLE DIFFICULTIES

1) Proportional error

Let us assume we have a 3D measurement space with axes x, y and z, where the "true" solution is a plane with $z=z_t$. Now make an infinite number of measurement triplets (x_m,y_m,z_m), assuming these measurements have Gaussian errors with standard deviations $\sigma_x=\sigma$, $\sigma_y=\sigma$ and $\sigma_z=\varepsilon.z_t$, for x, y and z. [The σ used here denotes standard deviation and is not to be confused with radar backscatter]. We note that the error in z is proportional to the true value z with proportionality constant ε. Given the PDF of measurements $p(x,y,z)dxdydz$ we try to estimate the solution plane $z=z_s$. Assuming we have no a priori knowledge and neglecting constant terms, we find the solution by minimising:

$$MLE=\left[\frac{z_m-z_s}{\sigma_z}\right]^2 \tag{B1}$$

over all measurements. Since we do not know σ_z we have to estimate it. The best estimate seems to be $\varepsilon.z_s$ where the subscript s refers to the estimated solution. Now if we minimise:

$$\iiint MLE.p(x,y,z)dxdydz \tag{B2}$$

we find:

$$z_s=(1+\varepsilon^4).z_t \tag{B3}$$

showing that the theoretical solution is not the "true" solution but, in fact, exceeds it. In the same way, one can show that if σ_z is estimated by $\varepsilon.z_m$ a solution below the "true" plane is found, with an error of second order, i.e. $0(\varepsilon^2)$.

The above example does not consider any non-linearities in the plane defined by all possible values of (x_s,y_s,z_s), i.e. solution plane. In our specific case, however, the solution surface is itself highly non-linear, which will further degrade the performance of the estimation procedure as a consequence of the proportional errors by introducing $0(\varepsilon^2)$ errors. An alternative is to do the estimation with σ^0 in dBs. The proportionality constant for σ^0 is approximately 5 %. As a consequence, the σ^0 error standard deviation in dBs has an approximately constant value of 0.2 dB. The drawback of using logarithmic rather than physical space, is that the σ^0 instrumental error standard deviation is expected to be Gaussian in physical space, whereas in logarithmic space the error distribution is expected to be slightly non-Gaussian and skew. In practice, it depends on the relative non-linearity in the formulation of the transfer function in physical and in logarithmic space, as to whether it is advantageous to do the estimation in one space, rather than the other (see section 3.3.1).

2) Non-linearity

A non-linear surface of itself will also lead to errors in MLE. A simple example illustrates this. Assume we have a 2D measurement space with axis x and y, and a true solution $x_t^2 + y_t^2 = 1$. We now make an infinite number of measurement pairs (x_m, y_m), which have Gaussian error standard deviations $\sigma_x = \sigma$ and $\sigma_y = \sigma$, and estimate a solution lying on a circle with $r = r_s$. Assuming no prior knowledge is present, we can define our objective function as:

$$\text{MLE} = \left\lceil \frac{r_m - r_s}{\sigma} \right\rceil^2 \tag{B4}$$

Minimising this function over the measurement distribution $p(x,y)dxdy$, and assuming $\sigma \ll 1$ gives the solution:

$$r_s = 1 - \sigma\sqrt{\frac{2}{\pi}} \tag{B5}$$

in which the error is first order in σ.

In a similar way it can be shown that if we try to fit the above measurement distribution with a solution like $(x+\beta)^2 + y^2 = r_s^2$, then we will introduce a positive term $0(\varepsilon)$ in Eqn (B5) increasing the solution radius r_s. One could regard β as a bias misfit term.

The assumption $\sigma \ll 1$ prevents "aliasing" problems. If $\sigma \approx 1$ then "true" values for example at $(x,y) = (0,1)$, i.e. the top of the circle, could be thrown by noise to the other side of the circle (eg around (0,-1). The distance of such measurement points to the "true" point would be large. In MLE, however, the likelihood of such points will be measured by the distance to the closest point on the circle, not the distance to the "true" point.

Obviously, non-linearity invalidates the use of a linear estimator (quadratic formulation) in a MLE problem. However, given the non-linearity and complexity of the transfer function estimation problem, a mathematically optimal solution will be difficult to find. Therefore, we will stick to a quadratic formulation, but try to pose the problem in a more linear and symmetric space. A misspecification of the bias term in the transfer function may lead to further $0(\varepsilon)$ errors. Aliasing effects will be present when the noise in wind direction is close to the period of the harmonic functions in the transfer function, and cannot easily be avoided. This will be the case for low wind speeds.

APPENDIX C: THE CMOD4 MODEL FORMULATION AND COEFFICIENTS

The form of the ECMWF CMOD4 model is:

$$\sigma^0_{lin} = b_0.(1+b_1 \cos\phi+b_3 \tanh b_2.\cos 2\phi)^{1.6}$$

where: $b_0 = b_r.10^{\alpha+\gamma.f_1(V+\beta)}$

and $f_1(y) = \begin{cases} 0 & if\ y \le 0 \\ \log y & if\ 0 < y \le 5 \\ \sqrt{y}/3.2 & if\ y > 5 \end{cases}$

and α, β, γ, b_1, b_2 and b_3 are expanded as Legendre polynomials to a total of 18 coefficients. b_r is a residual correction factor to b_0 and is given as a look-up table as a function of incidence angle.

$$\alpha = c_1P_0 + C_2P_1 + c_3P_2$$

$$\gamma = c_4P_0 + c_5P_1 + c_6P_2$$

$$\beta = c_7P_0 + c_8P_1 + c_9P_2$$

$$b_1 = c_{10}P_0 + c_{11}.V + (c_{12}P_0+c_{13}.V) \ . f_2(x)$$

$$b_2 = c_{14}P_0 + c_{15}.(1+P_1).V$$

$$b_3 = 0.42(1+c_{16}(c_{17}+x)(c_{18}+V))$$

$$b_r = LUT(\theta)$$

$$f_2(x) = \tanh\{+2.5(x+0.35)\} - 0.61(x+0.35)$$

where the Legendre polynomials are:

$$P_0 = 1 \quad P_1 = x \quad P_2 = (3x^2-1)/2 \text{ with } x = (\theta-40)/25.$$

V is the wind speed in ms^{-1}, ϕ the relative wind direction in degrees and θ the incidence angle in degrees.

CMOD4 coefficients

Model		CMOD4
α	c_1	-2.301523
	c_2	-1.632686
	c_3	0.761210
γ	c_4	1.156619
	c_5	0.595955
	c_6	-0.293819
β	c_7	-1.015244
	c_8	0.342175
	c_9	-0.500786
b_1	c_{10}	0.014430
	c_{11}	0.002484
	c_{12}	0.074450
	c_{13}	0.004023
b_2	c_{14}	0.148810
	c_{15}	0.089286
b_3	c_{16}	-0.006667
	c_{17}	3,000000
	c_{18}	-10.00000

Residual factors for CMOD4

θ^0	b_r	θ^0	b_r	θ^0	b_r
16	1.075	31	0.927	46	1.054
17	1.075	32	0.923	47	1.053
18	1.075	33	0.930	48	1.052
19	1.072	34	0.937	49	1.047
20	1.069	35	0.944	50	1.038
21	1.066	36	0.955	51	1.028
22	1.056	37	0.967	52	1.016
23	1.030	38	0.978	53	1.002
24	1.004	39	0.988	54	0.989
25	0.979	40	0.998	55	0.965
26	0.967	41	1.009	56	0.941
27	0.958	42	1.021	57	0.929
28	0.949	43	1.033	58	0.929
29	0.941	44	1.042	59	0.929
30	0.934	45	1.050	60	0.929